THE UNIVERSITY OF MANITOBA

SOURCE IDENTIFICATION USING SOUND AND VIBRATION INTENSITIES

BY

AMIT CHAWLA

A THESIS

SUBMITTED TO THE FACULTY OF GRADUATE STUDIES

IN PARTIAL FULFILMENT OF THE REQUIREMENTS FOR THE DEGREE

OF MASTER OF SCIENCE

DEPARTMENT OF MECHANICAL ENGINEERING

WINNIPEG, MANITOBA

CANADA

ISBN 0-315-33994-2

SOURCE IDENTIFICATION USING SOUND AND VIBRATION INTENSITIES

BY

AMIT CHAWLA

A thesis submitted to the Faculty of Graduate Studies of the University of Manitoba in partial fulfillment of the requirements of the degree of

MASTER OF SCIENCE

ACKNOWLEDGEMENTS

I would like to express my deepest gratitude to Dr. N. Popplewell for his guidance, patience and constant encouragement during the course of my program.

I acknowledge gratefully the financial support of Sperry Inc., Defence Systems Division, Winnipeg. Special thanks are due to Mr. J. Westergren for initiating this project and to Mr. D. C. Saxerud for his interest in this work. The enthusiastic support of Mr. A. F. Ma is appreciated deeply.

Finally, I would like to thank Messrs. J. Sewell, L. Wilkins, and J. Shewchuk for their technical assistance, and Mrs. D. Dennis for typing this manuscript.

ABSTRACT

After a brief literature review, a cross spectral technique using two microphones is described for measuring the sound power of a development computer even when the ambient noise is relatively high. Principal sound radiation regions are identified and recommendations are made for "quietening" the computer. These include acoustical treatment of the back panel, streamlining the airflow within the computer, and acoustical improvement of the EMI+ seal. Then an alternative but pragmatic approach is detailed which substitutes an accelerometer for the microphones. It is based on idealizing the computer as a sphere pulsating in an infinite baffle. This approach has been used advantageously to highlight the correlation between the sound and vibration of the computer. Finally, the mapping of structureborne vibration paths on the computer's cabinet is described. Once again, fundamental design flaws are identified and improvements are suggested. These recommendations include modifying the air flow within the computer, better isolation between the fan and the cabinet and local stiffening of the relatively flexible rear panel.

+Electromagnetic interference

TABLE OF CONTENTS

		Page
ACKNOWLEDGEMENTS		(i)
ABSTRACT		(ii)
TABLE OF CONTENTS		(iii)
LIST OF FIGURES		(iv)
LIST OF TABLES		(vii)
NOMENCLATURE		(viii)
Chapter I	INTRODUCTION	1
CHAPTER II	ACOUSTIC INTENSITY TECHNIQUE	9
2.1	Theory	10
2.2	Results	21
2.2.1	Sound Power Determination	27
2.2.2	Location of Sound Sources	34
2.3	Conclusions	45
Chapter III	CORRELATION BETWEEN THE SOUND AND VIBRATIONS OF THE COMPUTER	46
3.1	Theory	47
3.2	Results	49
3.3	Conclusions	57
Chapter IV	VIBRATION INTENSITY TECHNIQUE	58
4.1	Theory	59
4.2	Results and Discussion	69
4.2.1	Lead Plate	71
4.2.2	Computer	84
4.3	Conclusions	102
REFERENCES		104

APPENDICES

Appendix		Page
1	. . . .	109
2	. . . .	111
2A	. . . .	117
3	. . . .	119
4	. . . .	128

LIST OF FIGURES

Figure		Page
1.1	Showing the microphone locations recommended by ISO 3745 on a hemisphere enclosing the sound source.[7]	3
2.1	Microphone orientation of a) side-by-side and b) end-to-end configurations	11
2.2	Block diagram of acoustic intensity apparatus . . .	14
2.3	Approximation error, L_e, for different frequencies and microphone spacings	16
2.4	Comparison of the acoustic intensities measured in a pipe of length 1.2 m.	24
2.5	Comparison of the acoustic intensities measured in a pipe of length 4.0 m.	26
2.6	Comparison of acoustic intensity measured by using an ILG reference sound source and the acoustic intensity technique.	28
2.7	Overall sound pressure levels at the midpoint but 0.91 m. (3 ft) from each nearest computer panel. . .	33
2.8	View of computer showing the 56 and 25 measurement locations on the left side and rear panel, respectively	36
2.9	Overall air flow within the computer	37
2.10	One third octave band acoustic intensity levels at left side panel around 100 Hz. centre frequency .	38
2.11	One third octave band acoustic intensity levels by left side panel at 125 Hz. centre frequency	40
2.12	One third octave band acoustic intensity levels by left side panel at 500 Hz. centre frequency	41
2.13	One third octave band acoustic intensity levels by left side panel at 1000 Hz. centre frequency	42

Figure		Page
2.14	One third octave band acoustic intensity levels by rear panel at 50 Hz. centre frequency.	44
3.1	Accelerometer arrangement for measuring transverse and longitudinal accelerations at a "point".	51
3.2	Frequency response functions obtained by using the impulse technique [42] on: a)right, b) top, c) left and d) rear panel	53
3.3	Sound spectra of various fans	56
4.1	Representation of the vibration intensity vector at a measurement location on the computer	60
4.2	Forces, moments and displacements in a cross-section of a plate	62
4.3a,b	Dual accelerometer mount	70
4.4	Experimental setup	72
4.5	Comparison of vibration power levels measured by using force/velocity transducers and the vibration intensity technique	74
4.6	Comparison of vibration power levels measured by using force/velocity transducers, vibration intensity and Pavic's technique with accelerometer spacings of 2 cm. and 3 cm.	76
4.7	View of lead plate with 56 measurement locations . . .	78
4.8	One third octave band vibration intensity pattern and acceleration levels on lead plate at 63 Hz. centre frequency	79
4.9	One third octave band vibration intensity pattern and acceleration levels on lead plate at 80 Hz. centre frequency	80
4.10	One third octave band vibration intensity pattern and acceleration levels on lead plate at 100 Hz. centre frequency	81
4.11	Exploded view of computer showing 66 measurement locations	86

Figure		Page
4.12	One third octave band vibration intensity pattern on computer cabinet at 63 Hz. centre frequency with fan running	87
4.13	One third octave band accelerations at centre of left side panel of computer.	89
4.14	One third octave band accelerations at centre of right side panel of computer	90
4.15	One third octave band accelerations at centre of top panel of computer	91
4.16	One third octave band accelerations at centre of rear panel of computer	92
4.17	Frequency response function obtained by using the impulse technique [42]	94,95
4.18	One third octave band vibration intensity pattern on computer cabinet at 63 Hz. centre frequency with external excitation and no air flow	98
4.19	One third octave band vibration intensity pattern on computer cabinet at 500 Hz. centre frequency with fan running.	101
A.4.1	Intensity levels crossing sections AA' and BB' (dB re 10^{-12} W/m)	129
Plate 3.1	View of shaker attached to rear of computer	50

LIST OF TABLES

Table		Page
2.1	Measurement of computer's total sound power level using conventional and acoustic intensity technique	30
3.1	Measurement of computer's total sound power level determined by using surface velocities	54
4.1	Energy balance across various sections of the lead plate	83
A.1.1	Cartesian coordinates of microphone positions	110
A.2.1	Sound pressure levels of computer	112
A.2.2	Determination of Room constant R	113
A.2.3	Errors in L_p, Q and R	115
A.3.1	Octave band velocity squared values	121
A.3.2	Relative transverse and axial acceleration levels on top panel of computer	122
A.3.3	Relative transverse and axial acceleration levels on left panel of computer	123
A.3.4	Relative transverse and axial acceleration levels on right panel of computer	124
A.3.5	Relative transverse and axial acceleration levels on rear panel of computer	125

NOMENCLATURE

I	Acoustic intensity (magnitude)
p	Mean square sound pressure
ρ	Medium (air) density
c	Speed of sound in air
d	Diameter of Rayleigh disc
λ	Wavelength of sound
W	Total acoustic power
S	Closed surface area
$\vec{I}_n$	Intensity vector normal to the surface of a sound source
$\vec{u}_r$	Particle velocity in medium (air)
p_1	Pressure sensed by microphone 1
p_2	Pressure sensed by microphone 2
$\vec{\Delta}r$	Directional vector between microphone centres
lim	Limit
i	Complex number notation
ω	Variable circular frequency
T	Sampling period
G_{12}	Cross power spectrum between microphone/accelerometer channels
Im	Imaginary part
k	Acoustic wave number
$\vec{I}_{ex}$	Acoustic intensity of a point source determined analytically
S	Source strength of a monopole
$\vec{r}$	Distance of sound source from measurement location

M_x	Magnitude of moment on elemental area
M_{xy}	Magnitude of moment on elemental area
θ	Angular displacement (subscript denotes direction)
w_{xq}	Force component of intensity
w_{xb}	Bending moment component of intensity
w_{xt}	Twisting moment of intensity
Θ	Direction of vibration vector relative to horizontal
ε	Surface strain (subscript denotes direction)
γ_{xy}	Shear strain
w_x'	Modified component of intensity
a	Transverse accelerations (subscripts denote accelerometer #)
L_W	Sound power level
$L_{\bar{p}}$	Average sound pressure level
r	Radius of hypothetical hemisphere
S	Surface area of hypothetical hemisphere
So	Unit surface area (1 m^2)
N	Number of sound pressure measurement locations
C	Correction term to account for ambient pressure and temperature
Q	Directivity factor
R	Room constant
α	Absorbivity co-efficient
E	Expected value
Re	Real part
F	Fourier transform

$\vec{I}_{me}$ Acoustic intensity produced by a point source measured by using a finite difference approximation

r_1 Distance of source from microphone 1

r_2 Distance of source from microphone 2

G_{12s} Switched cross power spectrum between microphone/accelerometer channel

G_{12cal} Calibrated cross power spectrum between microphone channels

H_{12} Frequency response function for calibration signal between microphone channels

$|H_1|^2$ Auto power spectrum for calibration signal

H_{12s} Switched frequency response function for calibration signal

K_{12} Square root of ratio of H_{12}/H_{12s}

S Total area of vibrating surface on the "pulsating sphere"

ΔS_f Area of each individual vibrating surface element

n Number of individual vibrating areas

W_e Sound power radiated by an element on surface

$\vec{U}_e$ Volume velocity of pulsating sphere

a Radius of sphere

$< >$ Temporal average

D Flexural stiffness of a panel

h Thickness of a panel (assumed uniform)

ρ_t Material density

$\vec{w}$ Structureborne vibration vector

$\vec{w}_i$ Structureborne vibration vector (in some given direction)

Q_x Magnitude of shear force on elemental area

ν Poisson's ratio

CHAPTER I

Identification of the sources of noise and their reduction is the primary objective in noise control. However, it is desirable to have an accurate, quantitative measure of the sound intensity or power of a source before embarking on a noise reduction program. Sound power is generally emphasised because it provides a datum that does not change with ambient conditions [1]. Prior to the development of a viable method for directly measuring acoustic intensity, nearly all studies relied on the measurement of sound pressure. Sound pressure, however, is affected by ambient conditions so that it is necessary then to use special acoustical environments, such as that found in an anechoic chamber, to straightforwardly interpret the results [2].

Classical methods of sound power determination, like free, reverberant and semi-reverberant field testing, and duct testing, require special acoustical facilities [2,3,4]. These facilities essentially simulate free field or diffuse field conditions. In a reverberation chamber, for example, the boundaries are acoustically "hard" so that the sound field approaches a diffuse condition where the sound energy is statistically uniform throughout the room. In an anechoic chamber, on the other hand, the treatment at the room's boundaries effectively absorbs the incident sound, thereby producing an echo free or free field condition. Under echo free conditions, the methodology for determining the sound power of a source is described in ISO standards 3740 to 3746 inclusive and in ANSI S1. 31-1980 and ANSI S1. 32-1980 [5,6]. According to the method described in these standards, the sound source is placed on a reflecting plane in an anechoic chamber at the geometric centre of an imaginary hemisphere [6]. The sound power is determined from sound pressure measurements taken on the hemispherical control surface. The radius of the control surface is made sufficiently large to ensure that the sound waves are radiating freely and progressively outward from the surface. Typically, the hemisphere's radius is at least twice the major dimension of the sound source [1] so that the surface is in the acoustical far field of the source. The sound pressure produced by the source is measured by using a microphone, generally at 10 to 24 standard locations on the hemisphere as shown in Figure 1.1. The number of microphone locations depends upon the accuracy required, the directivity of the source and the symmetry of the radiation pattern. Usually ten is the number selected because it reasonably compromises between the two opposing requirements of accuracy and a short experimental procedure. The microphone locations are usually distributed such that each location is associated with the same proportion of the total surface area of the hemisphere. The sound power level is approximated by the procedure described in Appendix 1. For progressively outgoing waves under free field conditions, the mean square acoustical pressure, p^2, is related directly to the sound intensity, I, by [7]

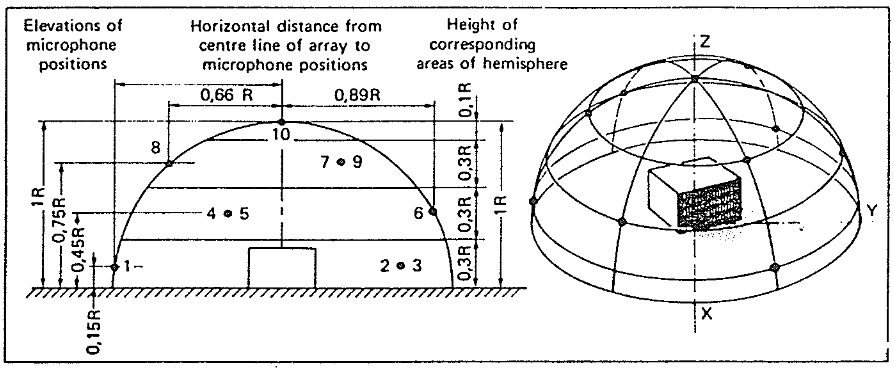

Figure 1.1 : Showing the microphone locations recommended by ISO 3745 on a hemisphere enclosing the sound source. [7]

$$I = p^2/\rho c \ . \qquad \{1.1\}$$

Here ρ is the medium's density and c is the speed of sound in the medium.

A major limitation of determining sound power from sound pressure measurements is that meaningful results can be obtained only in the far field of the sound source. Close to the source, the air's particle velocity is not necessarily in the direction of propagation of the sound wave so that an appreciable tangential velocity may exist [3]. Consequently, part of the acoustical energy radiated by the source may be undetected due to the directional characteristics of all microphones. It is this undetected velocity component which often causes an appreciable extraneous variation in sound pressure level at various distances from the source even under free field conditions [3]. Therefore, measurements must be in the far field where the particle velocity is primarily in the direction of propagation of the sound wave and the magnitude of the acoustic intensity is proportional to the square of the sound pressure [3]. Thus, special acoustical facilities have to be quite large with sound sources of considerable size, (e.g. 7m.X7m.X4m. to accommodate a truck) and, consequently, such facilities are quite expensive. [4]

Prior to the development of the acoustic intensity technique, no straightforward method existed for determining the individual sources of sound. It was necessary, therefore, to use a cumbersome and time consuming technique like lead cladding. Cladding has been employed extensively, for example,in the automotive industry. The procedure involves wrapping a lead sheet, lined with fibre glass or other absorbing material, around individual components and measuring the reduction in the overall sound pressure level (and, hence, the sound power level) due to selective wrapping. The reduction in the overall sound power level corresponds to the contribution of that particular wrapped component to the overall sound power level. There are, however, several drawbacks. First, an anechoic chamber is required to prevent reflected sound waves from interfering with the measurements. Second, this method fails at frequencies below about 300 Hz. because the lead then becomes "transparent" to the noise. This deficiency defeats the purpose of wrapping (i.e. to eliminate the effect of individual sources while measuring the reduction in the overall sound power level). Third, the lead sheet is situated close to the noise source so that there is a possibility of amplifying the sound due to the tight fitting enclosure at (low) frequencies where wavelengths are greater than the structural dimensions. Under such circumstances, it is extremely difficult to distinguish the noise generated by a particular component from that produced by other components. Finally, extreme caution has to be exercised during the wrapping procedure to prevent the lead from interfering physically with the vibration of the noise source. It is assumed generally that the sound field generated by the covered components does not interfere with the sound generated by the other components which, in turn, implies that these fields are uncorrelated.

Directional microphones have been used as an alternative to lead wrapping for identifying individual noise sources [3]. Although they provide good front to back discrimination, their major lobe is generally too broad at intermediate frequencies around 500 Hz. Hence, purpose built microphone arrays such as an "acoustic telescope" or "acoustic mirror" are employed to provide suitable directivity characteristics [3]. An acoustic mirror is a simple method of creating a reflecting acoustic telescope. The major limitation is the size of the mirror; it should be 50% to 75% of the measurement distance for good resolution or typically 8m. for the location of sound sources of an aero engine [3]. In an acoustic telescope a smaller array of microphones can provide an exceptionally directional detector. The entire array may be swung in any direction for good source discrimination. The disadvantage of this technique is that directional microphones are prohibitively expensive. Furthermore, many instrumentation channels are required and the array's optimum dimensions are a function of frequency so that they have to be varied as the analysis proceeds.

The first attempt to directly measure acoustic intensity under laboratory conditions was made by Olson [8] in 1932. In 1941, Clapp and Firestone [9] developed an intensity meter by using a ribbon velocity microphone. The ribbon microphone consisted of a strip of crinkled aluminum foil, 25 μm thick, which was held in terminal clamps between two permanent magnets. Any movement of the conducting strip caused by an impinging sound wave produced a measurable electric potential difference between the terminals proportional to the wave's velocity. However, such a microphone ceases to respond to a sound wave travelling parallel to the plane of the ribbon at frequencies above 2 kHz. [10,11] so that the device then behaves as a pressure microphone

[9,10]. Furthermore, ribbon microphones may have voltages induced in them by stray magnetic fields because of their electomagnetic nature. In addition, they are heavy but can be damaged by moderate winds. These limitations restrict the use of ribbon microphones except under strict laboratory conditions [11].

The measurement of particle velocity is also possible by using Rayleigh's disc [3]. The disc is usually about 20 μm thick and it is suspended vertically by a fine glass wire. The normal to this disc makes a chosen angle, θ, to the direction of the sound stream which is proportional to the speed of the stream. This apparatus is unsuitable for noise source delineation due to the important assumptions inherent to the theory. First, there should be no surface close to the disc. Second, the disc's diameter, d, should be small in comparison to the wavelength of sound i.e. $d/\lambda < 0.31$ [11]. This requirement places a physical limitation on the measurement of high frequency sound (e.g. for a disc diameter of 1.6 cm. the upper frequency limit is about 1800 Hz.). Furthermore, it is assumed that the fluid medium is incompressible and that the viscous forces and discontinuities of flow at the edge of the disc are negligible. As with other earlier devices, including Baker's directional hot wire anemometer or velocity transducer [12], the instrument is fragile, extremely sensitive to drafts and impractical for routine measurements outside of a laboratory.

With the advent of relatively inexpensive dual channel spectrum analyzers, direct intensity measurements may be made by using the cross power spectrum of two closely spaced microphone signals [13,14,15].

Subsequent integration of the component of intensity normal to a hypothetical control surface surrounding the source provides the total sound power. The significant advantage of this technique is that the acoustical power radiated by a source may be estimated both close and far from the sound source even in the presence of interfering sound fields [13]. Furthermore, the cross spectral technique provides a vectorial or visual definition of the acoustic intensity by indicating the energy flow patterns in the vicinity of sound sources, reflecting surfaces and absorbers. This additional information provides a valuable diagnostic aid in situations where knowledge of the propagation and dispersion of the sound is required. Although the requirements for the microphones and amplifiers are stringent vis-a-vis amplitude, phase matching and wide frequency response, it is possible to measure the acoustic energy over a continuous range of frequencies without a cumbersome and expensive anechoic chamber [2,13,15]. Consequently, the technique will be used to determine the total sound power of a development computer, with and without contaminating acoustic fields, and to identify its principal acoustical radiation regions.

CHAPTER II
ACOUSTIC INTENSITY TECHNIQUE

The theoretical basis of the acoustic intensity technique will be explained here. In addition, the assumptions inherent to the theory, major difficulties connected with these assumptions and techniques commonly used to overcome them will be discussed. Before embarking on major airborne testing of the development computer, preliminary experiments were performed by using a standing wave tube and an ILG reference sound source. The objective of these tests was twofold. First, it was necessary to verify and check microcomputer software written to manipulate data from a real time analyser. For this purpose, the standard standing wave tube [13] was adequate because it provided a means of generating plane waves with little or no interference from external sound sources. The plane waves were generated at one end of the tube by using a speaker driven by a random noise generator. An anechoic terminator was installed at the other end to minimise the reflection of sound waves from this boundary. Second, most machinery is associated with airflow so that it was necessary to determine the performance of the acoustic intensity technique under non-ideal conditions (e.g. in a semi-reverberant sound field with significant airflow). The results of the two sets of experiments will be reported here. The final part of the chapter deals with tests undertaken on the development computer to assess the viability of the acoustic intensity technique as a quality control method or diagnostic tool.

2.1 THEORY

The normal intensity vector, $\vec{I}_n$, is the net rate of flow of acoustic energy per unit area normal to a given surface [13,14]. Consequently, the total acoustic power, W, passing through a surface with area, S, is,

$$W = \int_S I_n dS, \tag{2.1}$$

where I_n is the magnitude of the normal intensity vector $\vec{I}_n$. The magnitude of intensity, I_n, may be defined mathematically as [2,13,14,15],

$$I_n = \lim_{T\to\infty} 1/T \int_{-T/2}^{T/2} p\ u_r\ dt \tag{2.2}$$

where p is the root mean square sound pressure, T is ostensibly the sampling period and $\vec{u}_r$ is the particle velocity with magnitude u_r at a point within a region of an isotropic and Newtonian medium with negligible mean flow, viscosity and field forces [13,14,15]. As noted in Chapter I, earliest attempts to directly measure the medium's particle velocity were largely unsuccessful. However, by using a finite difference approximation, the particle velocity, $\vec{u}_r$, may be determined by the sound pressures sensed by two closely spaced microphones. These microphones will be designated, for convenience, by subscripts 1 and 2. Two typical configurations are shown in Figure 2.1. In either case the magnitude of the velocity, u_r, at any instant, t, may be expressed as [13,14,15, 16,17,18,19,20]

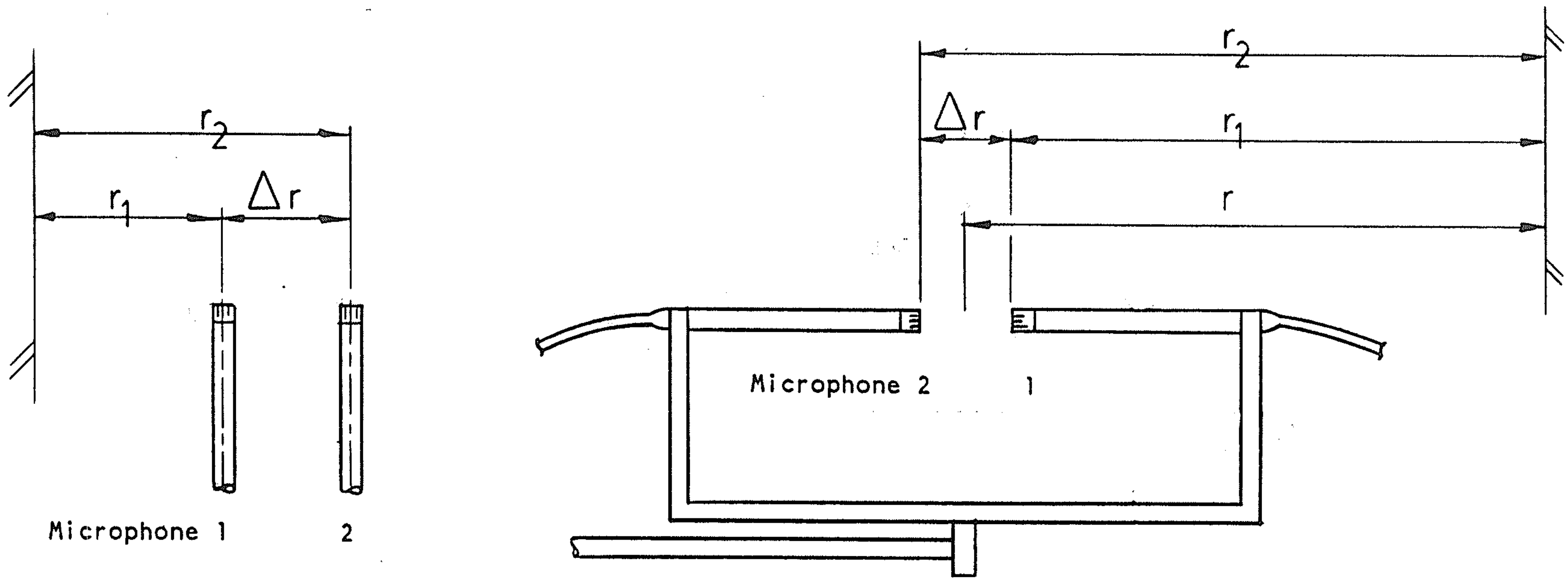

Figure 2.1 : Microphone orientation of a) side-by-side and b) end-to-end configurations.

$$u_r = (1/\Delta r\rho) \int_0^t (p_2 - p_1)dt \quad , \qquad \{2.3\}$$

and,

$$p = (p_1 + p_2)/2 \quad \text{with} \quad p(t) = 0 \text{ for } t < 0. \qquad \{2.4\}$$

The p_1 and p_2 are the pressures sensed by microphone 1 and 2, respectively, $\vec{\Delta r}$ is the directional vector between the microphones' centres, and ρ is the density of the medium. By substituting equation {2.3} and {2.4} into equation {2.2} and employing the definition of time average [15], the intensity may be rewritten as shown in Appendix 2A in the form [21]+

$$I_n = E \{Im (F_{p1} F^*_{p2})\} /\rho\Delta r\omega \qquad \{2.5\}$$

Here, E represents the expected value, Im is the imaginary part, F_p denotes the Fourier Transform of p and ω is the variable circular frequency. Then the magnitude of the intensity vector may be redefined as, [2,3,13,14,15,16,21]

$$I_n = Im (G_{12})/(\rho\Delta r\omega) \qquad \{2.6\}$$

by transforming equation {2.2} into the frequency domain. Here, $Im(G_{12})$ is the imaginary part of the cross power spectrum between the signals measured simultaneously by microphone 1 and microphone 2.

The right side of equation {2.6} may be computed by using a commercially available Fast Fourier Transform (FFT) analyser in conjunction with a microcomputer. A block diagram of the measurement

---

+

* denotes the complex conjugate

apparatus is shown in Figure 2.2. In order to improve the signal-to-noise ratio, an averaged value for the cross power spectrum is used. For the experiments described in subsequent sections, 64 averages were used to determine the cross spectrum G_{12} +. There are, however, two major limitations of such a procedure [13,14,17]. First, the spacing of the microphones, Δr, is extremely critical. Experience [2,13,14,15,17] suggests that the error in the intensity level is less than $\pm$ 1.5 dB provided the spatial gradients of the acoustical pressure and velocity are small in comparison to the predominant wavelength of sound being measured (i.e. $k\Delta r<1$ where k is the wave number). The following paragraphs explain in detail the procedures used for minimising the procedural and equipment related measurement errors associated with the acoustic intensity technique.

The acoustic intensity, I_{ex}, produced by a simple sound source like a monopole is [18],

$$I_{ex} = k^2 \rho c\ S^2/32\ \pi^2 r^2 \tag{2.7}$$

where S is the monople's strength and r is its distance from the measurement location. Assuming perfect instrumentation, the measured intensity using the finite difference approximation, I_{me}, has been evaluated as [17,18],

$$I_{me} = (k\rho c\ S^2/32\pi^2\ \Delta r\ r_1 r_2)\sin(k\Delta r). \tag{2.8}$$

+ The pressure signals are assumed to be ergodic and stationary [16]. Furthermore, the difference between successive averages was always within the limit of measurement error.

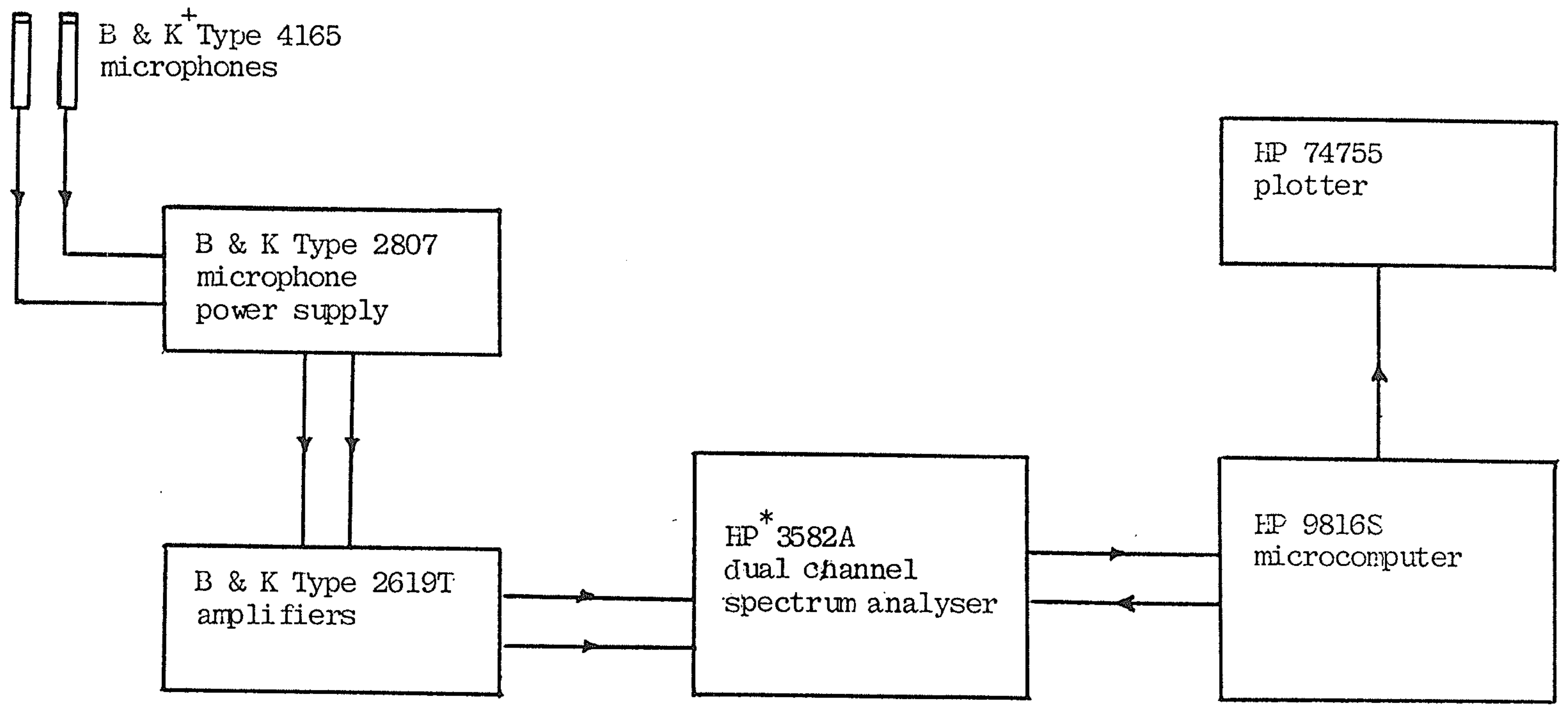

+ Bruel & Kjaer
* Hewlett- Packard

Figure 2.2 : Block diagram of acoustic intensity apparatus.

The error, L_e, between the measured and exact sound intensities may be defined as [17,18],

$$L_e = 10 \text{ Log } (I_{me}/I_{ex}) \qquad \{2.9\}$$

or, by using equation {2.7}and {2.8},

$$L_e = 10 \text{ Log } (\sin(k\Delta r) * r^2/(k\Delta r \; r_1 r_2)). \qquad \{2.10\}$$

Here, r is the mean distance of the sound source from a point midway between the microphones and r_1 and r_2 are the distances of microphones 1 and 2 from the source, respectively.

Equation {2.10} indicates that the approximation error, L_e, is a function of $k\Delta r$ as well as $\frac{\Delta r}{r}$. By approximating

$$r \simeq r_1 \cong r_2 \quad , \qquad \{2.11\}$$

equation {2.10} may be modified to ,

$$L_e = 10 \log_{10} \left[\frac{\sin(k\Delta r)}{k\Delta r}\right] \qquad \{2.12\}$$

which is plotted in Figure 2.3 . It may be seen that the intensity vector is grossly underestimated at all frequencies when $\Delta r/r << 1$. The above analysis assumes a simple monopole sound source which is normally representative of far but not near field measurements [17,18]. Parameters like microphone spacing for near field situations are usually assessed on the basis of a non-dimensional quadrupole analysis because of the greater and more representative modal complexity of the radiating surface. Then the following limits

$$0.1 < k\Delta r < 1.3 \;, 0 < \Delta r/r < 0.5 \qquad \{2.13\}$$

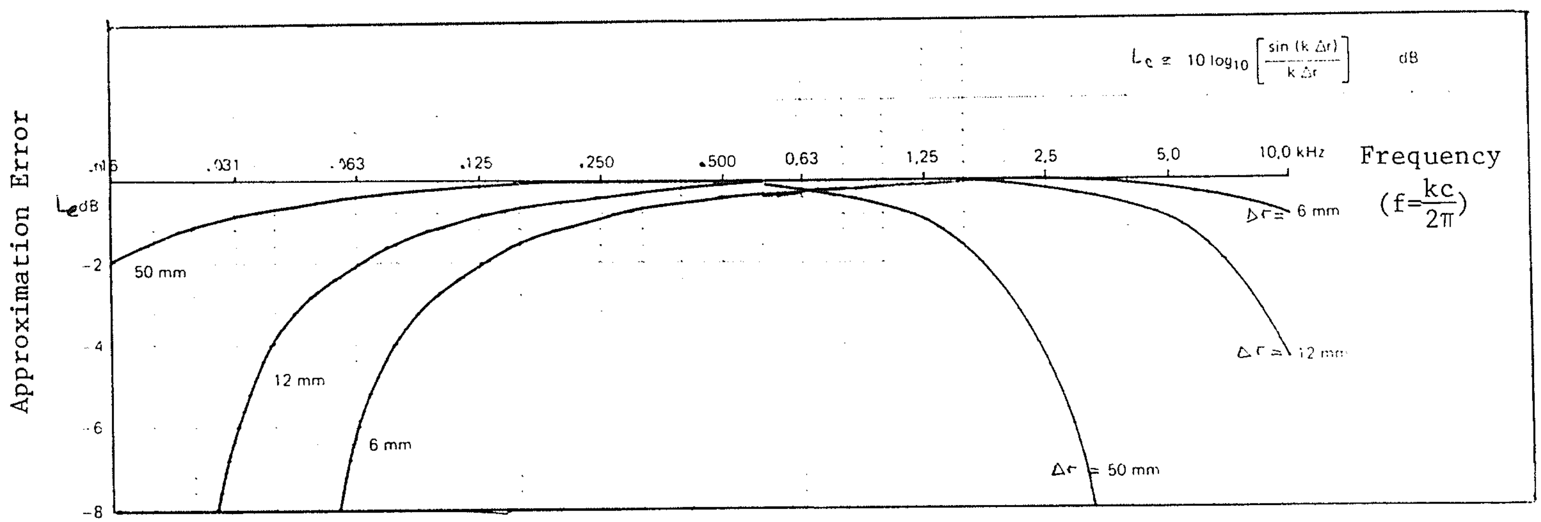

Figure 2.3 : Approximation error, Le, for different frequencies and microphone spacings.

have been proposed for errors typically within $\pm$ 1.5dB [19,20,23]. In addition to the error induced by the finite difference approximation of relation {2.3}, the imaginary part of the cross power spectrum, Im (G_{12}) in equation {2.6}, is extremely sensitive to phase mismatch between the two microphone channels [2,13,14,21]. This problem appears to be severe at frequencies less than about 250 Hz. where the signal to noise ratio may also be poor [21]. The signal to noise may be improved by ensemble averaging. However, expensive phase-matched instrumentation is necessary to directly overcome the phase related problem. Researchers like Chung [20,21], Krishnappa [13] and others [2,14] have described inexpensive but indirect techniques for avoiding errors due to phase mismatch. An overview will be given in the following paragraphs.

There are two techniques commonly used to overcome problems from mismatched phase between microphone channels. The first technique is commonly called the Switching Technique. In this procedure, the phase-corrected cross spectrum in equation {2.6} is approximated by the geometric mean of two cross spectra, G_{12} and G_{12s}. Here, G_{12} is the cross spectrum determined by the original microphone configuration and G_{12s} is the cross spectrum after interchanging or "switching" the two microphones and associated channels [14,20,21]. Consequently, equation {2.6} may be approximated as,

$$I_n = \mathrm{Im}\,(G_{12}\, G_{12s})^{1/2}/(\rho \Delta r \omega) \quad . \qquad \{2.14\}$$

The second method is known as the Transfer Function Method. In this procedure, the calibration of each microphone channel is accomplished by individually calibrating the microphone channels with a standard calibration source like a pistonphone. Two closely positioned microphones are then exposed simultaneously to the same signal by flush mounting them in a rigid circular plate attached to the end of a tube. Sound waves are generated at the other end of the tube by using a loudspeaker driven by a random noise generator. It is assumed during the calibration procedure that the microphones are subjected to one dimensional plane waves. However, this assumption is invalid at frequencies greater than 0.293 c/R, where c is the local speed of sound and R is the radius of the tube [1]. Thus, for a typical tube with a radius of about 50 cm., the upper frequency limit is 200 Hz. for plane wave propagation. At frequencies above this value, the transverse acoustical air modes in the tube are no longer negligible because they may be reflected back to the source with a significant amplitude buildup [1]. Another source of error is the incorrect pressure gradient on either side of the microphone diaphragm. Ideally, the air equalization hole located at the rear of the diaphragm should be exposed to a pressure gradient similar to that sensed by the two microphones. However, this condition cannot be satisfied due to the partial enclosure of the microphone in the duct. The improper exposure of the air equalization hole can lead to changes in the R.C. time constant of the internal volume behind the microphone's diaphragm and, hence, the response of the microphone. Providing these practical limitations are overcome, the calibrated cross spectrum $G_{12\,cal}$ may be written as [2,13,14],

$$G_{12cal} = G_{12}/(H_{12}\,|H_1|^2) \qquad \{2.15\}$$

where $H_{12}|H_1|^2$ is the calibration cross power spectrum between the two microphone channels and G_{12} is the measured cross power spectrum. [2,13,14]

The chief advantage of the Transfer Function Method over the Switching Technique is that G_{12s} need not be evaluated. Hence, the measurement of the cross spectrum G_{12} need be done only once which results in a significant time saving. On the other hand, it is extremely difficult to generate an accurate H_{12} for a broad band analysis. As mentioned earlier, the frequency limit of the plane wave assumption does not permit a sufficiently wide frequency band for calibration over the entire audio spectrum of 20 Hz. to 20 kHz. Thus, it may be necessary to repeat the calibration procedure by using tubes of different diameters to make corrections over the desired frequency range [2,13]. Another disadvantage is that the cumbersome calibration apparatus is difficult to transport.

In view of the conflicting arguments both for and against the two procedures, a modified switching procedure may be employed which overcomes the disadvantage of both techniques. The two microphone channels are subjected simultaneously to a broadband signal and the cross power spectrum is determined. The microphone channels are then switched and,while maintaining the broadband signal, the cross power spectrum in this switched configuration is obtained. Thus, the relative phase and gain factors of the two microphone channels may be determined from the square root of the ratios of the transfer functions between the two microphone channels (i.e. K_{12} in equation {2.17} on page 20). Thus, problems associated with obtaining a wide frequency response in a duct are overcome because the two microphone channels are presumably exposed to the same calibration signal in both configurations. This procedure also results in a halving of measurement time because calibration need be undertaken only once [2,13]. Mathematically, the procedure may be represented by,

$$G_{12cal} = G_{12}/(K_{12} \cdot |H_1|^2) \qquad \{2.16\}$$

where,

$$K_{12} = (H_{12}/H_{12s})^{1/2} \qquad \{2.17\}$$

and H_{12} and H_{12s} are the transfer functions measured in the original and switched configurations, respectively.

This section has outlined the practical feasibility of the acoustic intensity technique. The need for expensive purpose-built equipment is eliminated by using one of the corrective procedures described. The following sections detail tests using the acoustic intensity technique. The Switching Technique was employed invariably because it is particularly suitable for overcoming phase mismatch errors below about 125 Hz. [20,21,22,23]

2.2 RESULTS

The feasibility of the acoustical intensity technique was tested in a practical situation by using the development computer. The overall objective of these tests was to measure the total sound power level of the computer in the 500 Hz., 1000 Hz., and 2000 Hz. octave band centre frequencies. This procedure was dictated by a Sperry test procedure [24] based on the ANSI S1.31-1980 and ANSI S1.32-1980 standards. In addition to sound power measurements, the principal sound radiation regions of the computer were identified to determine a systematic basis for design changes in existing and future models. Preliminary experiments were carried out under non-ideal, semi-reverberant conditions by using a standing wave tube and an ILG reference sound source. These experiments enabled the microcomputer based software associated with the acoustic intensity technique to be checked. The reference sound source consisted of a motor to which a squirrel cage fan was attached. It produced calibrated intensity levels of 81 dB in the octave bands centered between 64 Hz. and 4 kHz. In addition, the reference sound source introduced a significant air flow (speed about 15 mph.) greater than that produced by the exhaust fan located at the rear of the development computer. The following sections describe in detail the preliminary experiments, the measurement of the sound power levels, the identification of the principal radiation regions as well as an explanation of the results.

Sound pressure levels were measured by using two carefully calibrated Bruel & Kjaer, Type 4165, 1.25 cm. diameter microphones connected to Bruel & Kjaer Type 2169T pre-amplifiers. The pre-amplifiers were powered by a Type 2807 power supply and resulting signals were processed on a Hewlett-Packard 3582A dual channel spectrum analyser and 9816S microcomputer. Microphones were used in both the end-to-end and side-by-side configurations to determine the advantages and disadvantages of both configurations.

Microphones were used in the end-to-end configuration as shown in Figure 2.1a to identify noise sources. A 50 mm. spacer between the microphones provided an adequate working frequency range of 32 to 1250 Hz. (It was suspected that the computer's airflow-induced sound occurred essentially below 500 Hz. Consequently, this range easily encompassed the lower and upper frequencies of interest.) The microphones were used in a side-by-side configuration, on the other hand, with a spacing of 2.5 cm. to determine the total sound power. Then the working frequency range was 220 to 2800 Hz. according to the limits given by equation {2.13}. This range allowed measurement of the computer's sound power at the 500 Hz., 1000 Hz., and 2000 Hz. octave band centre frequencies as specified by the test procedure [24]. Furthermore, the latter unlike the end-to-end configuration permitted the use of wind screens to protect the microphones from the airflow generated by the reference sound source or development computer. The distance from the centre of the probe to either of these sources was 18 cm. so that the requirements set by equation {2.13} were satisfied.

The acoustic intensity probe was inserted through an airtight slot in the standing wave tube. The tube's diameter of 10 cm. dictated the upper frequency limit of 2kHz. for plane wave generation. An adjustable sleeve sealed with plasticine ensured airtightness. A 10 cm. thick anechoic termination was used to reduce the effect of reflected sound waves. The spacing between the microphones was adjusted to encompass the desired frequency range. Great care was taken during the installation of the probe through the slot to ensure that the microphones measuring the normal intensity were normal to the longitudinal axis of the tube. This was done visually by using a spirit level. Furthermore, the microphones were flush mounted with the inner surface of the tube so that they did not disturb the sound waves. An octave band analysis was performed on the acoustic intensity determined from the two microphones. These values were compared with those obtained by employing the traditional method of measuring the sound pressure levels and using equation {1.1} to determine the acoustic intensity. The results are shown in Figure 2.4. Results at frequencies above 250 Hz. agree within 2 dB. However, there is a discrepancy of up to 16 dB below about 125 Hz. This difference occurred as a result of reflections from the tube's supposedly anechoic termination. The termination was effective at frequencies only above 800 Hz. [2,10]. Furthermore, the 1.2 m. length of the tube did not permit the probe to be positioned sufficiently far from the terminator to minimise "end effects". Thus, a 4m. tube of internal diameter 7.5 cm. was used in conjunction with a 0.5 m. anechoic termination to extend the lower frequency limit to about 180 Hz. with an

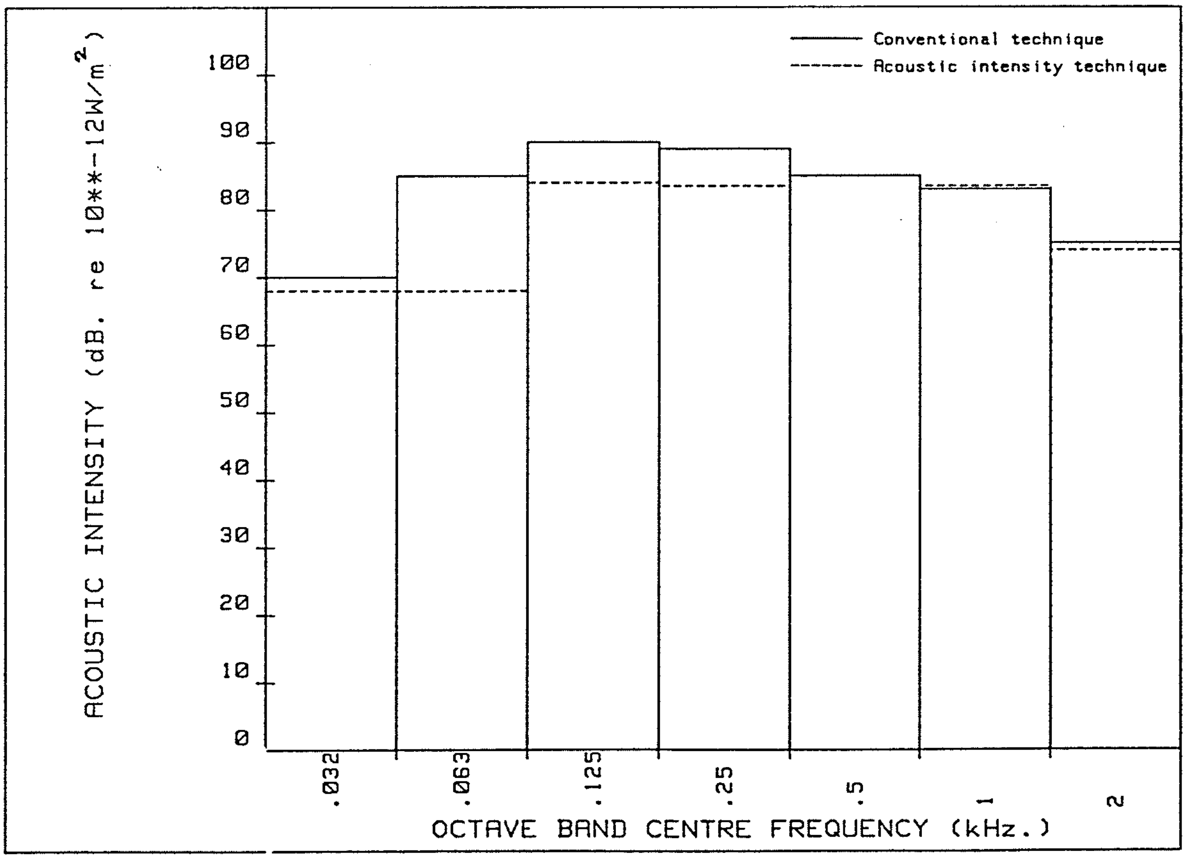

Figure 2.4 : Comparison of the acoustic intensities measured in a pipe of length 1.2 m.

upper limit of 2.6k Hz. These later results are shown in Figure 2.5. They correlate better even at the lower frequencies.

The results from the 4m. long tube confirmed the findings of other researchers that the measurement of airborne sound intensity by using two closely spaced microphones is relatively straightforward [2,13,14,20] . Problems arise with the conventional method of sound power determination when 1) there is a substantial movement of the medium [22]; 2) the predominant frequency of the major sound source is lower than about 100 Hz. [13] and 3) intensity measurements are made in areas of high environmental noise. Noisy conditions are typical of most industrial environments where the acoustical intensity technique is of greatest value. Thus, an ILG reference sound source was employed to conveniently simulate such conditions (i.e., to provide high levels of background noise and a significant airflow). However, the acoustic intensity given by equation {2.6} is valid only if there is no mass movement of the medium (i.e. no air flow) [22]. Ducting was considered to divert the air flow away from the microphones. However, this procedure was found impractical because it required the fan to be encompassed within the duct so that its sound would be attenuated by a not absolutely determinable amount. Hence, a thin, light polythene diaphragm was used to protect the microphones from the flow but the diaphragm added extraneous noise due to vibrations of its surface. Finally, a standard polyurethane wind screen was fixed over each microphone. The sound attenuation due to these wind screens is less than 2 dB up to

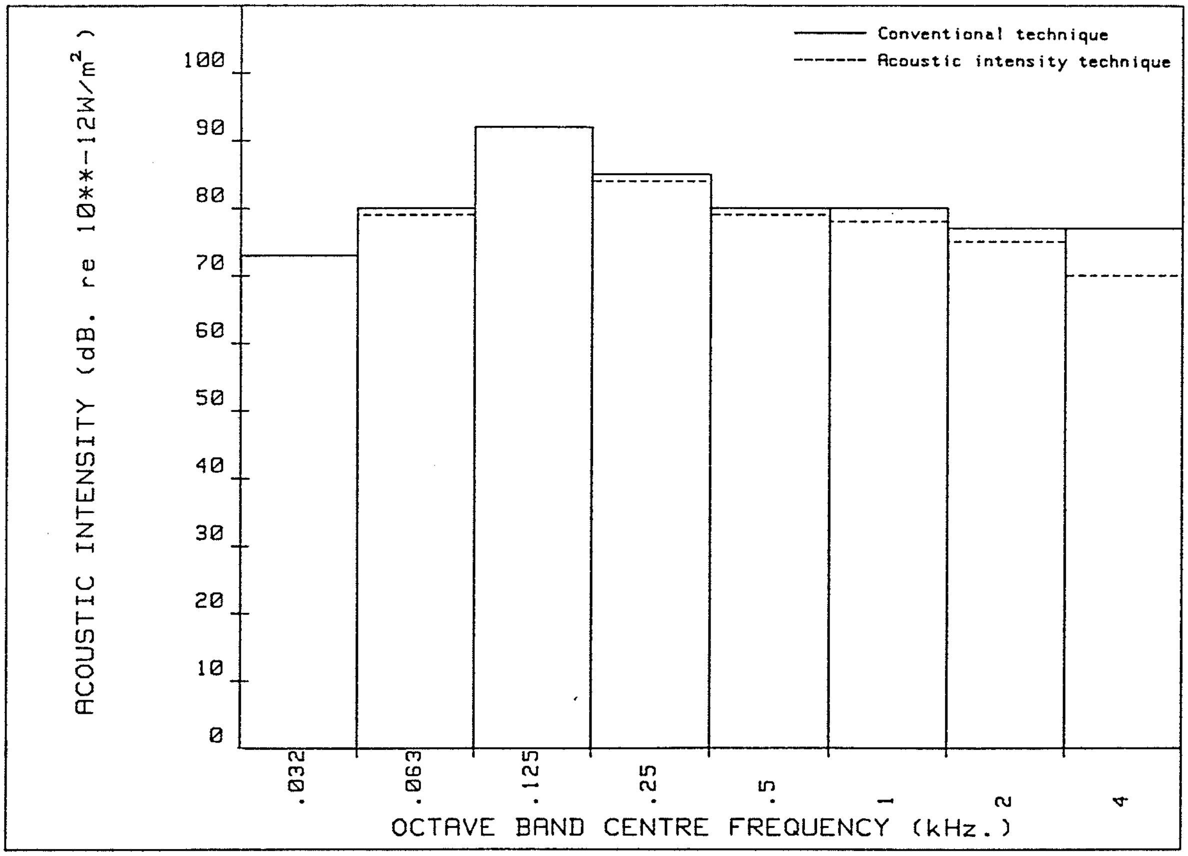

Figure 2.5 : Comparison of the acoustic intensities measured in a pipe of length 4.0 m.

8kHz for wind speeds less than about 0.3M, where M is the Mach number [2 6]. This range, of course, encompasses the speed of interest.

A one third octave band analysis was performed on the acoustical intensity determined by the two microphone method and compared with the manufacturer's specifications of the reference sound source. These results are presented in Figure 2.6. There is excellent agreement at all frequencies even as low as 63 Hz. These tests, therefore, showed the wind screens to be extremely effective for air flows of concern.

Having tested the software, an investigation was initiated 1) to determine the sound power of the development unit, with and without the presence of contaminating acoustic fields; and 2) to identify and rank its principal radiation regions. The findings of a feasibility study regarding the use of acoustic intensity to determine the sound power and, in addition, to identify sources of noise will be presented next.

2.2.1 SOUND POWER DETERMINATION

The objective of these experiments was to conventionally determine the sound power of the development computer [24] and to compare the data with that from the acoustic intensity technique. The total sound power of the computer was evaluated in accordance with the procedure detailed in specified standards [24]. However, tests were made in a large room under semi-reverberant conditions due to the unavailability of an anechoic chamber. The test fixture supporting the computer was basically an H frame with four vertical columns

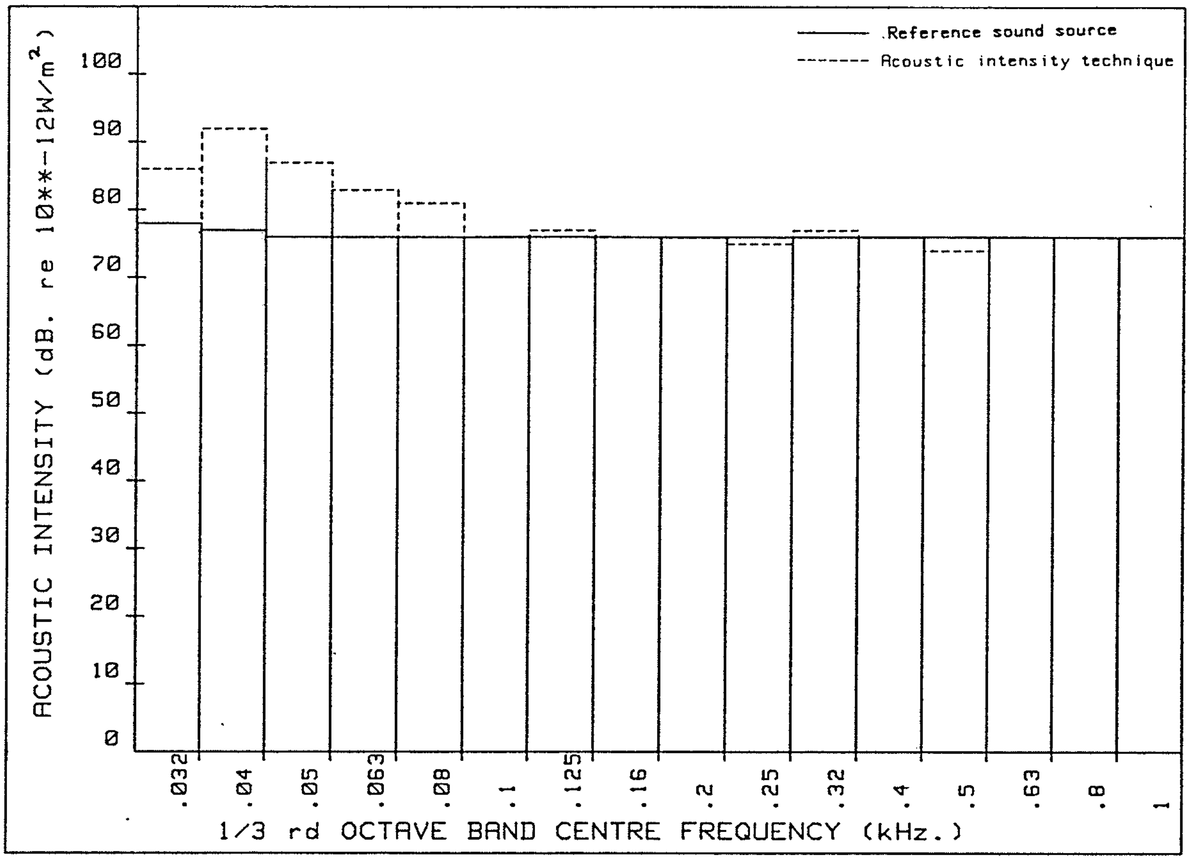

Figure 2.6 : Comparison of acoustic intensity measured by using an ILG reference sound source and the acoustic intensity technique.

and four horizontal supports from which the computer could be suspended 90 cm. above a hard reflecting plane. The total sound power of the computer was measured by using the acoustic intensity technique. A closed imaginary measurement surface parallel to the sides of the cabinet was chosen in the nearfield of the computer, 18 cm. from the cabinet. The normal component of the sound intensity was measured at a total of twenty equally distributed points on the imaginary surface. The total sound power was then determined conventionally by summing the sound power radiated over each section of the imaginary surface. The sound power of the computer was evaluated next in the presence of interfering acoustic sources. This evaluation entailed the positioning of an ILG reference sound source 1.0 m behind the unit with a reflecting screen 1.2 m. to the left of the computer. Such conditions reasonably simulate a noisy, reflective environment with a fairly substantial air flow. The corresponding sound power levels invariably determined by the acoustic intensity technique are presented in Table 2.1.

The total sound power measured either in the presence or absence of the reference sound source are in good agreement in Table 2.1. The observed differences of up to 3 dB are well within the limits of experimental error determined in Appendix 2 under semi-reverberant [26] conditions. A formal measurement error analysis is quantified in Appendix 2 so that only the two major errors will be mentioned briefly here. One primary error with the acoustic intensity technique is the $\pm$ 1.5 dB deviation associated with the finite difference formulation

Case	Sound power at octave band centre frequency		
	500 Hz.	1000 Hz.	2000 Hz.
1	70.6±4.0+	60.2±3.4	58.1±3.3
2	69.6±1.8	57.4±1.8	55.0±1.8
3	68.2±1.8	63.8±1.8	63.2±1.8
Reference Sound Source	72.0±1.5	72.0±1.5	72.0±1.5

(+dB. re. 10.0 E-12 W.)

Table 2.1 : Computer's total sound power level determined 1) conventionally 2) by using the acoustic intensity method, and 3) as in 2) but in the presence of the reference sound source. Sound power level of ILG reference sound source given for comparison.

of equation {2.6}. Another is the $\pm$ 1.0 dB error inherent to the averaging mode of the spectrum analyser when the invariably employed 64 averages is used [25]. Despite these measurement errors, the measured values of the sound power by using the acoustic intensity technique agree well with those measured conventionally. The significant advantage of the acoustic intensity technique is the speed with which the sound power of the development computer was determined (typically 20 minutes as compared to about 3 hours when measured conventionally). There are, however, serious discrepancies when measurements were performed in the presence of the reference sound source. In case (3), for example, the measured sound power agrees with that determined conventionally in the 500 Hz. octave band. However, differences of up to 8 dB can be observed in the octave bands centred at 1000 Hz. and 2000 Hz. These discrepancies may be explained by examining the characteristics of the sound sources. Intensity levels of 81 dB were produced independently by the reference sound source in each of the octave bands centred between 64 Hz. and 4kHz. Such levels exceed by more than 15 dB those values generated by the computer alone. It was difficult, therefore, to distinguish the noise produced only by the computer. This observation is corroborated by the nearly equal sound powers measured at the 1000 and 2000 Hz. octave band centre frequencies. Consequently, these results confirm the findings of other researchers [28,29,30], that the acoustic intensity technique cannot be used if the noise levels of the background exceed those of the source alone by 10 dB or more. In addition to the quantitative measurement errors associated with the acoustic intensity technique mentioned in Appendix 2, some qualitative errors warrant discussion. First, the test procedure [24] is based on the premise that the measurement of the sound pressure levels is in the free field e.g. in an anechoic chamber. However, an anechoic chamber was unavailable so that measurements had to be undertaken in a large (8.3m X 5.6mX 3.6m) room. The resulting sound field was essentially reverberant so that the normally employed standard for free field measurements [24] was replaced by the more appropriate ANSI S1.21-1976. A comparison of the sound of the computer evaluated in free field and semi-reverberant field conditions produced a difference of up to 3 dB. This difference reflects primarily the effect of the environment on the measured sound power levels. This observation highlights the chief advantage of the acoustic intensity technique i.e. it is unaffected by environmental conditions. Furthermore, the directivity characteristics of the sound source are extremely important in determining the number of measurement locations. The overall sound pressure levels in Figure 2.7 suggest that the predominant radiation regions lie towards the rear of the computer. Hence, accuracy could be improved if extra measurement locations were included around the sides and rear of the computer where changes in sound pressure levels are greatest. However, it would be obtained at the expense of a significant increase in measurement time. Thus, a total of twenty measurement points represented a reasonable compromise between these requirements.

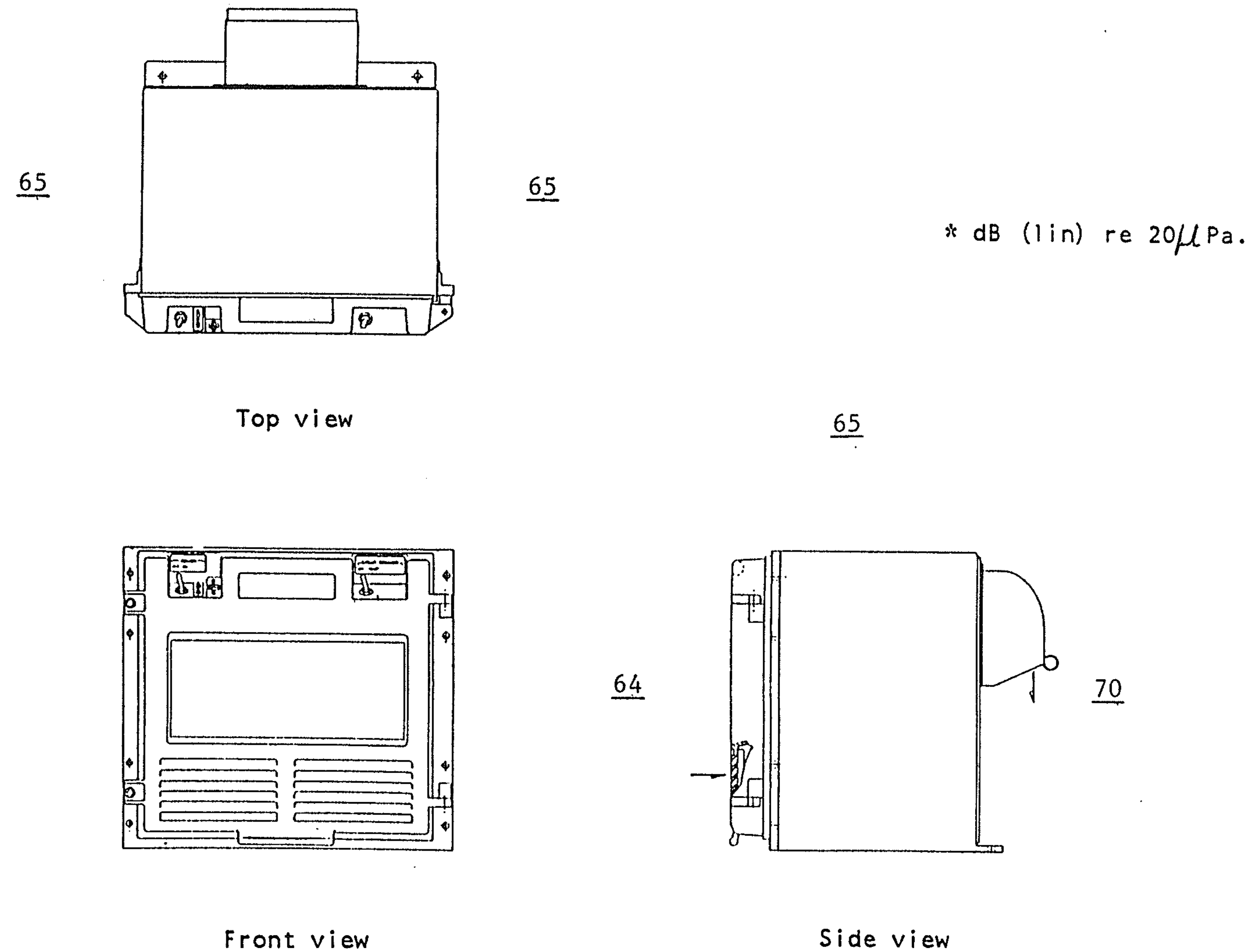

Figure 2.7 : Overall sound pressure levels at the midpoint but 0.91 m. (3 ft) from each nearest computer panel.

The previously described experiments illustrate the advantages of the acoustic intensity technique. First, the sound power of a sound source may be determined with a lower measurement error than with the conventional procedure. Second, the acoustic intensity approach may be used advantageously under difficult measurement conditions without special acoustical environments.

2.2.2 LOCATION OF SOUND SOURCES

This section deals with the identification of the principal radiation regions of the development computer by using the acoustic intensity technique. However, overall sound pressure levels were first measured in the near field of the computer at a distance of 3 feet from each panel to obtain a "feel" for the overall sound radiation pattern. These pressure levels are shown in Figure 2.7. It can be seen that the predominant radiation regions are towards the rear of the computer. This is the extent of the information that is available by utilising conventional equipment such as a sound level meter. Measurement of sound pressure levels is unlikely to reveal further details without the use of, say, the lead cladding technique [31,32,33]. A near field analysis is more likely to determine the cause-sound effect relationship of various components with the computer. Consequently, the acoustic intensity technique was used to more closely identify the principal radiation regions. A 7 x 8 and a 5 x 5 element grid was marked, respectively, on the left side and rear panel of the computer as illustrated in Figure 2.8. The numbering system employed for the grid is also shown. The printed circuit board (PCB) chassis and power supplies within the computer are located towards the front half of the computer. Consequently the front half of the computer is more complex in its construction compared to the relatively "symmetrical" rear half. Thus, a narrower grid was marked on the left compared with the rear panel. The probe was mounted horizontally on two sturdy tripod stands with the aid of a spirit level. The probe was visually positioned normal to the panel and the acoustic intensity determined at each location. A three dimensional plot of intensity was charted at one-third octave centre frequencies. Typical plots are presented in Figure 2.10 through 2.14. The discussion that follows is based, in part, on comprehensive air flow studies carried out earlier by the computer manufacturer.

Figure 2.10 shows the acoustic intensity emitted to the side of the left panel in the 1/3rd octave band centered at 100 Hz. It is clear from this figure that the predominant noise radiation regions at frequencies around 100 Hz. lie toward the rear of the computer. This is expected because the fan is mounted on the rear panel and operates at 56 Hz. However, there is also significant acoustic energy radiated at location 31, 38 and 45. This phenomenon may be explained in relation to the airflow within the computer. The air enters the computer through a grille at the lower end of the front panel and impacts the metal plate located at the base of the PCB chassis shown in Figure 2.9.

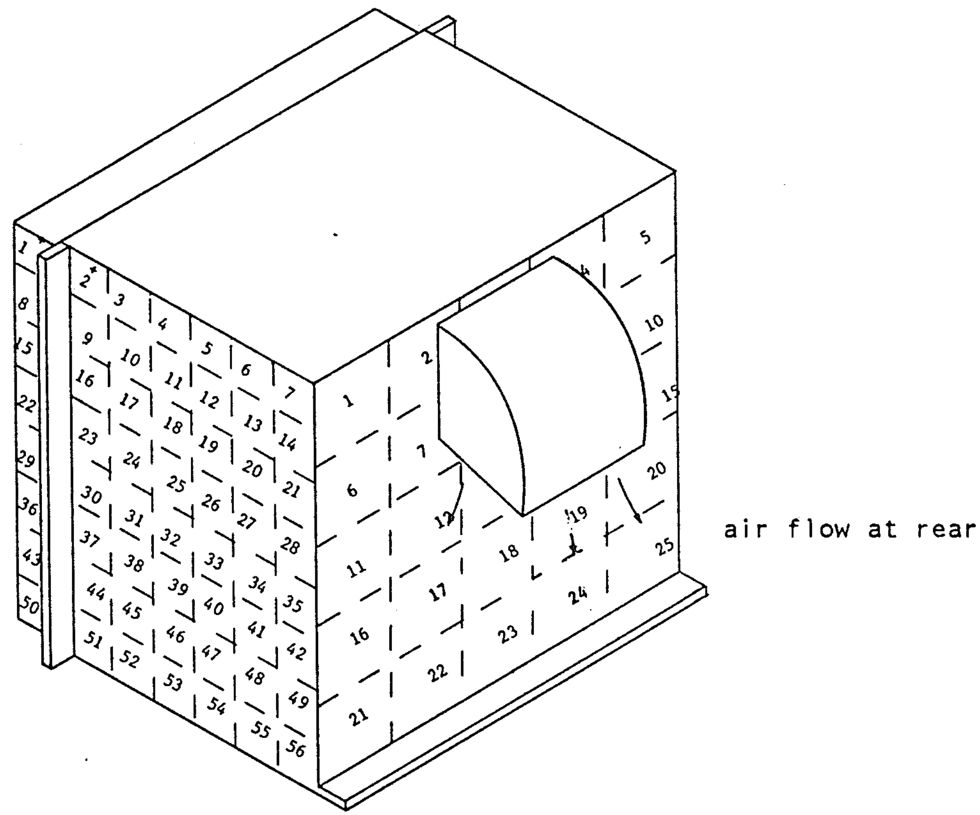

+measurement locations (used also in subsequent figures)

Figure 2.8 : View of computer showing the 56 and 25 measurement locations on the left side and rear panel, respectively.

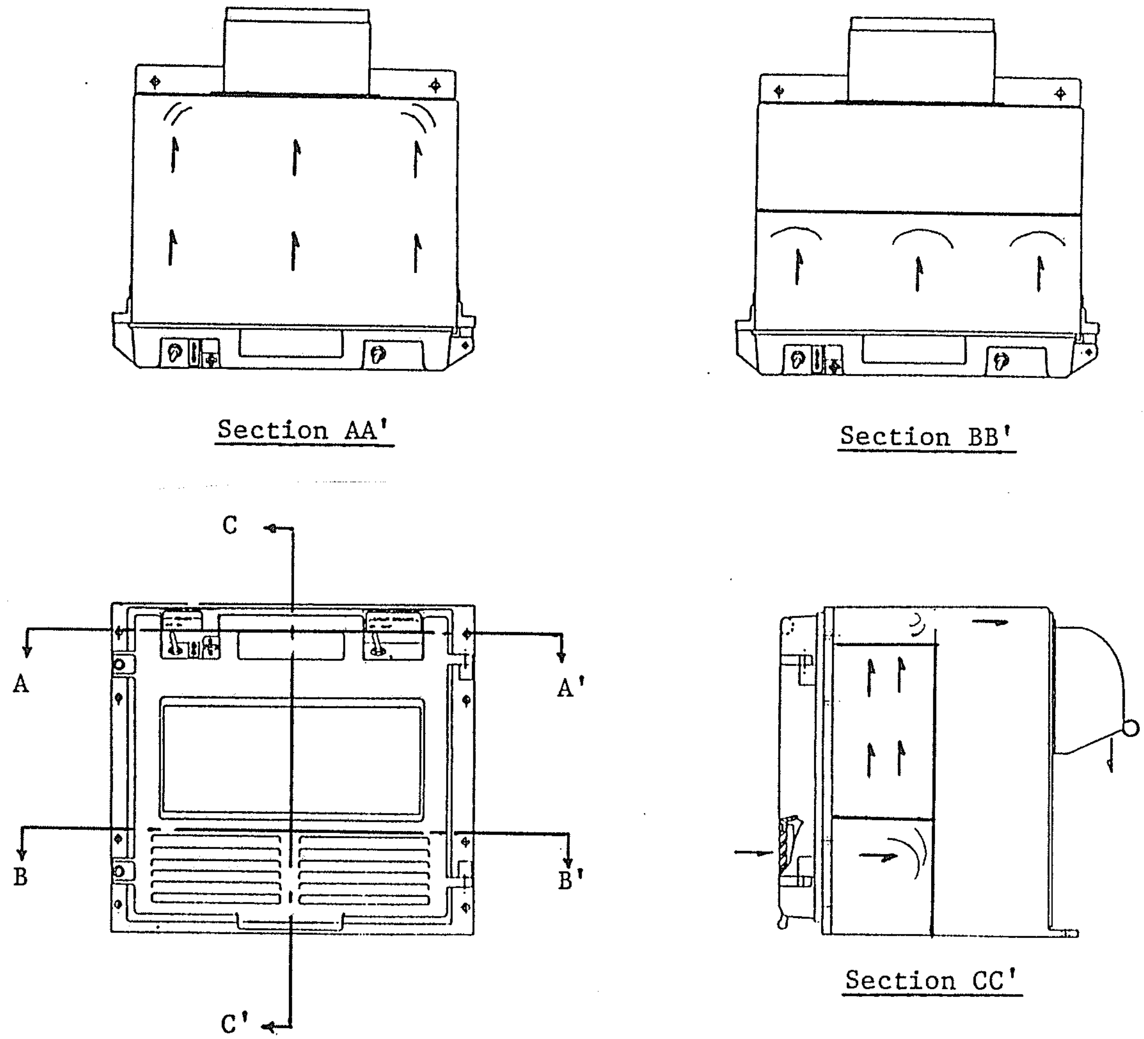

Figure 2.9 : Overall air flow within the computer.

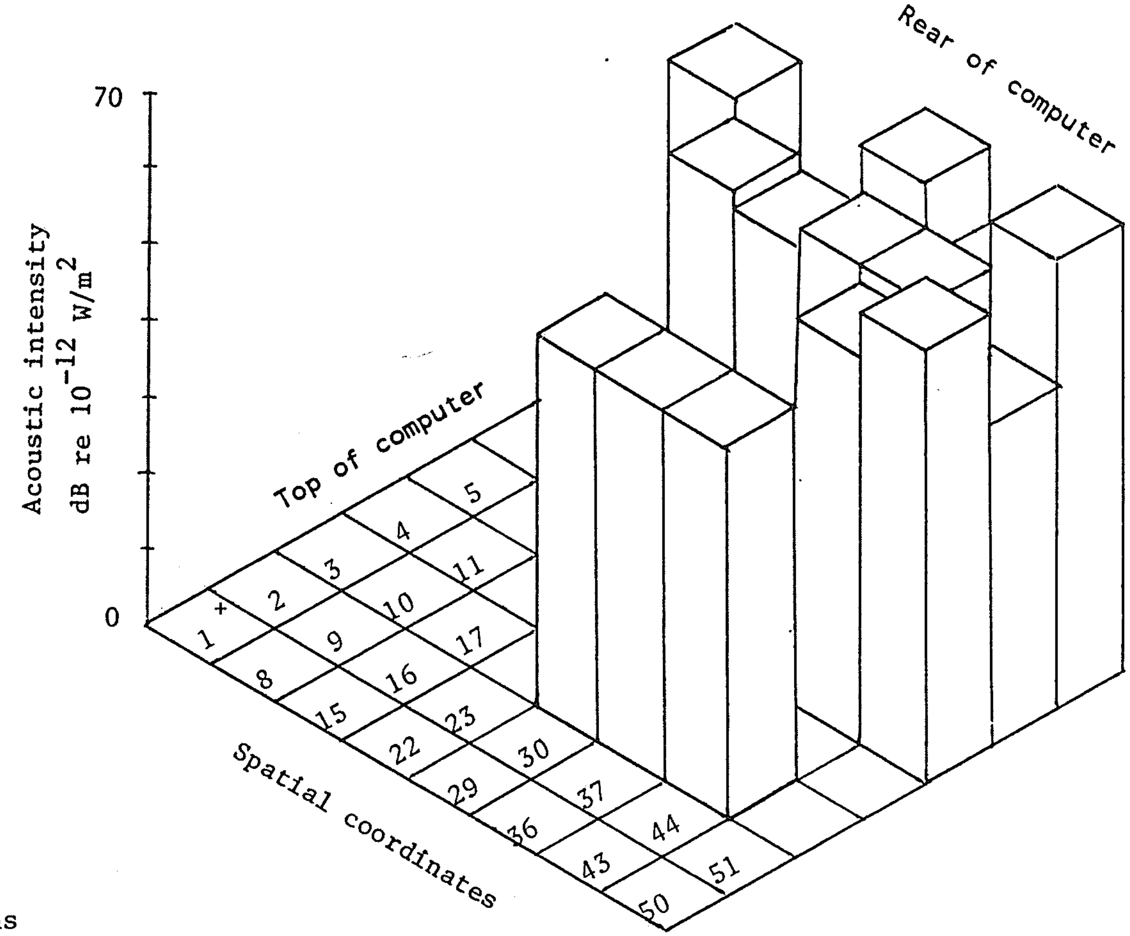

+measurement locations shown in Figure 2.8

Figure 2.10 : One third octave band acoustic intensity levels at left side panel around 100 Hz. centre frequency.

Upon impact, part of the air stream is deflected through 90 degrees to pass through the spacing between the printed circuit boards before turning through another 90 degrees and exiting at the rear. A substantial proportion of the air entering the unit, however, is also deflected towards the left and right side panels. Based upon the primary location of "impact" determined by the manufacturer, it is believed that the airstream striking the side panels behaves as a noise source at location 31, 38 and 45.

Figure 2.11 indicates that the left panel radiates little sound around 125 Hz. except towards the rear. This observation suggests that there is considerable sound "leakage" from the spacing between the cabinet and the rear panel. On the other hand, Figure 2.12 intimates that significant acoustic energy is radiated at all the measurement locations around 500 Hz. It is possible that the air, which is forced through a narrow gap between the cabinet and the PCB chassis, causes the panel to radiate sound essentially uniformly over its surface. Then the minor variation in intensity over the surface of the panel is probably due to locally changing airflow created by components fixed to the PCBs. Figure 2.13 indicates that the major radiating regions at about 1000 Hz. again lie towards the rear of the computer. The slightly higher values of 4 dB at location 21 and 28 relative to that at location 14 are possibly from "singing" caused by air passing through a honeycomb mesh at the exit. Once again, sound radiation was detected towards the front of the computer at location 32 and 39. This is also due, presumably, to the deflected air stream

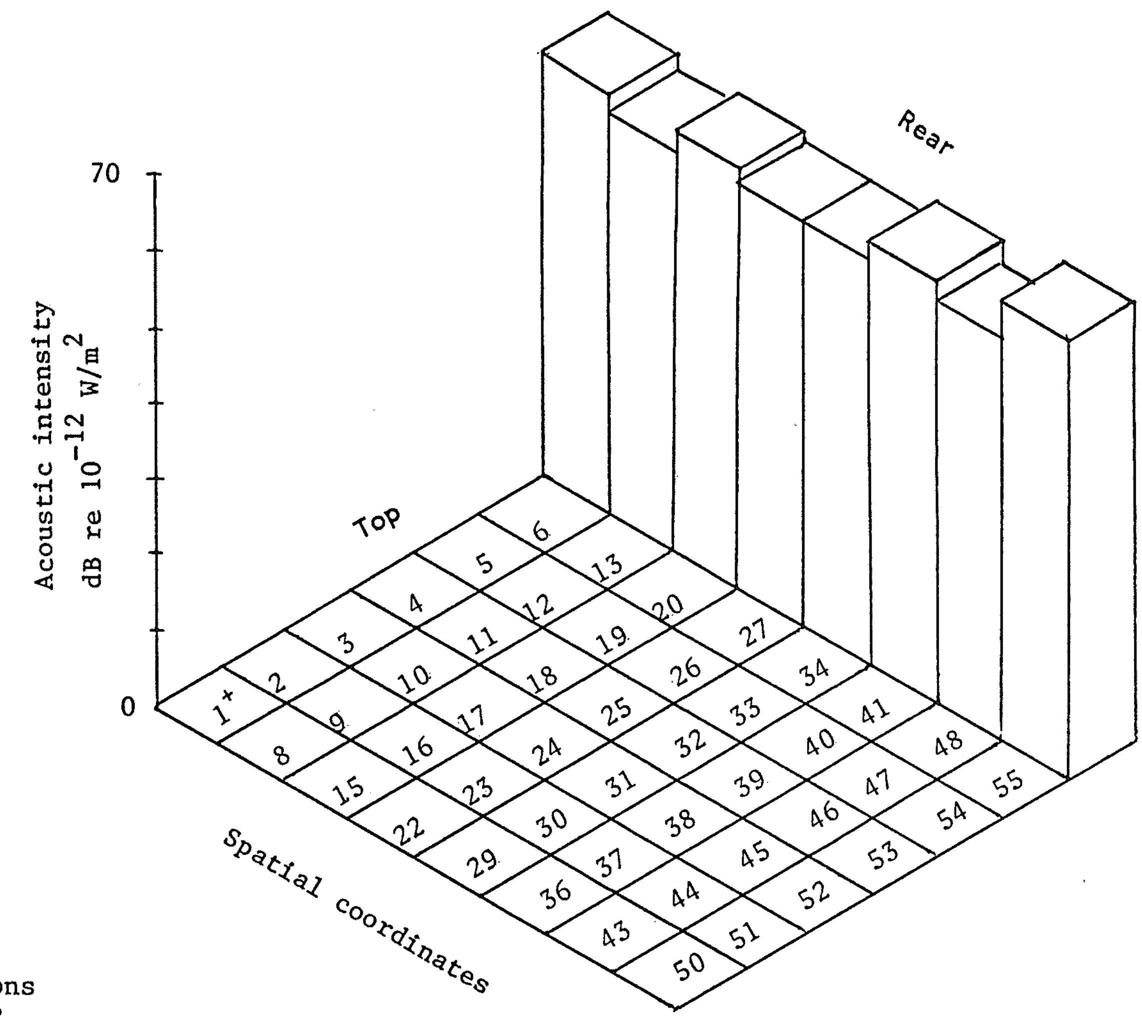

+measurement locations shown in Figure 2.8

Figure 2.11 : One third octave band acoustic intensity levels by left side panel at 125 Hz. centre frequency.

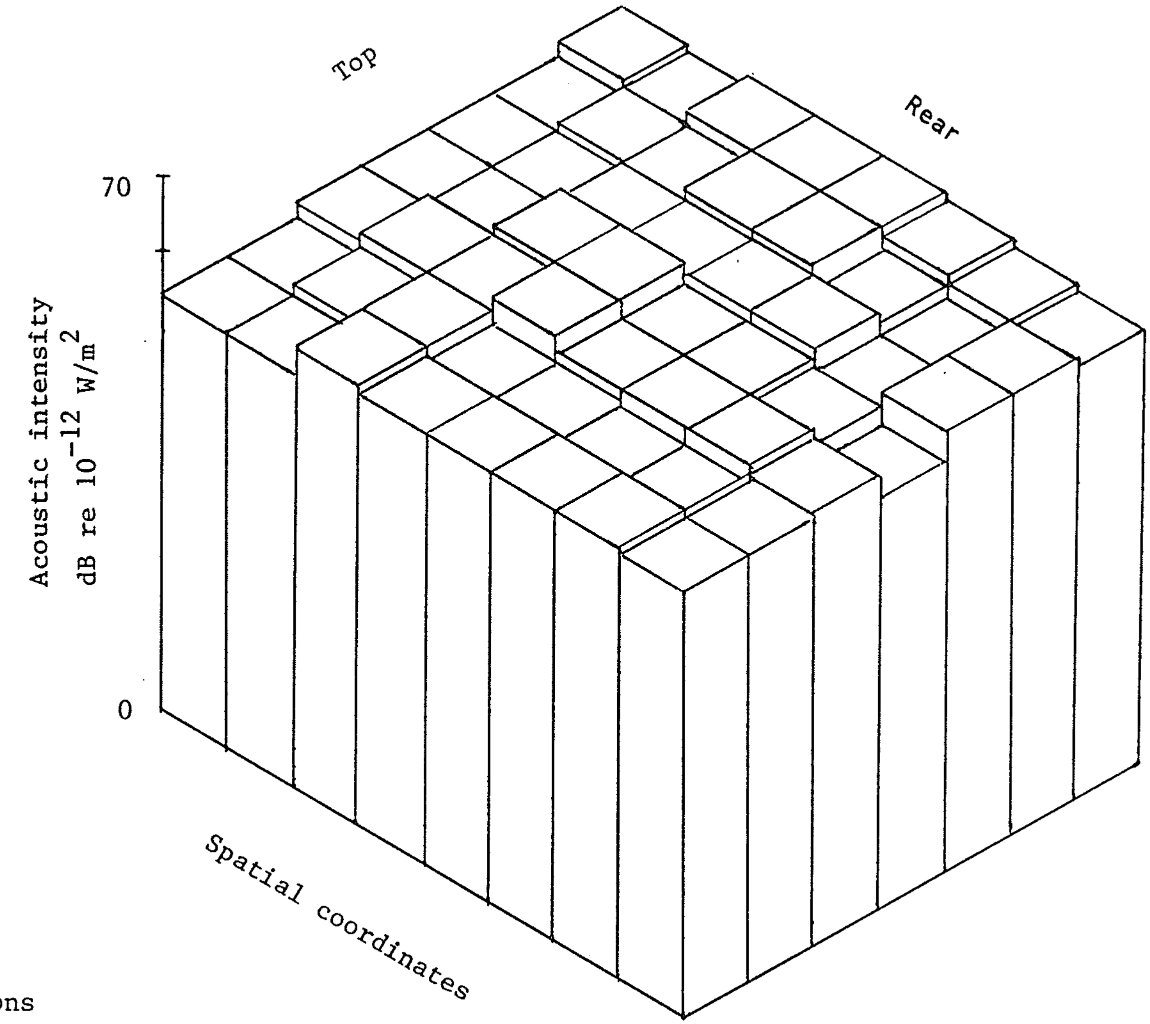

+measurement locations shown in Figure 2.8

Figure 2.12 : One third octave band acoustic intensity levels by left side panel at 500 Hz. centre frequency.

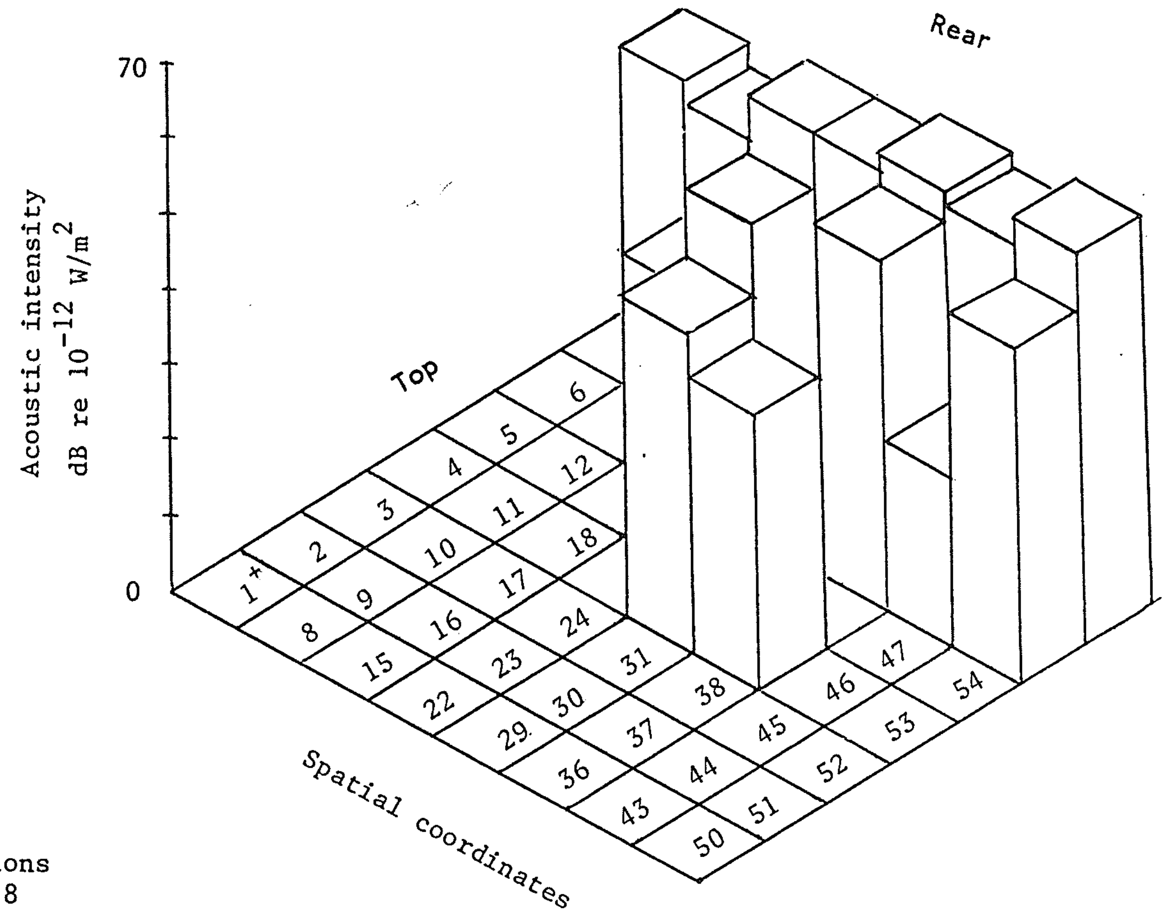

+measurement locations shown in Figure 2.8

Figure 2.13 : One third octave band acoustic intensity levels by left side panel at 1000 Hz. centre frequency.

striking the side panels. There is an apparent "lack" of sound being radiated in Figure 2.14 at locations 2,3,4,7,8 and 9. This implies that the acoustical hood on the rear panel was effective at frequencies lower than about 125 Hz.

The above phenomena could not be verified by a conventional technique like lead wrapping because of the danger from high voltage condensors. Ordinarily it is easy to identify the exact location of a noise source. However, it becomes increasingly difficult when the sound is propagating through module gates, wire loops, stiffeners etc., in a confined space because the directional characteristics of the sound are distorted. If the magnitude of the acoustic intensity radiated by each individual component is required, further work is necessary to quantitatively identify, as in reference [34], loss factors to account for distortions as the sound travels from the source to the microphone.[35,36]

The results obtained by using the acoustic intensity technique will be summarized.

1. Sound power levels may be determined quickly and accurately even under difficult measurement conditions.
2. The following changes are necessary to improve the acoustical performance of the computer
   a) The back panel of the computer requires acoustical treatment.
   b) The airflow within the computer needs streamlining to reduce turbulence and, hence, the vibration of the internal components mounted on the PCB chassis.

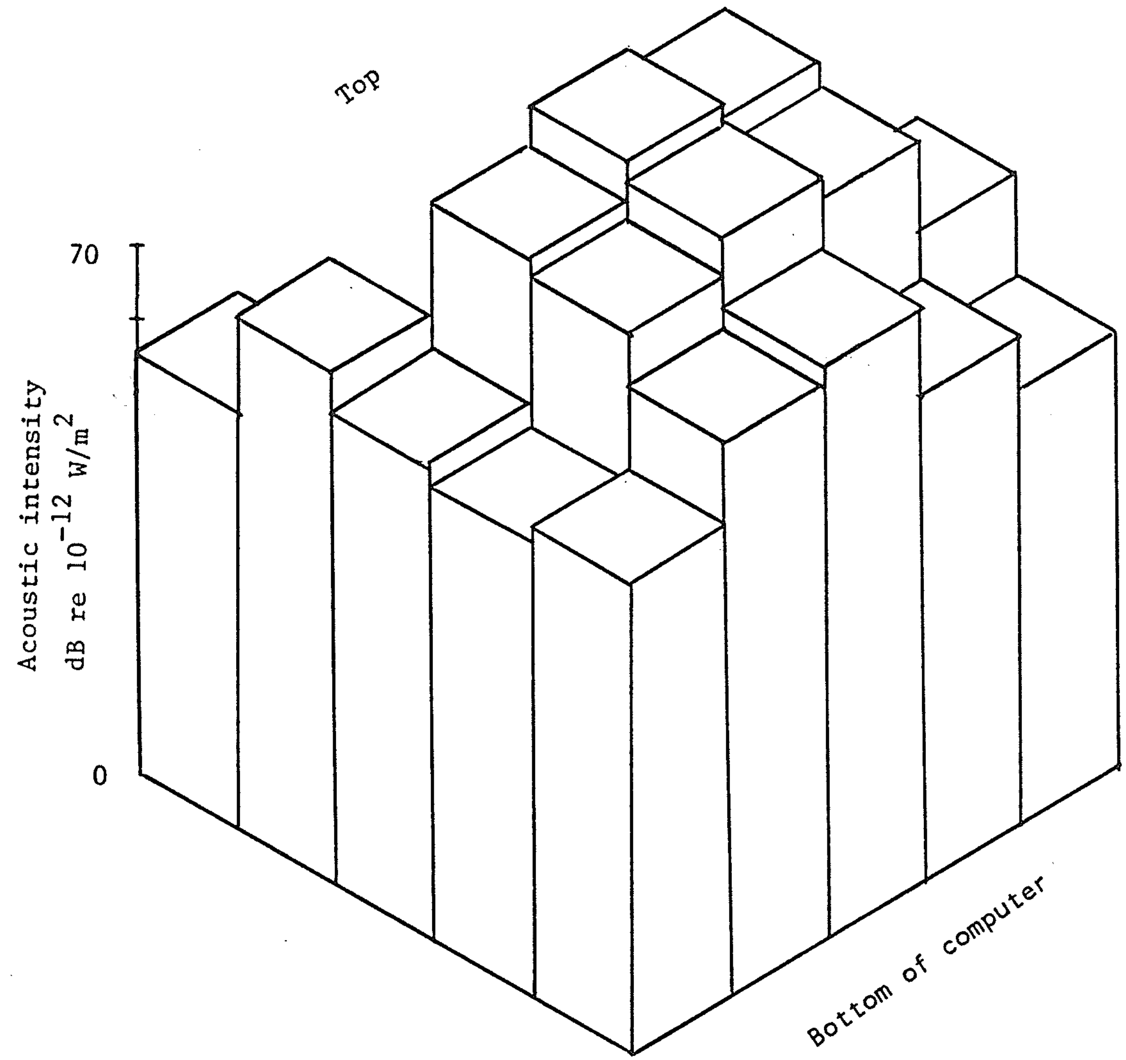

+measurement locations shown in Figure 2.8

Figure 2.14 : One third octave band acoustic intensity levels by rear panel at 50 Hz. centre frequency.

c) The combined acoustic and EMI seal between the cabinet and the rear panel needs improvement.

2.3 CONCLUSIONS

This study has demonstrated the feasibility of applying the acoustic intensity technique to digital computer systems. First, the sound power can be determined accurately and without a special acoustical environment. The measurement time may be further reduced by using the modified switching procedure to eliminate the need for switching channels after each measurement. Second, the source identification tests have yielded a better understanding of the sound sources within the computer. Tests on this computer have yielded valuable insight into the mechanism of sound radiation and illustrate the potential of the cross spectral intensity technique.

CHAPTER III

CORRELATION BETWEEN THE SOUND AND VIBRATIONS OF THE COMPUTER

This chapter explains a pragmatic approach to determining sound power by using a simple empirical procedure involving velocity measurements on the computer's panels. [37] It is expected that the results will highlight the degree of correlation between the radiated sound and the vibration of the computer. [38,39] The computer is idealized as a pulsating sphere - an idealization which has been used successfully to represent an internal combustion (I.C.) engine [40,41]. Fukuda et al [40] took measurements on an I.C. engine block where there was essentially one "flexible panel" supported by an essentially rigid casing. The test computer has a similar configuration because the back panel is much more "flexible" than the other panels. The modeling of a sound source as a pulsating sphere is based on the premise that there exists a strong correlation between the vibration of a solid boundary and the sound radiation from that surface [37]. Any vibrating surface will radiate sound if it is in contact with an elastic medium. The layer of the medium in immediate contact with the surface moves with the surface. The resulting movement is sufficient to initiate a train of compressions and rarefactions which generate a sound wave [37]. Consequently, the movement of a boundary transfers energy to the particles of the medium which travels through the medium as a sound wave. Thus, it should be possible to determine the sound power of the computer by simply using surface velocity measurements [37,38,39,40,41].

It is widely known that sound travels from a source to the observer along both airborne and structureborne transmission paths [38]. The correlation between structureborne vibration and airborne sound, however, is not well defined. This chapter explains the idealizations used and the results obtained by modeling a computer as a pulsating sphere whose surface vibrates radially. The analysis is confined to radial pulsations of the sphere and invariably presumes symmetry to simplify the analysis [39,40]. It is assumed that the panels of the computer are continually subjected to excitations caused by the constant rotational speed of the fan. Mean square velocity levels were measured at various locations on the surface of the computer and the sound power determined as shown in Appendix 3. Once again, sound power levels were obtained in the 500 Hz., 1000 Hz., and 2000 Hz. octave bands [24].

3.1 THEORY

The theory of sound radiation from a pulsating sphere is well defined [37,38,39,40,41]. It is strictly valid only at the fundamental or "breathing" mode. To extend the analysis to higher frequencies, the total area of the vibrating surface, S, is divided into $n(S/\Delta S_f)$ identical components each having surface area ΔS_f [40]. This simplification reasonably permits the further assumption that each component vibrates in its own breathing mode. Then the overall sound power is the sum of the sound powers radiated from each component.

The sound power radiated by an element on a hemi-spherical source pulsating with volume speed U_e in an infinite baffle is [40]

$$W_e = (\rho c U_e^2/2\Pi a^2)\ k^2a^2/\ (1 + k^2a^2) \quad . \qquad \{3.1\}$$

Here k is the acoustic wave number and a is the radius of the hemisphere which is approximately $\sqrt{\Delta S_f/2\Pi}$ [40]. It is assumed that a) the amplitude of motion is small i.e. much less than the radius of the sphere; b) the sphere is embedded in an infinite medium so that there are no reflected waves [1]; and c) the n radiating surfaces are independent, incoherent and distributed uniformly over the surface. Thus, by substituting a in equation {3.1} and summing, the expression for the total sound power, W_s, becomes,

$$W_s = {}_n\Sigma W_e = \rho\langle\dot{\xi}^2\rangle S(k^2\Delta S_f/(2\Pi + k^2\Delta S_f)) \ . \qquad \{3.2\}$$

The < > is the temporal average of n individual components of the surface speed, $\dot{\xi}$. For a broadband frequency analysis, the wave number, k, and the unit surface area, ΔS_f are taken, for convenience, to correspond to those values at the centre frequency of each band [40].

A value of ΔS_f is necessary to determine an appropriate number of measurement points. According to reference [40], for example, reasonable accuracy may be obtained if ΔS_f is approximated by the area covering the fundamental mode of a comparable simply supported rectangular plate. Then the following ΔS_f have been suggested

$$\Delta S_f = (\Pi/f)\sqrt{D/\rho_t h} \quad , \text{ for } f > (\Pi/S)\sqrt{D/\rho_t h} \qquad \{3.3\}$$

$$\Delta S_f = S \quad , \text{ otherwise} \qquad \{3.4\}$$

from which n may be obtained straightforwardly. In the above, ρ_t denotes the material density, h is the thickness and D is the flexural stiffness of a panel. In determining h, ρ_t, and D, it is assumed that each panel is homogeneous and uniform and that any deviations from the simple unstiffened hollow box model do not affect the vibration pattern.

3.2 RESULTS

Preliminary experiments were undertaken to determine if the major movement of each computer panel was flexural or axial. This information is necessary because the idealization of the computer as a pulsating sphere is realistic only if the transverse motion of every panel predominates. The computer was clamped on a sturdy table by using C-clamps to prevent the computer from "bouncing". An electro-magnetic shaker was attached to the hood at the rear of the computer as shown in plate P.3.1. A white noise source was used to drive the shaker. The output of the shaker was delivered to the computer through a fairly weak spring to simulate the force produced by the fan but without any accompanying air flow. This simulation is reasonable because the spectrum of the excitation imparted by the shaker encompasses the excitation frequency range of both the air flow and the fan. The corresponding axial and transverse accelerations of the computer's exterior panels were measured by using two B & K type 4344 accelerometers mounted on an aluminum block shown in Figure 3.1. The ensuing accelerations are presented in Appendix 3. They indicate that at frequencies greater than 250 Hz, the transverse accelerations of the panels were, indeed, greater than the

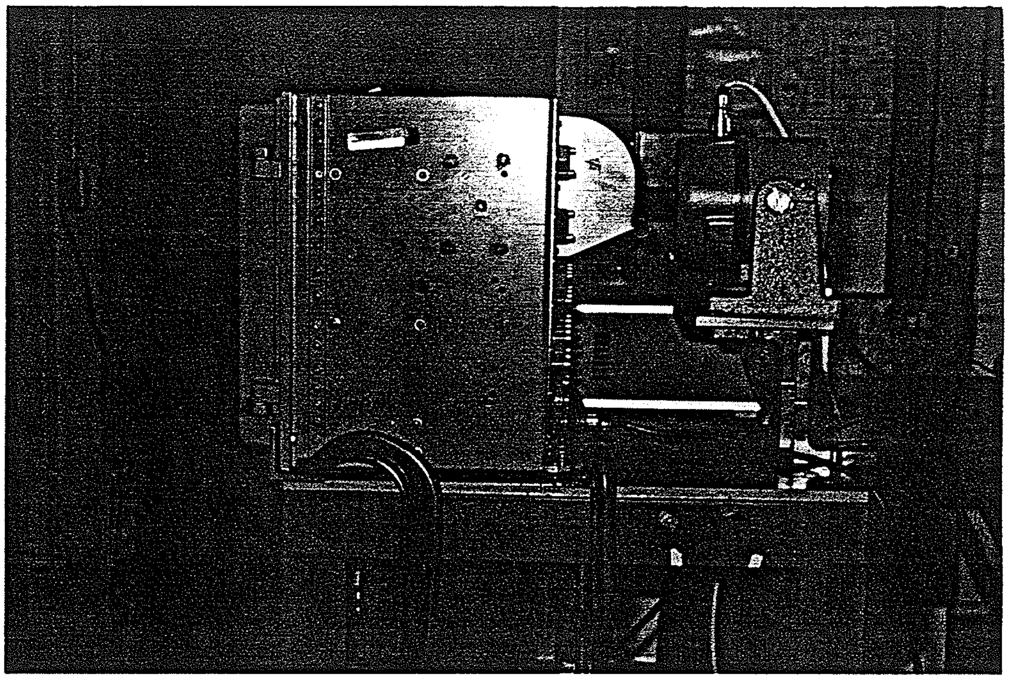

Plate P.3.1 : View of shaker attached to rear of computer.

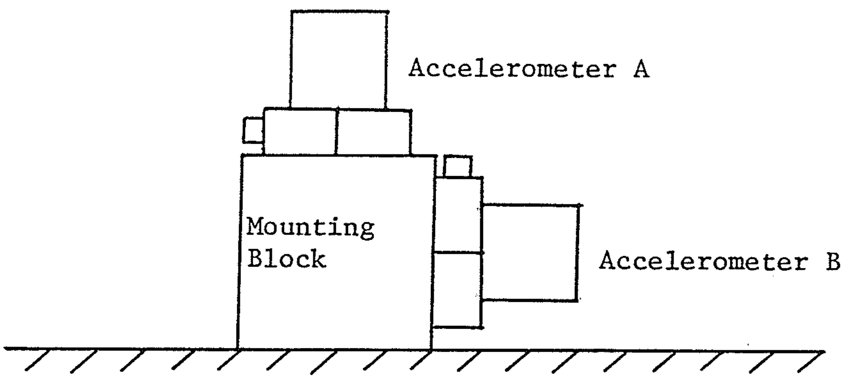

Figure 3.1 : Accelerometer arrangement for measuring transverse and longitudinal accelerations at a "point".

corresponding axial accelerations by up to 15 dB. Therefore, exterior panels certainly vibrate primarily transversely in frequencies related to the measurement of the computer's sound power.

Still finer knowledge of the computer's dynamic behavior is needed to better assess if the uniformly radial motion of the assumed breathing mode is reasonable. Modal behavior was found most conveniently by impacting each panel with an instrumented hammer [42] to obtain the frequency response functions given in Figure 3.2a through 3.2d. Natural frequencies are identified in these figures by peak amplitudes corresponding to a phase shift in excess of 60 degrees and a coherence value better than 0.8 [42]. A fair number occur below 200 Hz. which approximates the lower cut-off frequency of the lowest, 500 Hz centred octave band of concern. Consequently, flexural modes with wavelengths smaller than each panel's dimensions must predominate in the frequency span covered by the sound power measurements. Then inevitable out-of-phase motions even on an individual panel contradict the uniform breathing assumption. Hence, every exterior computer panel must be idealised as a set of components each pulsating essentially incoherently.

The computer's sound power measured conventionally or by using the acoustic intensity technique are presented for reference in row 1 and 2, respectively, of Table 3.1. Analogous octave band sound power levels obtained from surface velocity measurements are given in row 3 and 4. (A typical computation is shown more conveniently in Appendix 3.) The number of measurement locations suggested by equation {3.3} and {3.4} were employed to compute the data of row 4 whereas somewhat fewer locations were used for row 3. Differences between corresponding

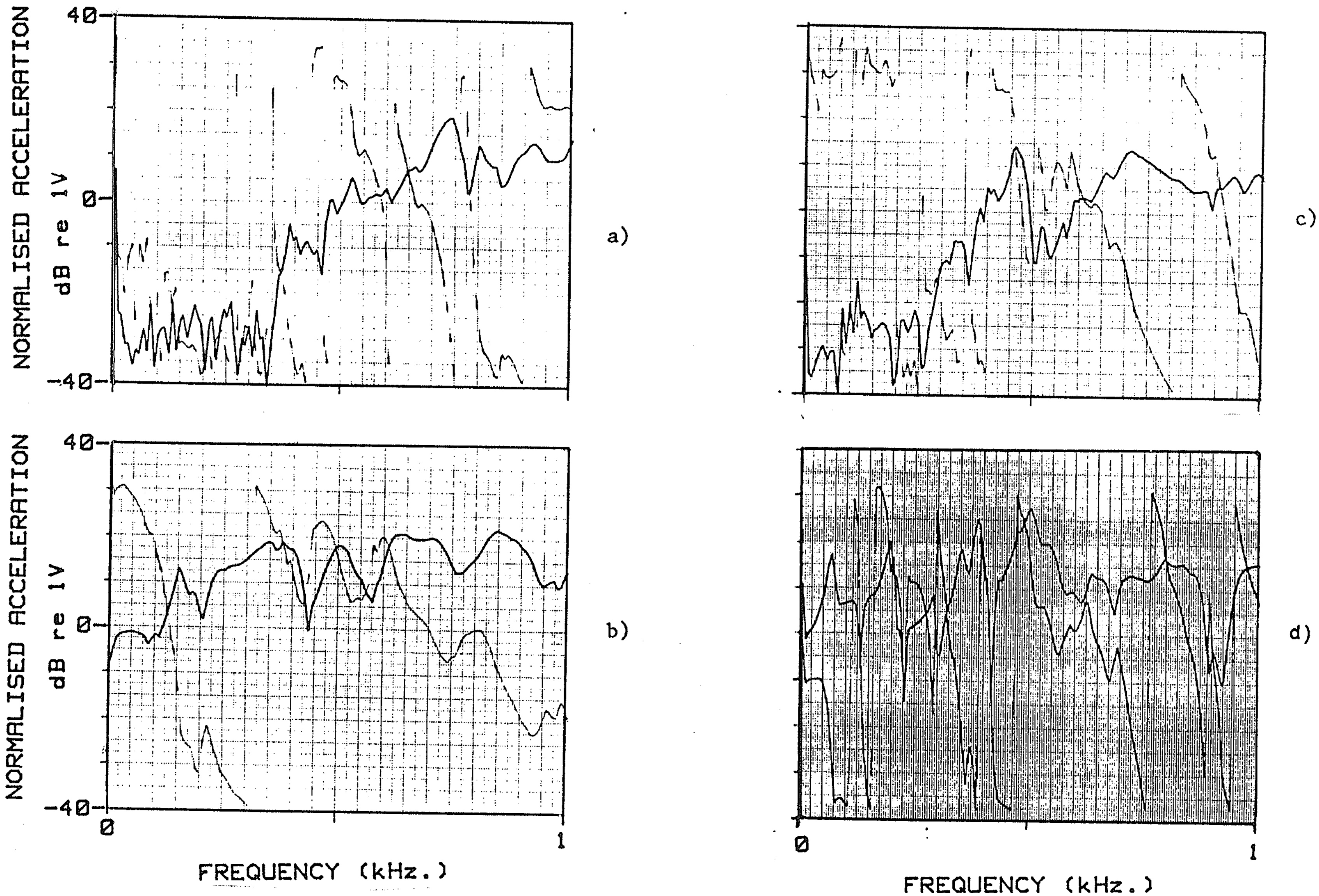

Figure 3.2 : Frequency response functions obtained by using the impulse technique [42] on : a) right, b) top, c) left and d) rear panel.

Case	Sound power at octave band centre frequency		
	500 Hz.	1000 Hz.	2000 Hz.
1	70.6±4.0	60.2±3.4	58.2±3.3
2	69.6±1.8	57.4±1.8	55.0±1.8
3	64.6±0.0	63.1±0.0	65.3±0.0
4	72.8±0.0	61.3±0.0	61.0±0.0

(in dB re 10.0 E-12 W.)

Table 3.1 : Computer's total sound power level determined 1) conventionally; 2) by using the acoustic intensity method; 3) using surface velocity measurements at 20, 40 and 80 locations; and 4) as in 3) but with 25,50 and 100 locations, respectively, for the 500, 1000 and 2000 octave bands.

sound power levels in these two rows are generally apparent and particularly so in the 500 Hz octave band. Results in row 4 invariably correlate better with the reference data of row 1 and 2. Consequently, the number of measurements suggested by equation {3.3} and {3.4} should at least be employed. On the other hand, the sound powers in row 4 are constantly the highest followed consistently by those in row 1 and row 2. The greatest differences of about 3dB and then a further 3dB between these rows happen in the 2000 Hz octave band. Presumably the complex structural interactions between interior components and exterior panels as well as panel regions adjacent to local stiffeners can no longer be ignored completely there. Therefore, equation {3.3} which is based pragmatically upon the simplest uniform hollow box becomes somewhat less accurate. Further "incoherent" sources implicit to additional measurement locations may produce an improvement but only at the cost of substantially longer measurement periods.

This pragmatic approach implicitly assumes that the mechanical vibration of the computer's exterior panels radiates the sound. However, this approach would fail at frequencies below 200 Hz where the "air flow noise" of an axial flow fan is known to predominate. The sound intensity spectrum of such a fan is shown in Figure 3.3 [43]. Fortunately, at frequencies related to the measurement of the computer's sound power (500, 1000 and 2000 Hz), the mechanical vibration of the computer's exterior panels is predominant, thereby satisfying the implicit assumption. [40,45,46,47]

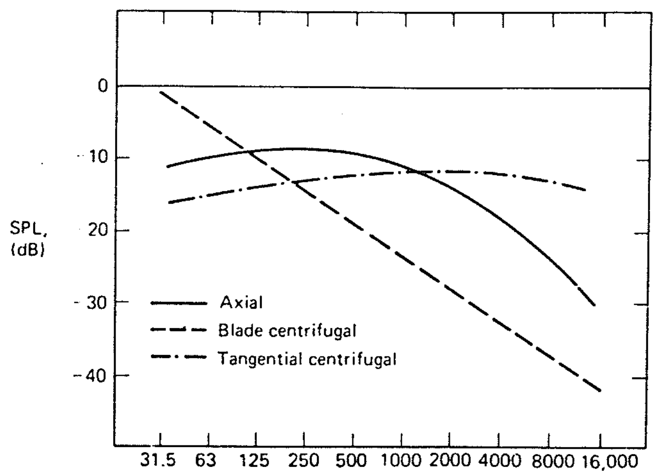

Figure 3.3 : Sound spectra of various fans [43] with axial fan data applicable here.

3.3 CONCLUSIONS

The importance of the idealised model cannot be over-emphasized. In Chapter II, for example, the sound power of the computer could not be determined accurately when the ambient noise levels exceeded those from the computer alone by about 15 dB. Under such circumstances, the sound power of the computer could be determined by using the surface velocity technique because the velocity is hardly affected by ambient noise. This assertion would only apply, of course, to circumstances where contaminating vibrations are minimal. Furthermore, the correlation between the vibration and sound radiation has been highlighted. Thus, the sound power of a source may be measured under even the most trying conditions. In addition, the enhanced understanding of the physical process of sound radiation may be used advantageously to suggest future structural remedies on the cabinet.

CHAPTER IV

VIBRATION INTENSITY TECHNIQUE

Combustion and aerodynamic noise are major noise components for many power systems like fans and engines [48]. After these two noise sources have been attenuated, structureborne vibration often becomes important [48]. As mentioned in Chapter III, the typically predominant normal surface component of vibration produces acoustic pressure waves which become significant when large surface areas, typical of industrial blowers, are encountered [49]. Then the vibrations themselves have to be controlled to reduce acoustical radiation from the surface. Suitable controls will generally require the significant vibration sources and the structureborne transmission paths to be identified so that the mechanical energy along the propagation paths may be absorbed or deflected.

A new cross spectral technique will be described which may be used to identify sources of vibration by employing intensity vectors. Following a presentation of the theory [49,50,51,52], the results of preliminary tests on a lead plate will be given. These tests provided experience on a relatively simple homogeneous plate and formed the basis for further tests on the computer which is basically an assemblage of beams and panels. A major aim was to better understand the mechanism and propagation of structureborne vibration energy and, if feasible, attenuate excessive vibrations in the development computer. A secondary consideration was to provide a standard for the design of future computers.

4.1 THEORY

The plateborne vibration vector, $\vec{w}$, is defined as the net flow of vibration energy per unit width. The magnitude of the plateborne vibration intensity in a given direction, w_i, is the projection of the intensity vector in that direction as shown in Figure 4.1. In formulating the vibration intensity flowing through a small section of a stiffened panel of the computer, the following assumptions are made. 1) Flexural vibrations predominate and 2) losses occur only at the ends of a panel or reinforcing beam. The first assertion has already been confirmed experimentally in Chapter III. Rotational inertia and shear deformation, therefore, are reasonably negligible [51]. The second assumption may be justified by the argument described in reference [49] for a one dimensional structure. The analysis may then be extended to a two dimensional structure such as a plate by describing the flexural behaviour of a plate in terms of two perpendicular beam functions. This is easily accomplished by appropriately modifying the subscripts defining the directions. For a one dimensional structure, the vibration's complex wave number, k, has four roots; two of which are usually real and two imaginary. [50] These roots imply a harmonic solution consisting of "travelling waves" (implying free field) and a "near field", exponentially decreasing solution with waves moving in both the outward and inward directions. This latter situation is analogous

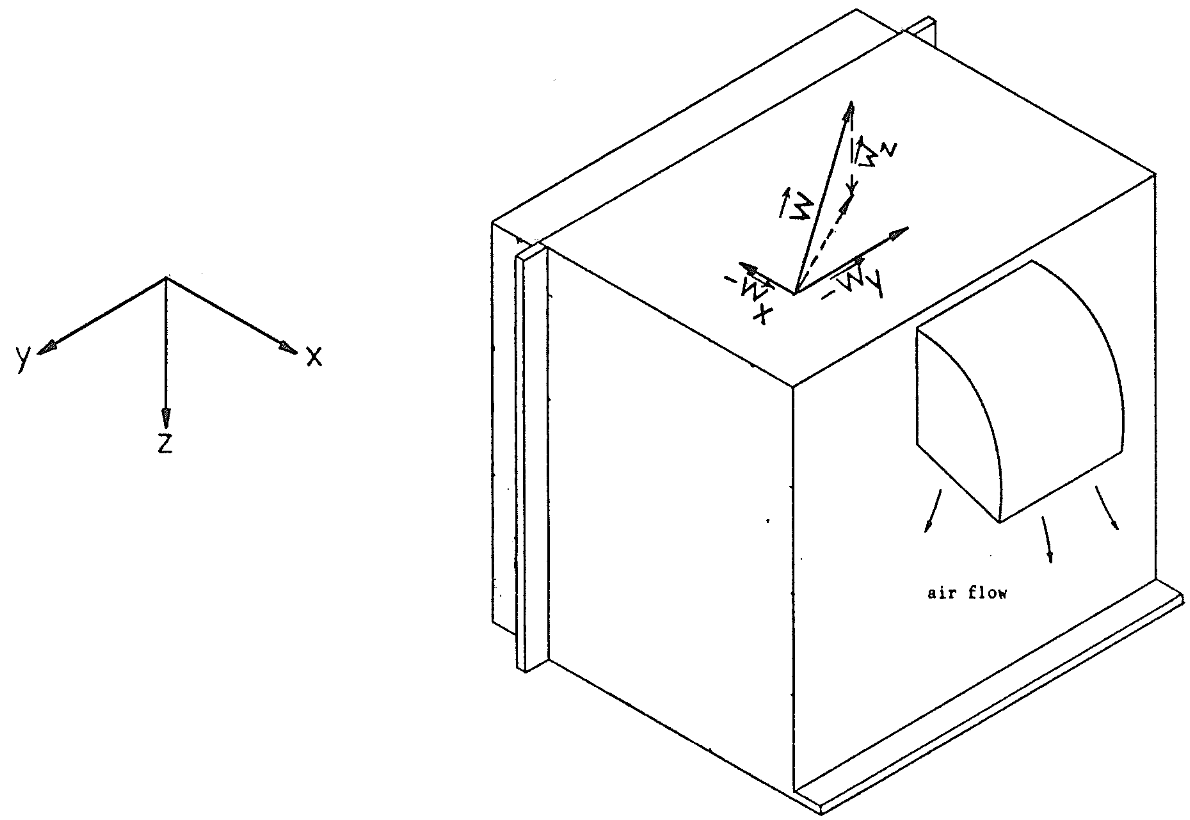

Figure 4.1 : Representation of the vibration intensity vector at a measurement location on the computer.

to the near field of a sound source where the acoustic waves do not travel freely and progressively from the source. The near field component usually decreases rapidly from the boundaries of the wave medium and usually does not carry energy so that progressive waves are more important. The present analysis is limited to this type of wave. For travelling progressive waves, the existence of a near field is attributed to the necessity for satisfying mechanical equilibrium at boundaries where continuity of the physical properties of the wave medium are disrupted. Therefore, the amplitude of the near field can be expected to be similar to that of the progressive waves at these boundaries [50].

Consider initially a flat, uniform and homogeneous plate section of the computer with its neutral plane in the x-y plane as shown in Figure 4.2. At any point of a cross-section which is perpendicular to the x-axis, there exists the component of shear force, Q_x[+], and two moment components, M_x and M_{xy}. The scalar product of the corresponding vectors with their own velocity vectors gives the vibration intensity vector through the cross section in the x-direction [49,51,52]. Now [52]

$$M_x = -D(\partial^2\xi/\partial x^2 + \nu\,\partial^2\xi/\partial y^2) \quad , \qquad \{4.1\}$$

$$M_{xy} = M_{yx} = D(1-\nu)\partial^2\xi/\partial x\partial y \quad , \qquad \{4.2\}$$

$$Q_x = -D\frac{\partial}{\partial x}\left(\frac{\partial^2\xi}{\partial x^2} + \frac{\partial^2\xi}{\partial y^2}\right) \quad , \qquad \{4.3\}$$

+ The notation Q_x will be used to designate the magnitude of vector $\vec{Q}$ in the x-direction. An extension to other subscripted variables is straightforward.

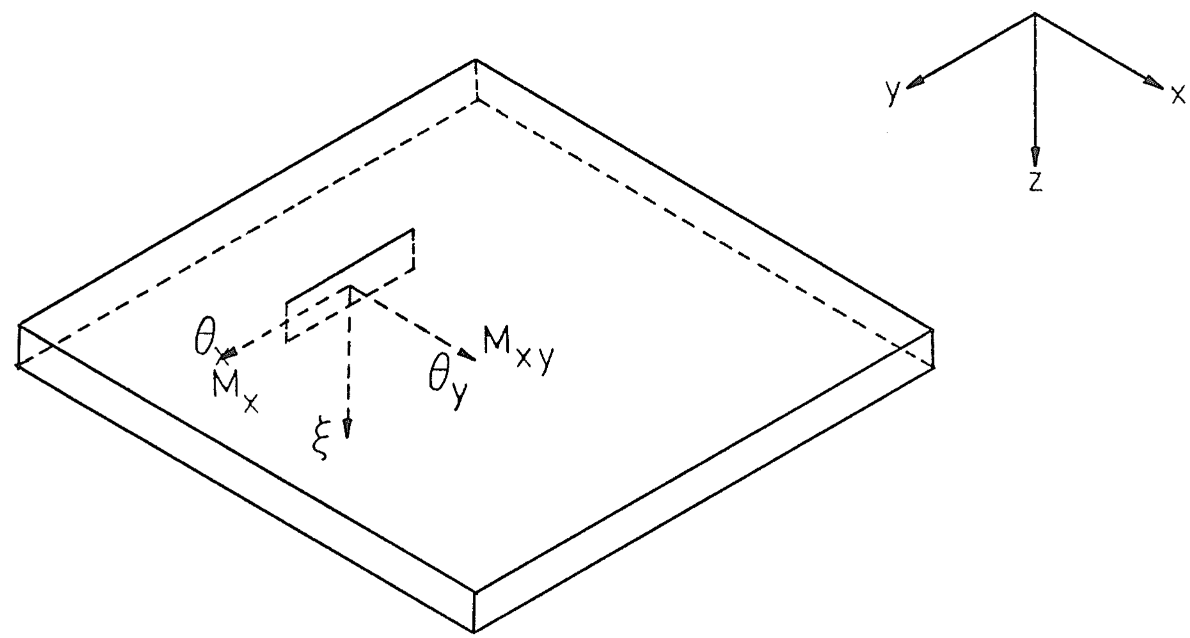

Figure 4.2 : Forces, moments and displacements in a cross-section of a plate.

where D is the plate's flexural stiffness and ξ the transverse displacement in the z direction. The x and y components, θ_x and θ_y respectively, of the angular displacement, θ , are

$$\theta_x = -\frac{\partial}{\partial x}(\xi) \qquad \{4.4\}$$

and

$$\theta_y = -\frac{\partial}{\partial y}(\xi) . \qquad \{4.5\}$$

Therefore the x-component of the intensity vector is composed not only of the contribution of the force,

$$w_{xq} = Q_x \, \partial \xi/\partial t \quad , \qquad \{4.6\}$$

but also those from the bending and twisting moments, respectively given by [49]

$$w_{xb} = M_x \,(-\partial^2\xi/\partial y\partial t) \text{ and } w_{xt} = M_{xy}(\partial^2\xi/\partial x\partial t) . \qquad \{4.7\}$$

Consequently, the magnitude of the total vibration intensity in the x-direction, w_x, is [51,52]

$$w_x = \langle Q_x\dot{\xi} \rangle + \langle M_{xy}\dot{\theta}_y \rangle + \langle M_x\dot{\theta}_x \rangle . \qquad \{4.8\}$$

A dot superscript invariably denotes a time derivative and < > designates a temporal average. The intensity component in the y direction, w_y, can be combined to give the magnitude, w, and direction, θ, of the net intensity vector, $\vec{w}$, as

$$w = \sqrt{(w_x^2 + w_y^2)} \text{ and } \theta = \text{arc tan } (w_y/w_x) . \qquad \{4.9\}$$

All six variables in equation {4.8} should be ideally measured simultaneously. This is impractical, however, for two reasons. First, as in the acoustic intensity case where the velocity could not be determined directly, the force and moments cannot be measured straightforwardly. Second, even with the modifications described below, this procedure would require an expensive six channel data acquisition system. Hence, further simplifications are necessary to reduce costs. Fortunately, the force and moment components of intensity are equal for flexural waves in the free field region [49,51]. Thus, only the moment need be measured and its components M_x, M_y, and M_{xy} can be determined easily in terms of the surface strains $\varepsilon_x, \varepsilon_y$ by using the simple relationships [51,52]

$$M_x = 2D/h(\varepsilon_x + \nu\xi_y) \quad , \qquad \{4.10\}$$

$$M_y = 2D/h(\varepsilon_y + \nu\varepsilon_x) \quad , \qquad \{4.11\}$$

and

$$M_{xy} = 2D/h(1-\nu)\,\gamma_{xy} \quad . \qquad \{4.12\}$$

Although the strains ε_x and ε_y can be measured easily by using strain gauges, the shear strain γ_{xy} is almost inaccessible because it involves attaching a strain gauge along the edge of the plate. This poses an obvious difficulty with thin plates where the thickness is much less than the width of the strain gauge. The problem may be overcome by introducing a modified component of intensity, w_x', where

$$w_x' = <[(M_x+M_y)/(1+\nu)]\dot{\theta}_x> \qquad \{4.13\}$$

is an approximation to the true moment contribution w_x given by equation {4.8} . This approximation has been explained in detail in reference [51]. It has been found to be reasonable for panels and beams like those forming the exterior of the computer. Now the sum required in equation {4.13} of M_x and M_y may be determined from equation {4.10} and {4.11} as

$$M_x + M_y = 2D/h(1+\nu)(\varepsilon_x + \varepsilon_y) \quad . \qquad \{4.14\}$$

However [51],

$$\varepsilon_x + \varepsilon_y = -h/2(\partial^2\xi/\partial x^2 + \partial^2\xi\ /\partial y^2) \qquad \{4.15\}$$

so that equation {4.14} becomes

$$M_x + M_y = -D(1+\nu)(\partial^2\xi/\partial x^2 + \partial^2\xi/\partial y^2) \ . \qquad \{4.16\}$$

For plane waves in a free field, the sum of the partial derivatives in equation {4.16} is [51]

$$\partial^2\xi/\partial x^2+\partial^2\xi/\partial y^2 = k^2\xi \qquad \{4.17\}$$

where $k^4 = \omega^2 m/D$, ω is the angular frequency and m is the mass per unit area [51,52,53]. Substituting equation {4.17} into equation {4.16} yields,

$$M_x + M_y = -D(1+\nu)k^2\xi \ . \qquad \{4.18\}$$

Under free field conditions the force and moment components, w_{fx} and w_{mx}, of the intensity are equal so that [49,51]

$$w_{fx} = w_{mx} = w_x/2 \qquad \{4.19\}$$

and, hence,

$$w_x = 2w_{mx} \approx 2w_{mx}' \, . \qquad \{4.20\}$$

The last relationship together with the further substitution of equation {4.13} gives

$$w_x = - <2Dk^2 \xi \, \dot{\theta} x > \, , \qquad \{4.21\}$$

or, by integrating the acceleration $\ddot{\xi}$ twice to give the expression in terms of the displacement, ξ

$$w_x = <2Dk^2 \dot{\theta}_x \int_0^t \int_0^t \ddot{\xi} \, dt \, dt > \, . \qquad \{4.22\}$$

Thus, w_x may be determined by simultaneously measuring the time averaged angular speed $\dot{\theta}_x$ and transverse acceleration $\ddot{\xi}$. Variables $\dot{\theta}_x$ and $\ddot{\xi}$ may be obtained by using the two accelerometer configuration shown in Figure 4.3 [51,52]. This arrangement is analogous to the two microphone configuration described in Chapter II where the pressure, p, and magnitude of the particle velocity, u_r, now correspond to the acceleration, $\ddot{\xi}$, and rotational speed, $\dot{\theta}_x$, respectively. By modifying the procedure involving the microphones to accommodate the accelerometers, it may be seen that the acceleration, $\ddot{\xi}$, at the measurement point may be approximated by the mean acceleration from the two accelerometers. These accelerometers may be distinguished by subscripts 1 and 2 again. The mean acceleration, therefore, is

$$\ddot{\xi} = (\ddot{\xi}_1 + \ddot{\xi}_2)/2 \, . \qquad \{4.23\}$$

The angular speed $\dot{\theta}_x$, on the other hand, can be determined from the finite difference approximation,

$$\dot{\theta}_x = \int_0^t (\ddot{\xi}_2 - \ddot{\xi}_1) / \Delta r \, dt \quad ; \qquad \{4.24\}$$

where Δr is the spacing between the accelerometers. Once again, the spacing, Δr, is a function of the vibration wavelength and, therefore, must be set appropriately. There is presently no nomogram for setting the spacing so that a reasonable value was determined experimentally. The procedure will be described later. Substituting for $k^2, \dot{\theta}_x$ and $\ddot{\xi}$ in equation{4.22}, the intensity component, w_x, may be rewritten as

$$w_x = (2\ D/\omega\sqrt{\frac{m}{D}} < \int_0^t \int_0^t (\ddot{\xi}_1 + \ddot{\xi}_2)\ dt\ (\ddot{\xi}_1 - \ddot{\xi}_2)/\Delta r\ dt >. \quad \{4.25\}$$

It is shown in Appendix 2 that the last equation can be transformed into the frequency domain to yield

$$w_x = 2\sqrt{Dm}\ \mathrm{Im}\ (G_{12})/\omega^2\Delta r \qquad \{4.26\}$$

where G_{12} is the cross power spectrum between accelerations 1 and 2 [52,53]. This expression is now similar to equation {2.6} in Chapter II. Once again, 64 averages were invariably used to improve the signal to noise ratio of the accelerations.

From the experience with the acoustic intensity technique, the practical implementation of equation {4.26} was anticipated to be even more sensitive to phase mismatch between channels because of the lower frequency characteristics of the vibrations. Thus, the switching technique was used again to overcome phase mismatch between the two accelerometer channels. If the measured cross spectrum is denoted by G_{12s} in the switched configuration, then equation {4.26} can be approximated by

$$w_x = 2\sqrt{Dm}\ \ \mathrm{Im}[G_{12} \circ G_{12\,s}]^{1/2} /\omega^2\Delta r \ . \qquad \{4.27\}$$

Due to the inherent assumption of the force and moment components of intensity being equal in equation {4.6} through {4.11}, equation {4.26} is valid only for the "free field" case. However, for the more complex "near field" condition, Pavic [49] has similarly formulated equation {4.25} at any instant, t, as

$$w = D/\Delta^3 < 4\int_0^t\int_0^t a_3\int_0^t a_2\, dt\, dt\, dt - \int_0^t\int_0^t a_4\int_0^t a_2 dt\, dt\, dt - \int_0^t\int_0^t a_3\int_0^t a_1 dt\, dt\, dt >. \tag{4.28}$$

Subscripts 1 through 4 now refer to four accelerometers whose orientation is such that energy flows in the direction of an accelerometer with a lower number. Although expression {4.28} is general, signal processing in the time domain is cumbersome because elaborate electronic circuitry is required. Consequently, Verheij [54] transformed the expression developed by Pavic into the frequency domain as

$$w = D/_{\omega^3\Delta^3}(4\mathrm{Im}[G_{23}] - \mathrm{Im}[G_{24}] - \mathrm{Im}[G_{13}]) \tag{4.29}$$

so that a dual channel spectrum analyser may be used straightforwardly in conjunction with a microcomputer. It can be seen, however, that this procedure is slower than that associated with equation {4.26} because three cross spectra have now to be evaluated. On the other hand, equation {4.29} will be used in the following section to corroborate the experimental results obtained by using equation {4.27}.

4.2 RESULTS AND DISCUSSION

The overall objective of the vibration intensity measurements was to identify the predominant structureborne vibration paths through the computer in the 63 and 500 Hz. centred one-third octave bands. These bands were selected because previous preliminary vibration tests [55] had yielded high structureborne levels there. However, experiments were first undertaken on the 1 m. X 1 m. X .006 m. lead plate shown in Figure 4.4 to provide valuable practical experience and a simple means of calibration. A lead plate was chosen because lead has a high loss factor compared to other metals. The incident wave is absorbed rapidly as it progresses through the material and this inhibits reflections or reduces their magnitude significantly so as not to interfere with the incident wave. Consequently, this arrangement is analogous to the calibration of the 4m. long pipe described in Chapter II. The results of these calibration experiments will be presented in the following section.

A dual accelerometer mount shown in Figure 4.3a was designed and fabricated to meet certain requirements. First, the accelerometer mount and accelerometers (or probe) had to be light so as to inconsequentially affect the vibrations of the plate. Second, the fundamental resonance frequency of the probe had to exceed the upper frequency of interest (i.e. 500 Hz. for the computer) to prevent the dynamics of the probe from distorting the measurements. The fundamental resonance frequency of the probe was found to be around 1400 Hz.

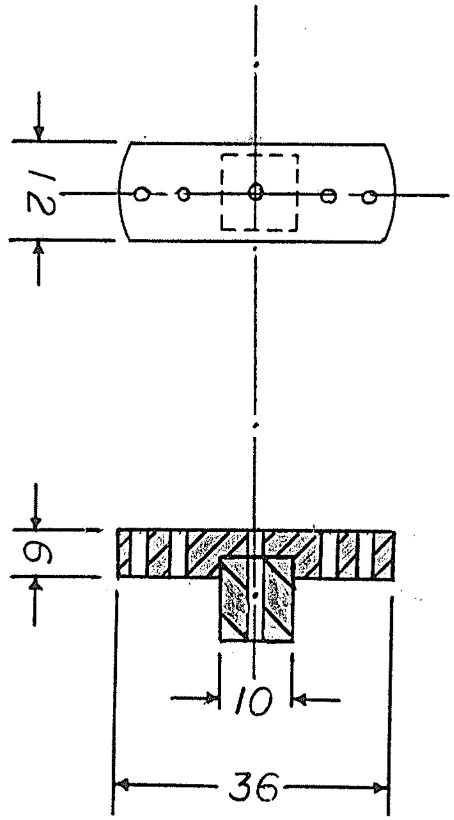

a)

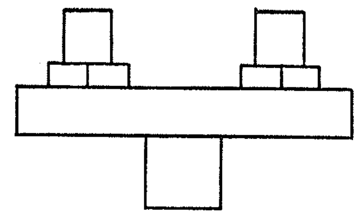

b)

Figure 4.3a : Dual accelerometer mount.

Figure 4.3b : Dual accelerometer mount with acclerometers.

which is well above the upper frequency of interest. Third, the accelerometers had to be protected from electromagnetic interference (EMI) generated by the high voltage transformers within the computer. Consequently, the accelerometer mount was fabricated from low density aluminum which provides an excellent EMI shield. Fourth, the spacing between the accelerometers had to be adjustable to encompass any desired frequency range. A slot arrangement was considered where the accelerometers could slide across the mount and be locked in place. However, firmly securing the accelerometers was too difficult. Hence, two sets of tapped holes were drilled on the mount such that there was a choice of a 2 cm. or 3 cm. spacing between the accelerometers.

4.2.1 LEAD PLATE

The lead plate was suspended from two corners by a 3 mm. steel cable as shown in Figure 4.4. The lower edge of the plate was embedded in a sand pit so that the sand could act as a vibration absorber. An electro-magnetic shaker was attached to a point on the central axis of the panel, 20 cm. from the plate's upper edge. A white noise signal from the HP 3582A spectrum analyser was fed to the shaker which then generated essentially flexural waves in the lead plate. The shaker was coupled to the plate through a spring and a force transducer so that the input power could be measured directly. An accelerometer was attached at the input and the integrated output provided the velocity. Two supports were also attached to the plate, 50 cm. from the

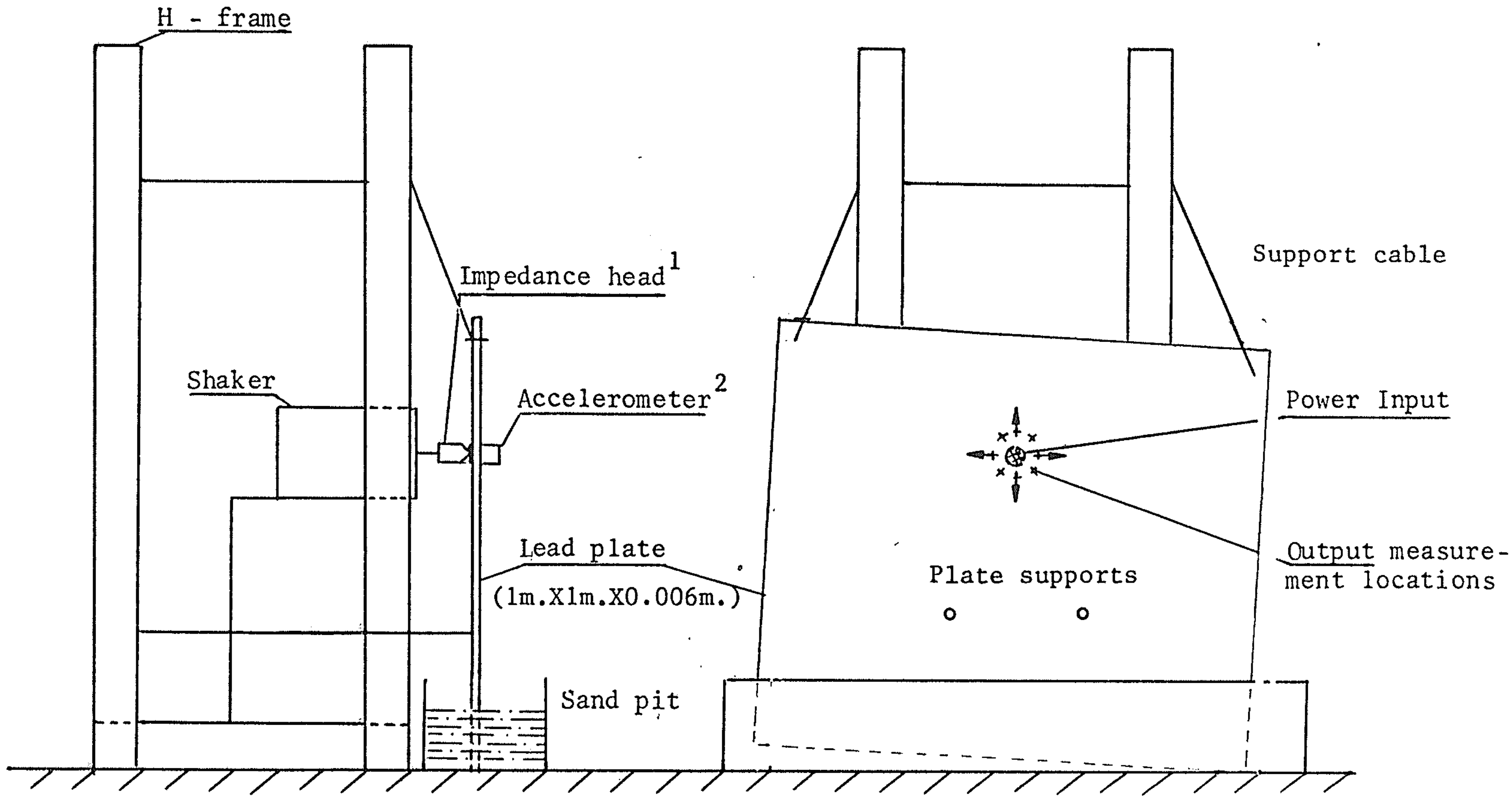

1. Bruel & Kjaer type 8001
2. Bruel & Kjaer type 4366

Figure4.4 Experimental setup

upper edge, to stabilize the panel and prevent it from "flapping". After installation, an unavoidable 5 degree tilt was observed relative to the horizontal so that the complete arrangement was not quite symmetrical.

A preliminary but important cross-check was performed by comparing the vibration power to the plate measured by using two different techniques. The power input was determined from the product of the force and velocity at the connection of the shaker assembly to the plate. The output was measured by using the two accelerometer arrangement. The two accelerometer probe was placed on the plate and located progressively at eight equispaced positions on a circle around the contact point as illustrated in Figure 4.4 Intensity levels were integrated along the segments associated with each measurement location and the total output power level was calculated. A comparison of the input and output levels is presented graphically in Figure 4.5. It can be seen that discrepancies of up to 5 dB occur at frequencies less than 50 Hz. but that there is good agreement otherwise. Thus, the employed spacing of 3 cm. between the probe's two accelerometers should be adequate for measurements at or above 63 Hz. However, the spacing between the accelerometers would have to be increased for measurements below 63 Hz. This comparison confirms the measurement capability of the two accelerometer technique.

The technique developed by Pavic [49] and modified by Verheij [54] was used to further check the power levels imparted to the plate. This procedure involved a linear array of four accelerometers and the

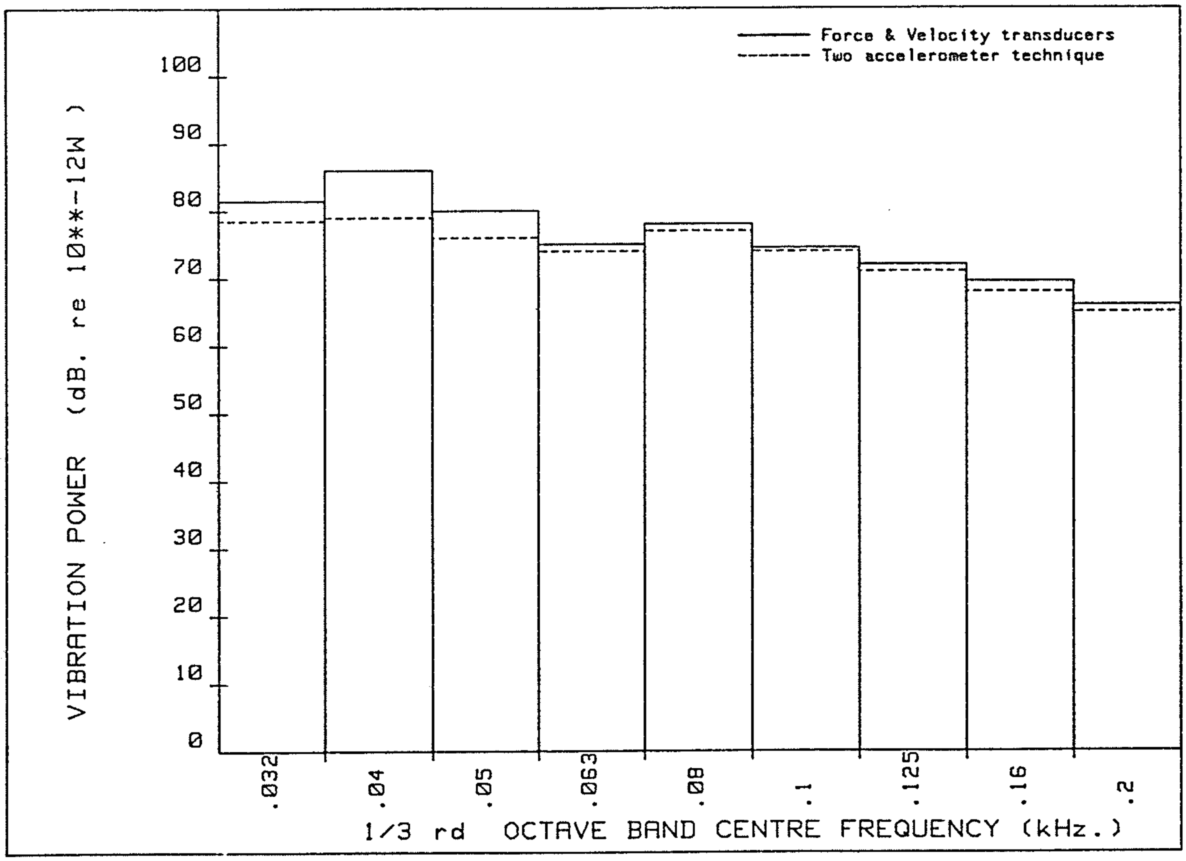

Figure 4.5 : Comparison of vibration power levels measured by using force/velocity transducers and the vibration intensity technique.

vibration intensity was calculated by using expression {4.29}. Once again, the switching technique was used to overcome phase mismatch between the accelerometer channels. A comparison of the vibration power levels determined by using the force/velocity transducer, two accelerometers and Pavic's four accelerometer technique is presented graphically in Figure 4.6. It can be seen from the figure that the input power agrees again with the values from Pavic's technique where a spacing of 3 cm. was employed between the accelerometers. There are significant errors, however, when the spacing between the accelerometers was only 2 cm. It would seem, therefore, that a spacing of 3 cm. is reasonable for measurements in the frequency range of 50 - 200 Hz. so that this spacing was invariably used.

The agreement between the power levels determined by using the various techniques is expected. Although the measurement locations on the circumference of a 5 cm. radius circle were in the far field, they were sufficiently close to the input that vibration losses were small. However, measurements made within a radius less than 4 cm. from the input yielded significant discrepancies of up to 10 dB. On the other hand, measurements on the circumference of a circle of radius 12 cm. from the input showed little deviation from the measured input. Consequently, it may be concluded that the reason for the discrepancy was the "near field" effect mentioned in the theory. Another interesting observation from these tests concerns Pavic's four accelerometer technique. Although this technique permits measurements in the near and far fields, there are serious practical problems associated with it.

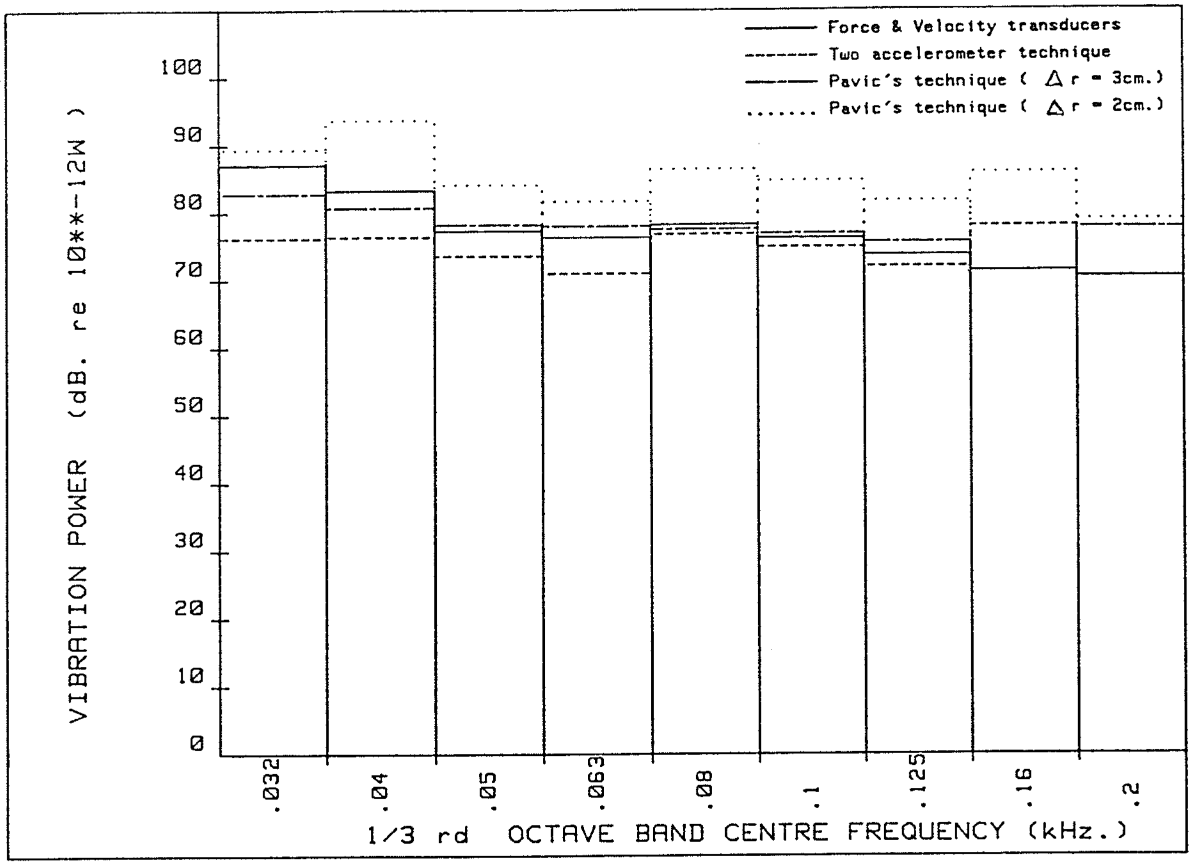

Figure 4.6 : Comparison of vibration power levels measured by using force/velocity transducers, vibration intensity and Pavic's technique with accelerometer spacings of 2 cm. and 3 cm.

First, it is thrice as time consuming as the two accelerometer technique because about 10 minutes is required typically per location for each vibration intensity vector component. Second, the increased physical length of the accelerometer array restricts the use of this procedure to large unencumbered surfaces which were generally not present on the computer. Third, the vibration intensity vector is no longer measured at a point so that the indistinct measurement location may limit the technique's use in locating vibration sources.

Further tests were performed on the lead plate to provide experience for the mapping and interpretation of the directions as well as the magnitudes of the intensity vectors. Consequently, 56 measurement locations together with a reference axes system were marked on the panel as illustrated in Figure 4.7. The two accelerometer probe was positioned at each location along the x-axis and then reversed through 180 degrees to measure the horizontal component of the net vibration intensity. In each case, switching was used to overcome phase mismatch between the accelerometer channels. Then a similar procedure was followed along the y-axis to determine the vertical component. The magnitude of the intensity vector is simply the resultant of these two components as indicated by equation {4.9}. This method was repeated at each location for the one-third octave bands centred between 63 and 100 Hz. Typical intensity patterns are presented in Figure 4.8 through 4.10.

Before considering the propagation paths, a cursory examination of the vibration energy away from the shaker coupling reveals several

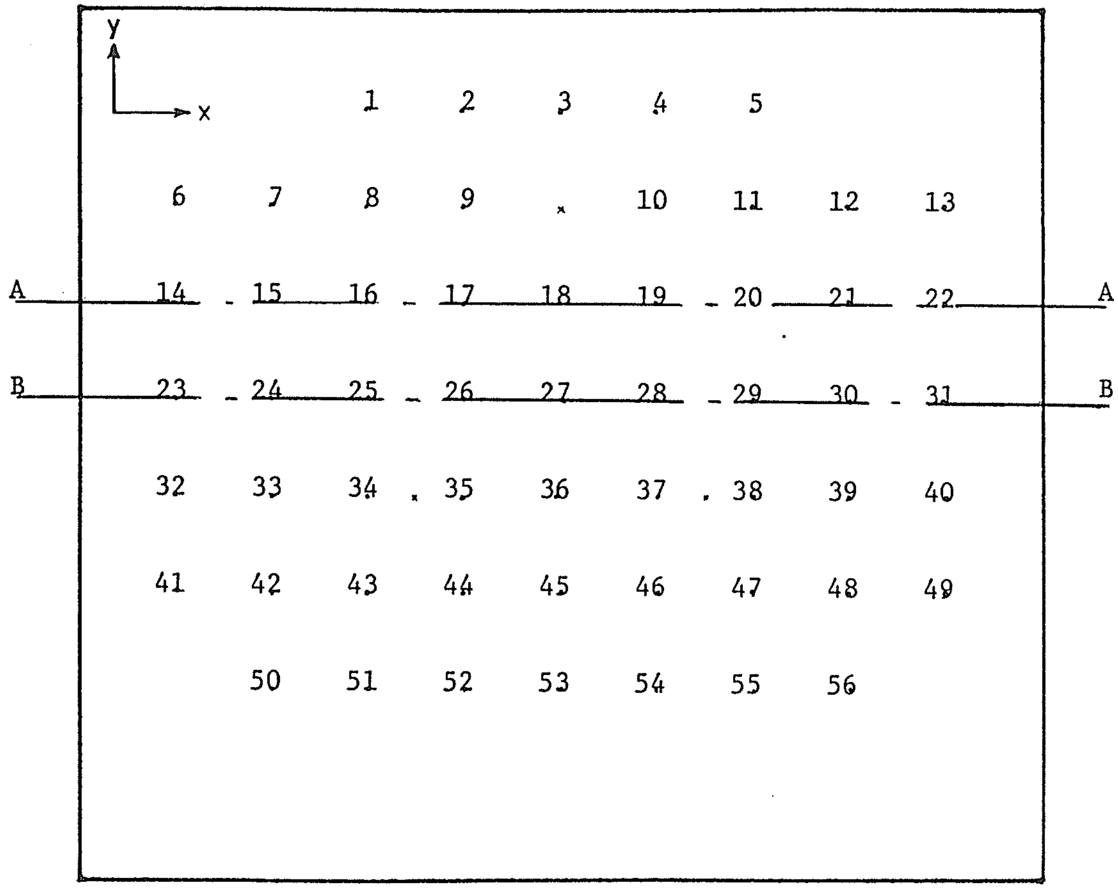

Figure 4.7 : View of lead plate with 56 measurement locations.

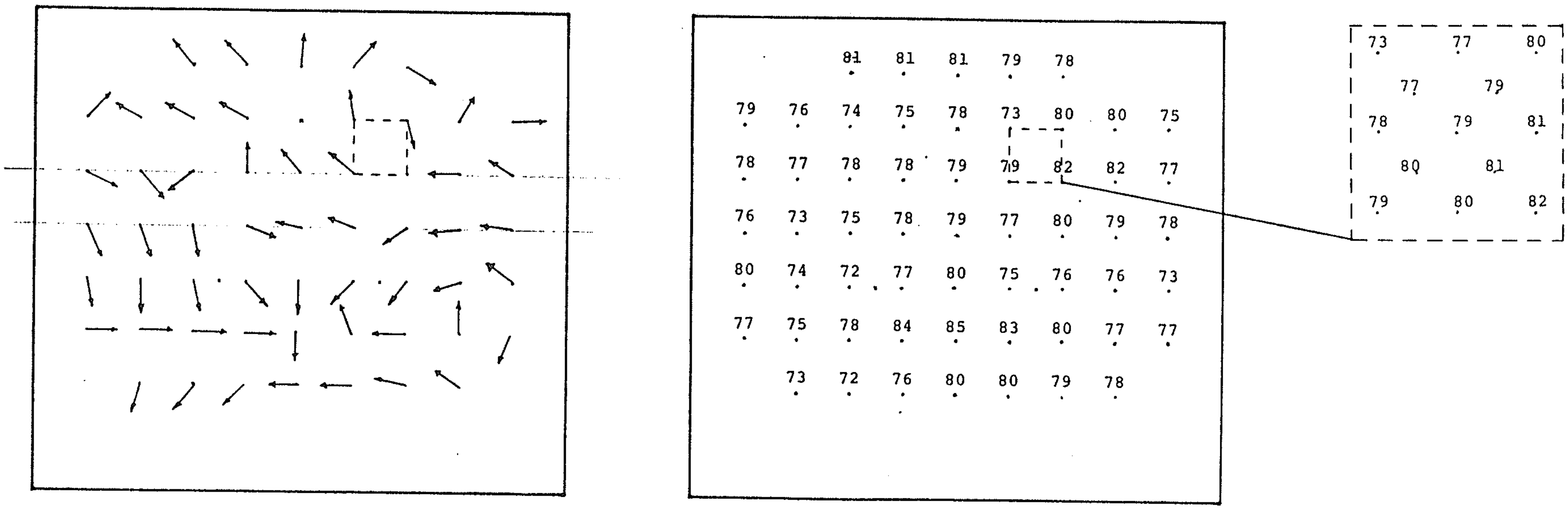

Intensity pattern

Acceleration levels

Closeup of acceleration levels within "circulation"

Figure 4.8 : One third octave band vibration intensity pattern and acceleration levels on lead plate at 63 Hz. centre frequency.

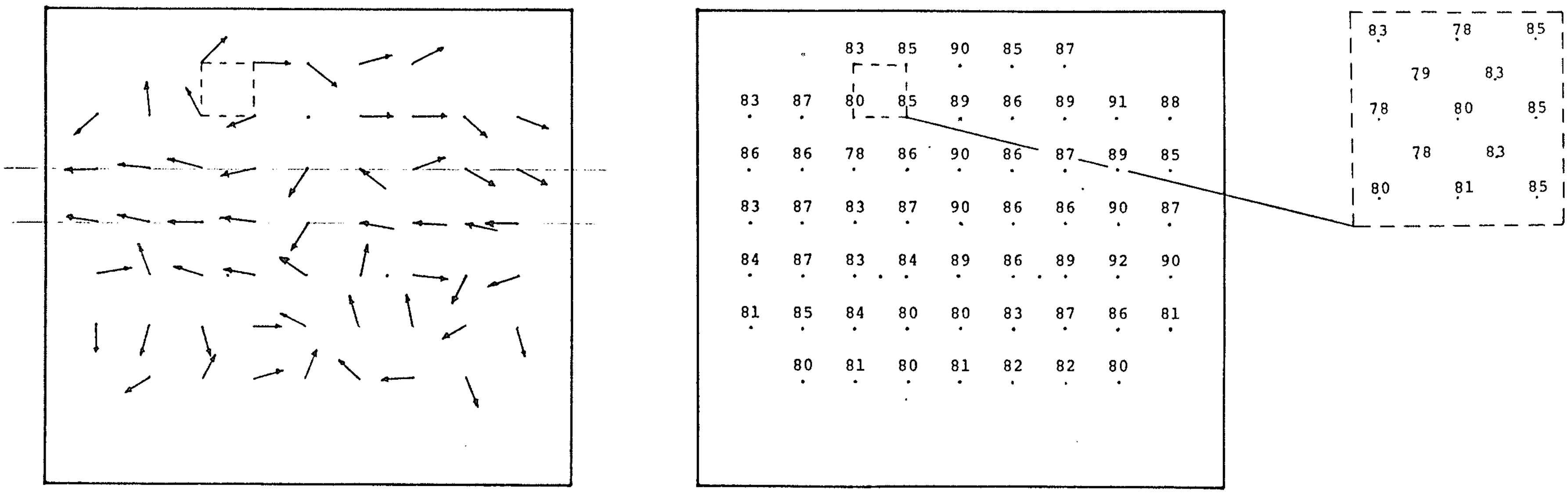

Intensity pattern

Acceleration levels

Closeup of acceleration levels within "circulation"

Figure 4.9 : One third octave band vibration intensity pattern and acceleration levels on lead plate at 80 Hz. centre frequency.

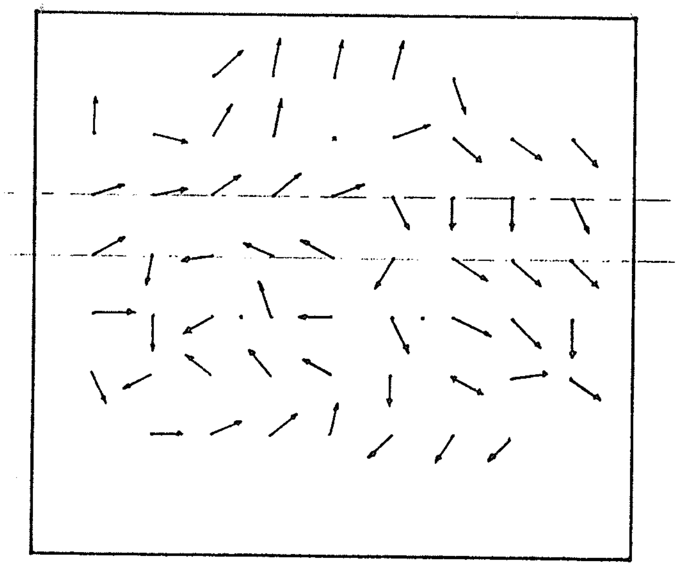

Intensity pattern

		80	77	78	76	78		
81	80	83	85	84	82	81	82	85
77	80	84	85	84	81	78	72	77
84	84	80	76	78	80	78	85	86
84	85	82	84	86	83	82	89	87
82	82	82	84	83	80	85	86	77
	80	80	83	81	80	79	82	

Acceleration levels

Figure 4.10 : One third octave band vibration intensity pattern and acceleration levels on lead plate at 100 Hz. centre frequency.

interesting phenomena. First, the total energy crossing sections AA' and BB' in Figure 4.8 through 4.10 generally agrees favourably with the input power. This result is not surprising because the energy should intuitively flow towards the vibration absorbing sand. The intensity directions in the lower plate regions generally corroborate this observation. There are discrepancies, however, of up to 14 dB at the sections listed in Table 4.1 . Such discrepancies may be caused by internal stresses within the plate due to the sagging under its own weight. Furthermore, several intensity vectors in Figure 4.8 through 4.10 are predominantly horizontal along sections AA' and BB'. Consequently, an energy balance in the vertical direction is likely to generate discrepancies because of the comparatively little energy flow there. This assertion may initially appear to contradict the intuitive direction of flow. However, the plate is two dimensional so that the vibration energy flows in both the x and y directions. The absorbing sand pit, however, is the only active vibration absorber and it is located distantly from sections AA' and BB'. Consequently, the "horizontal" component of the intensity vector has to "turn" through approximately 90 degrees to eventually flow towards the absorber. This feature is reflected in Figure 4.9 by the generally increasing magnitude of the vertical component of the intensity towards the bottom of the plate. Second, an inspection of the acceleration magnitudes in Figures 4.8 through 4.10 clearly shows that the energy usually flows from locations with high accelerations to ones with lower accelerations. The acceleration, of course, is proportional to the force so that the basic

One-third octave band Centre Frequency Hz.	Force and velocity transducer Input Power dB*	Input Power two accelerometer technique dB	Power across Section AA' dB	Power across Section BB' dB
63	67.7	71.0	71.9	73.9
80	78.2	76.8	75.9	64.0
100	76.2	74.9	66.6	73.0

* dB re 10^{-12} W.

Table 4.1 Energy balance across various sections of the lead plate. (Details of the calculations are shown in Appendix 4).

concept of energy flow from a point of higher to one with a lower potential is reinforced. Third, there exists a circulation or vortex type phenomenon which can be seen within the dotted boundaries of Figure 4.8 and 4.9. Accelerations recorded in a narrow grid within a vortex are also given in these figures for reference. However, no definite pattern is discernible in these regions. This phenomenon has been mentioned by Noiseux [51] who connected vortices with individual circulation cells. It is most probably due to edges initiating reflections which interfere locally with the original waves to produce the circulatory pattern. However, similar effects may also emanate from local stiffners (like those on the computer panels) or may indicate the overall flow from a source to a sink. Elaboration requires further detailed studies.

4.2.2 COMPUTER

After completing the tests on the lead plate, the two accelerometer probe was used to identify the computer's structureborne vibration paths in the 63 and 500 Hz. centred one-third octave bands. Sixteen measurement locations were marked on each of the left, right and top panels. These panels were relatively free of external attachments but the rear panel not only had 18 connector caps but also had the fan hood attached. Hence, somewhat more measurement locations were thought necessary on this panel due to its additional complexity. Unfortunately, the 4 cm. X 1 cm. dimensions of the probe were such that its location on the back was difficult because of the space restrictions between the connector caps. The size of the probe could not be reduced because its major dimension depends largely upon the necessary 3 cm.+ spacing between the accelerometers. Therefore, only the 18 locations shown in Figure 4.11 were employed.

Intensity vectors mapped on the exterior panels of the computer are shown in Figure 4.12. At first glance it would seem that the vectors are orientated randomly except, perhaps, towards the right of the top panel at locations 20, 24, 28, 32 in Figure 4.11. A close examination inside the computer revealed the presence of PCBs towards the left side panel with a void towards the right side. Consequently, the computer was not quite symmetrical about the vertical plane bisecting the top and bottom. Due to the consistent, recognisable pattern to the right of the top panel, it was suspected that vibration sources other than purely structural were present. They were thought to be associated with the internal air flow because the previous sound tests had highlighted the importance of this flow. Therefore, it was considered necessary to determine the magnitude of the airflow induced vibrations and to compare these levels with the structureborne vibrations generated mechanically by the fan. Consequently, the following three configurations were adopted. The development computer was 1) in its original configuration; 2) with the rear panel isolated from the cabinet by polyurethane foam to minimise the drop in the internal static air pressure; and 3) as in case (1) but with internal components removed so that the air could be ducted by using a polythene tube

+The fundamental wavelength on the lead plate and the computer panels in a given direction are comparable. Hence the spacing of 3 cm. between the accelerometers is still reasonable.

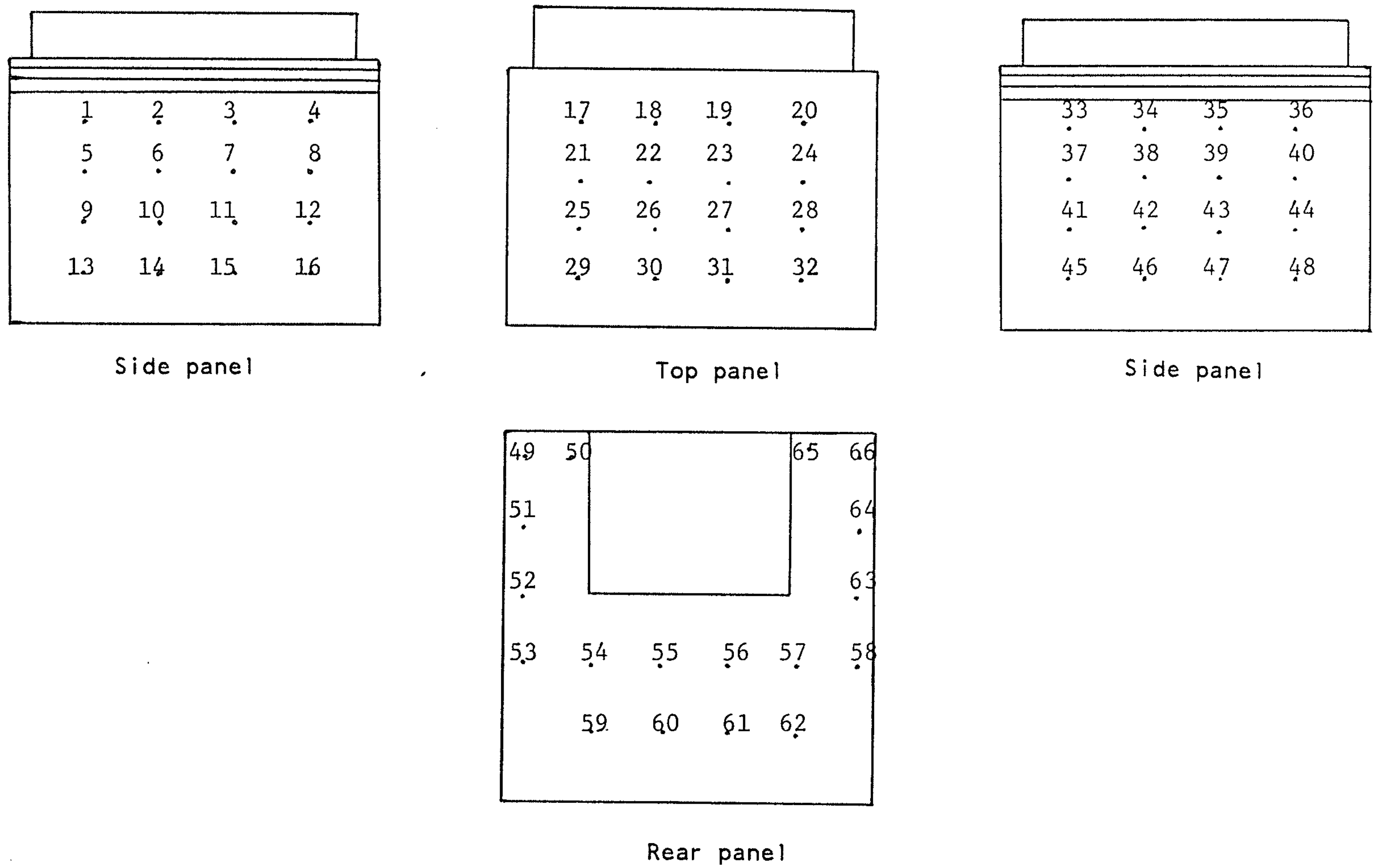

Figure 4.11 : Exploded view of computer showing 66 measurement locations.

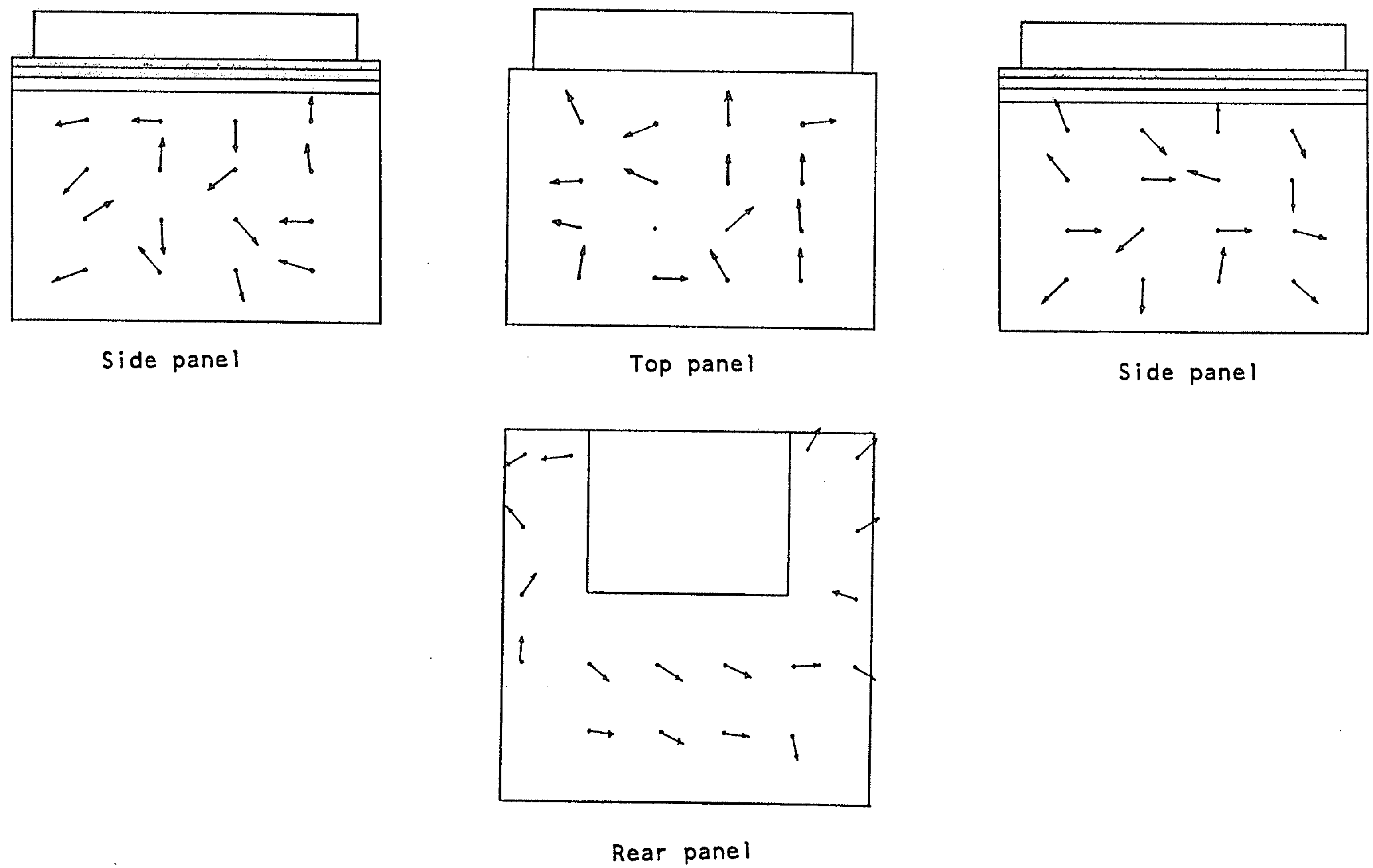

Figure 4.12 : One third octave band vibration intensity pattern on computer cabinet at 63 Hz. centre frequency with fan running.

from the front entrance directly to the exit at the rear of the computer. These assemblies respectively and reasonably simulated a combination of air and fan induced vibrations, largely airflow induced vibrations and, finally, almost a purely fan induced mechanical vibration. The ensuing accelerations are presented in Figure 4.13 through 4.16. The predominant features of all these figures may be subdivided into three main groups. First, there is a generally increasing acceleration level up to about 160 to 200 Hz. Second, a peak occurs around 160 to 200 Hz. and, third, the spectra are relatively horizontal above 250 Hz. In Figure 4.16, however, there is also a pronounced peak in the area of 50 to 63 Hz. on the rear panel. This peak corresponds to the fan's operating frequency of 3250 rpm or 54.12 Hz. which, due to the resolution of the one-third octaves, is observed in two frequency bands. Furthermore, the acceleration levels at frequencies below 50 Hz. increase dramatically by up to 15 dB with the back panel isolated - thereby implying a "resonant condition". This increase happens at substantially lower frequencies (below 50 Hz.) than on the other panels. The frequency response function shown in Figure 3.2d shows the fundamental resonant frequency of the back panel to be 64 Hz. Consequently, the increase seems to be due to the greater flexibility of the back panel because of the isolation. Therefore, it is reasonable to suggest that the response of the back panel is primarily stiffness controlled at frequencies below about 80 Hz. Consequently, it would be beneficial there if the excitation imparted to the rear by the fan could be reduced by redesigning the fan mounts to provide better isolation. Furthermore, the rear panel may also be isolated better from the cabinet by using an improved EMI seal and

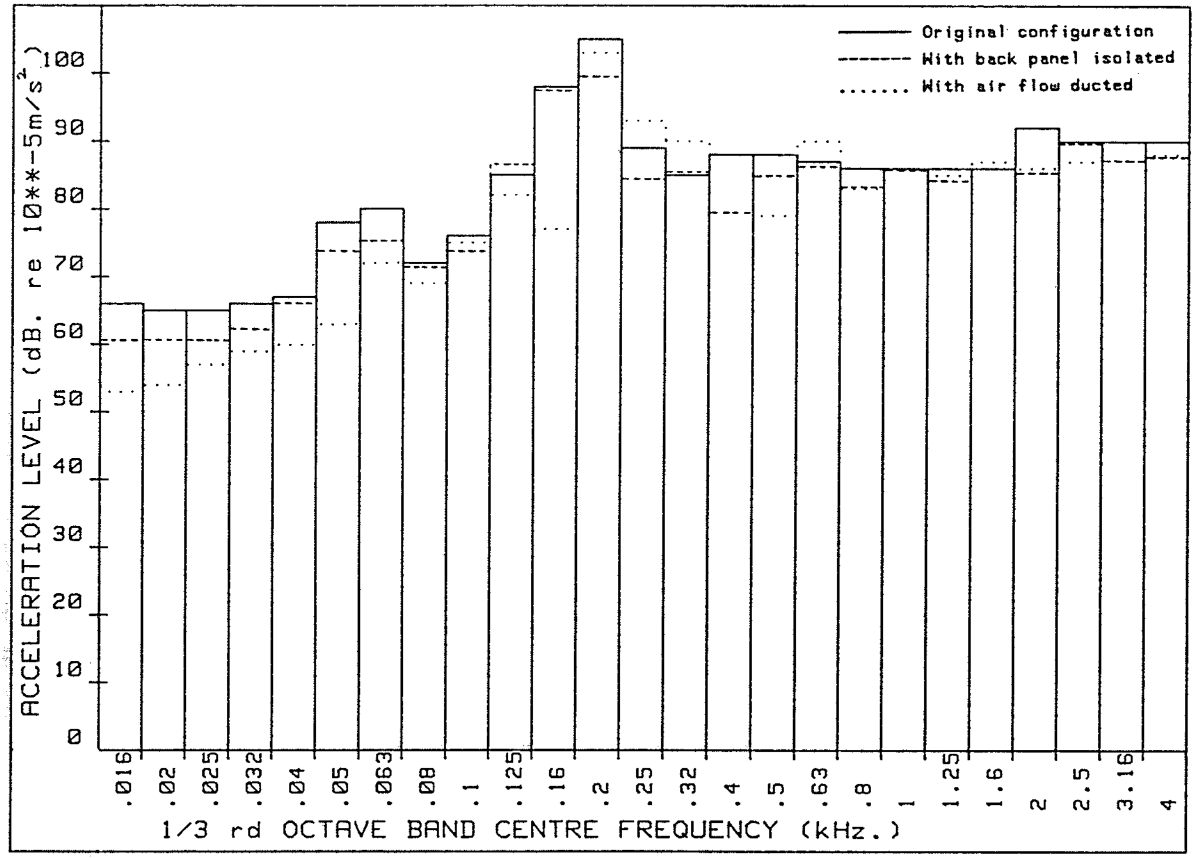

Figure 4.13 : One third octave band accelerations at centre of left side panel of computer.

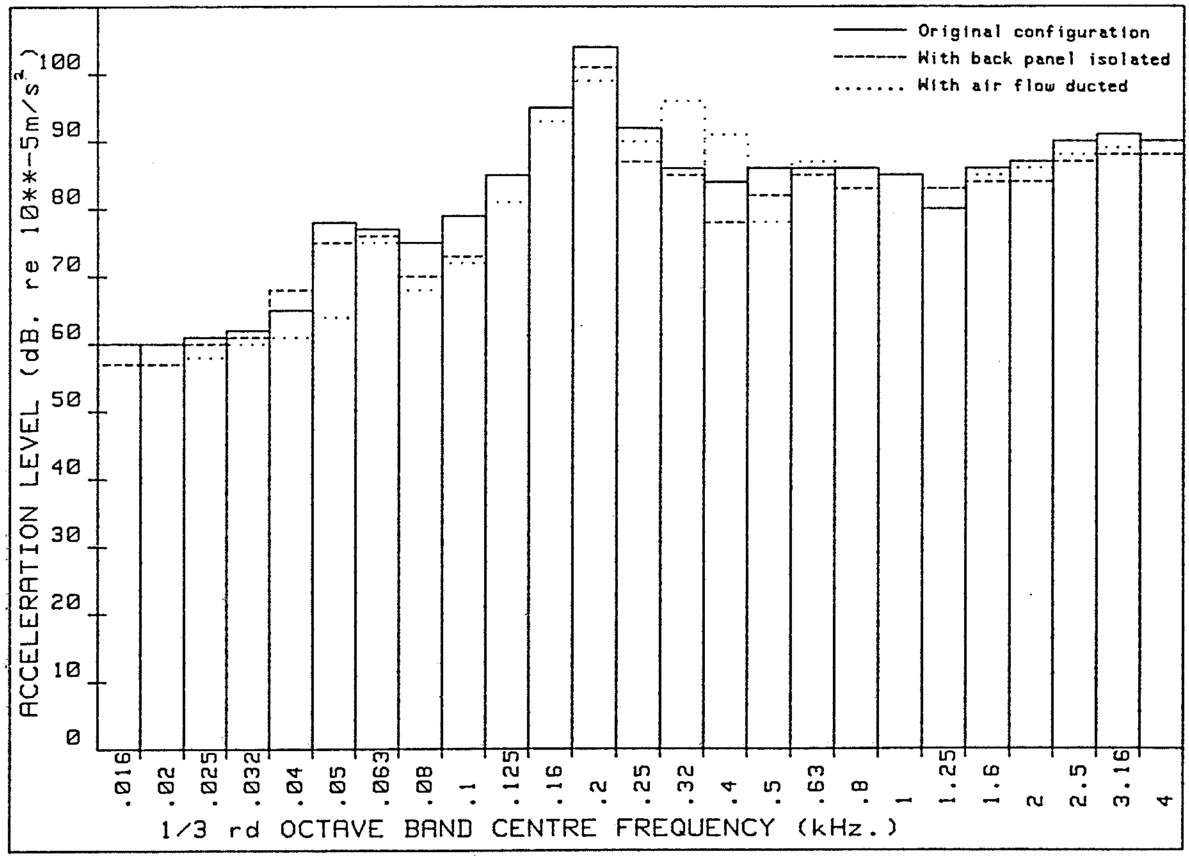

Figure 4.14 : One third octave band accelerations at centre of right side panel of computer.

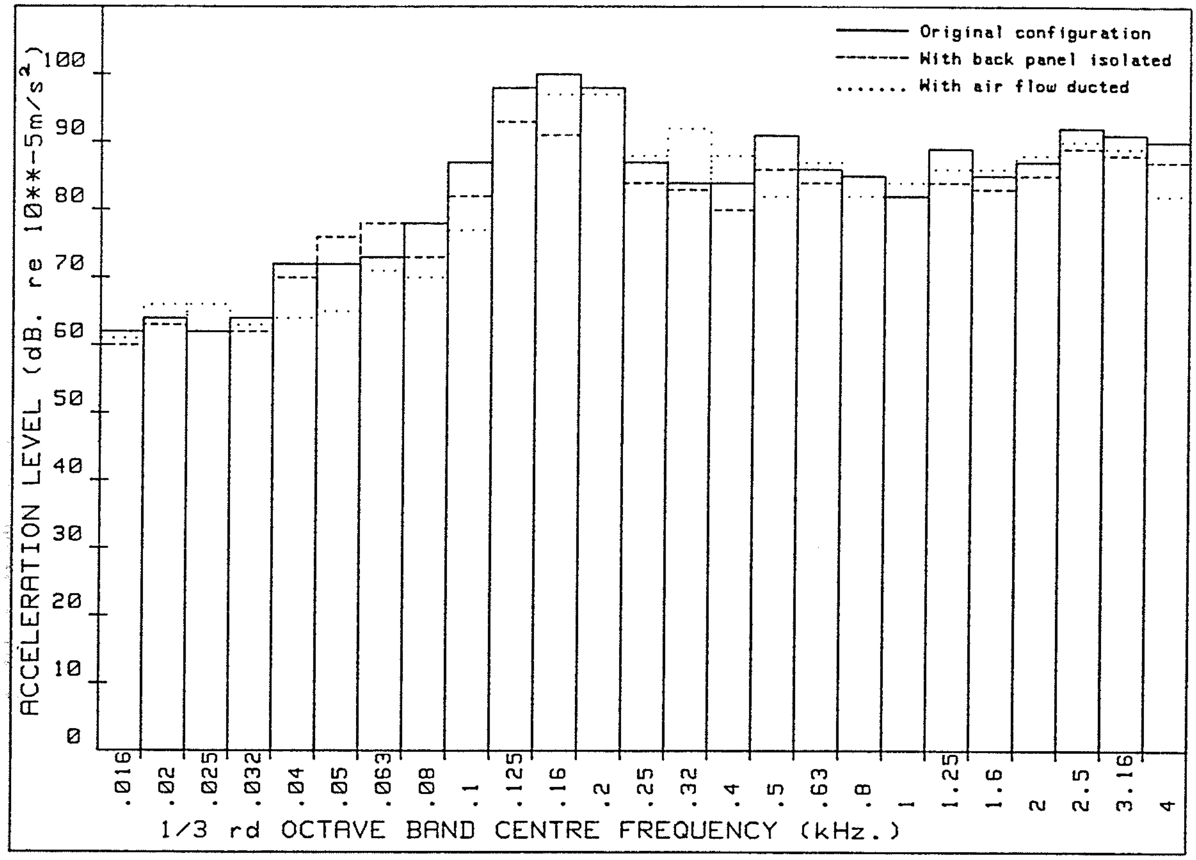

Figure 4.15 : One third octave band accelerations at centre of top panel of computer.

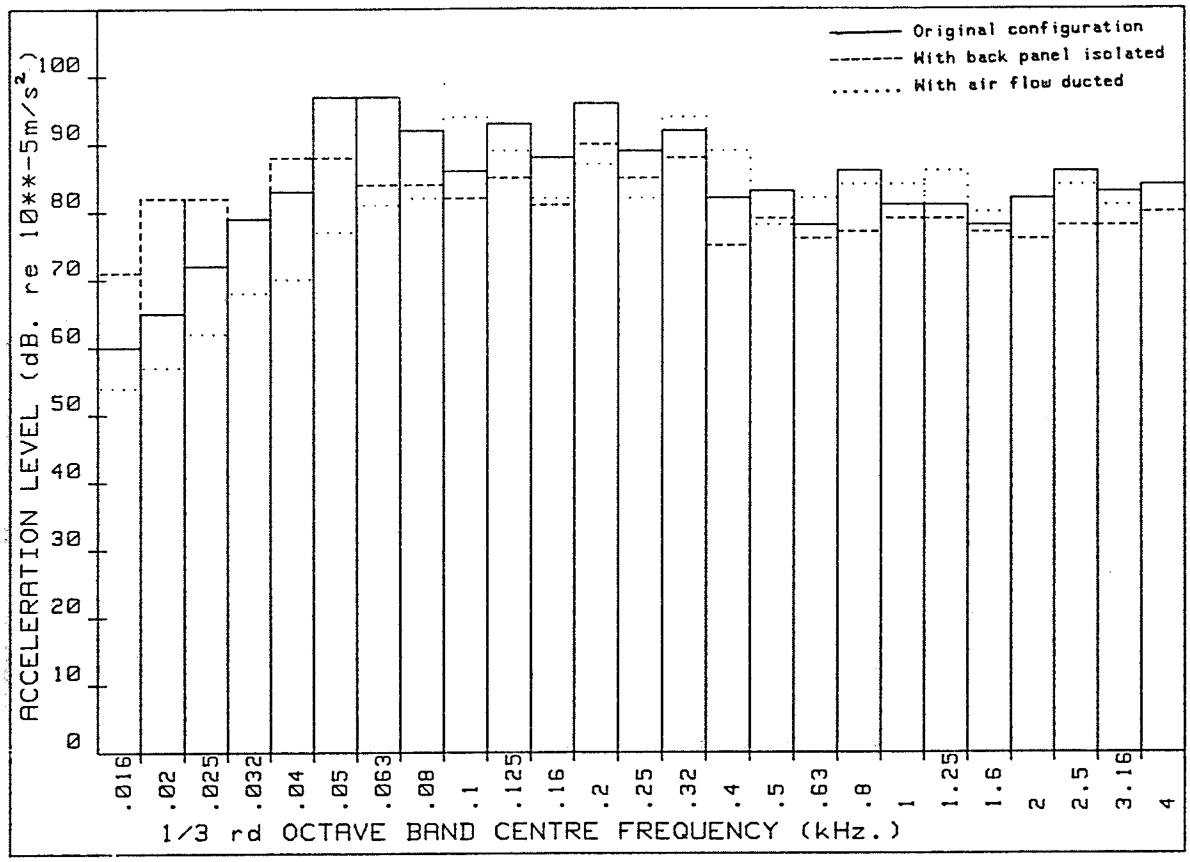

Figure 4.16 : One third octave band accelerations at centre of rear panel of computer.

eliminating the direct vibration transmission through solid screws. The second salient feature of Figure 4.13 through 4.16 is the further and greater peak occurring around 160 to 200 Hz. Virtual elimination of the airflow marginally lowers the peak so that it appears to be influenced largely by structural factors. From Figure 3.2b and 3.2d it is clear that this peak is a structural resonance dictated by the computer's top/back panel. The frequency region above about 250 Hz. is uniformly resonant with structural interactions between the interior and exterior panels possibly coming into play. Good correlation between the sound power measured by the surface velocity and acoustic intensity techniques supports this hypothesis because the sound radiated from about 500 to 2000 Hz. is largely due to structural vibrations of the cabinet. However, components within the computer may influence this behaviour to some degree. Consequently, the structural properties of internal components were analysed in detail by utilising the Impulse Technique again [42]. The instrumented hammer was used to impact the components whose responses were detected with an accelerometer. Each acceleration was normalised automatically with respect to the magnitude of the impact by the spectrum analyser. Typical normalised frequency response functions are shown in Figure 4.17a through 4.17g. It can be seen that there are invariably peaks in the 500 Hz. region which correspond to resonant structural frequencies of the PCB chassis, cards and cross members etc. The following sections draw upon the salient features of Figure 4.13 through 4.16 and Figure 4.17a through 4.17g to explain the results obtained by using the two accelerometer vibration

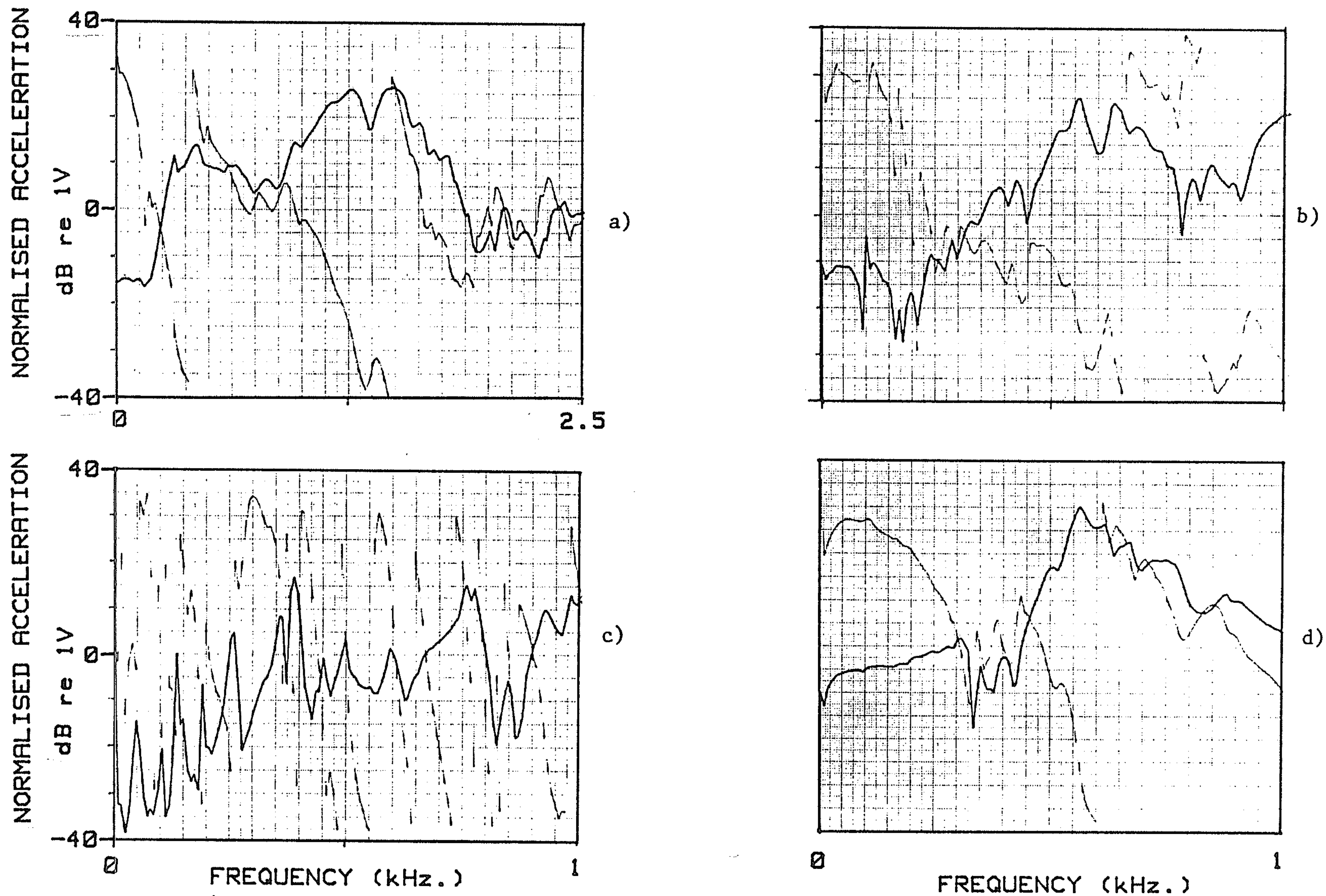

Figure 4.17 : Frequency response function obtained by using the impulse technique. [42]

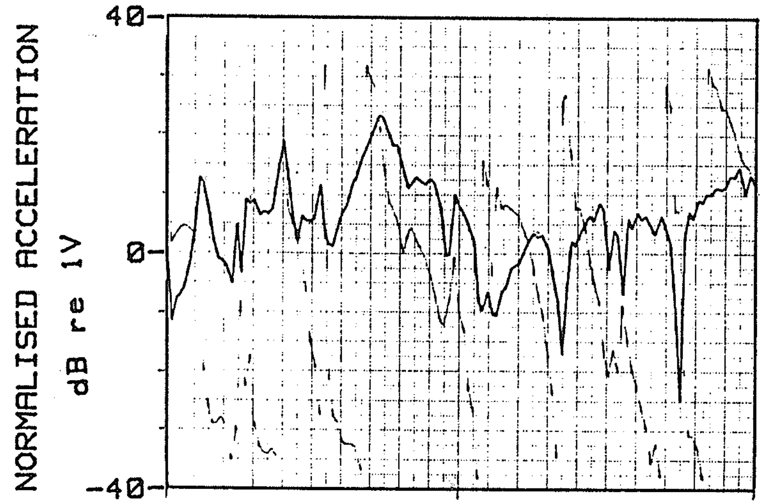

e)

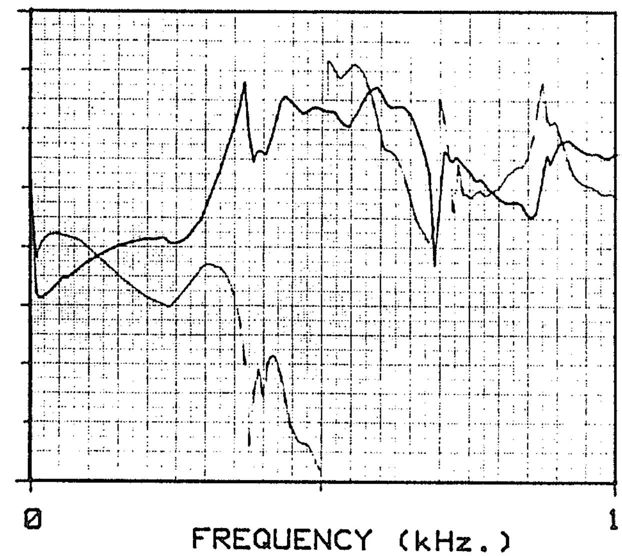

f)

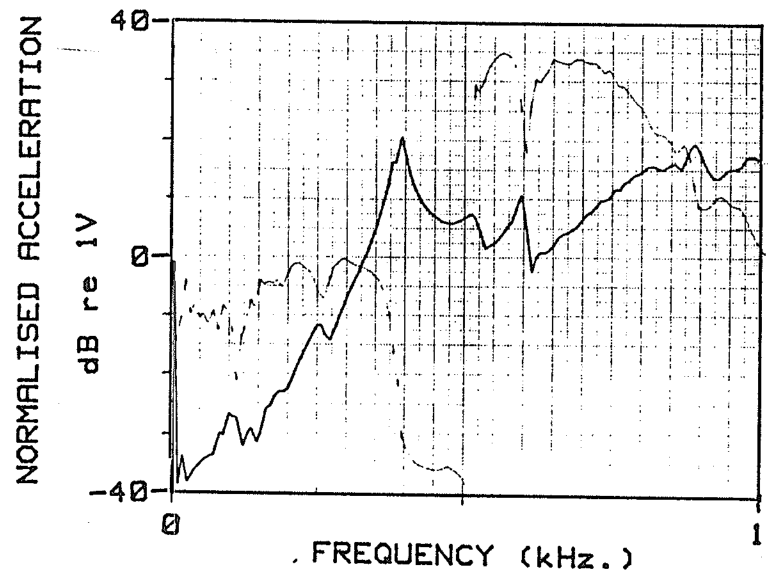

g)

<u>KEY:</u>

a) Cross panel at base of PCB chassis.
b) PCB cross member (z- direction).
c) Cross transfer function of PCB chassis and PCB.
d) PCB cross member (x-direction).
e) PCB
f) Front display panel.
g) Panel on PCB chassis.

intensity technique.

Comparing accelerations of different computer configurations at the same location (Figure 4.13 through 4.16), it is clear that at frequencies less than 100 Hz. the air flow induced vibration levels generally exceed those generated purely mechanically by the fan by up to 12 dB (re 1 E -5 m/s^2). Consequently, it is not surprising that the intensity patterns seem to be behaving randomly in Figure 4.12 because the primary source is the turbulent air which strikes the panels haphazardly. To corroborate the importance of the air flow in generating structureborne vibrations, it was necessary to examine the vibration intensity patterns in the one-third octave band centred at 63 Hz. in the absence of air flow. Thus, an external vibration source devoid of any air flow was required. The primary objective was to simulate purely the mechanical forcing of the fan at the rear of the computer. Consequently, the computer was clamped to the base of an essentially rigid table with a shaker attached to the fan hood as shown in Plate P3.1. The vibration was transmitted mechanically to the computer through a weak spring to produce a force-like excitation. The white noise input to the shaker was filtered through a one-third octave band centred at 63 Hz. to reasonably simulate the main frequency characteristics of the fan. The internal configuration of the computer, now without power, was similar to that used in the previously described air flow experiment. Once again, vibration intensities were measured at the same locations and the resulting intensity patterns are given in Figure 4.18. The vibration energy now flows towards the front right of the computer on the top panel. The right half of the top panel has a transmission path fairly similar to that shown in Figure 4.12 where air was flowing internally. However, the intensity pattern on the left half of the top panel has changed quite appreciably. This discrepancy corroborates the earlier conclusion that the air flow does, indeed, act as a vibration source at locations where air strikes the panels. For example, Figure 2.9 shows the air flow path within a symmetrical computer. However, due to the asymmetrical construction of the development computer with the presence of PCB's on the left side of the interior chassis, the impact of the air is restricted to locations 17,18,21,22,25, 26 shown in Figure 4.11. Furthermore, it can be seen from Figure 4.18 that there is generally a net flow of vibration energy from the top edge of the right panel towards the computer's base. Indeed, it is clear that on the lower half of the rear panel there is a net energy flow towards the base of the computer. This is not surprising because the computer's mounting to the table is through solid angle brackets which provide good transmission to the table. However, there is a net flow towards the hood area in the upper half of the rear panel. A similar behaviour can also be seen in Figure 4.18 at the top left corner of the right panel (at locations 41,25,46 in Figure 4.11). This evidence clearly corroborates the obvious that the fan and hood assembly is the source of vibration. It appears that structureborne transmission of energy occurs as a result of the hood pivoting about the upper edge

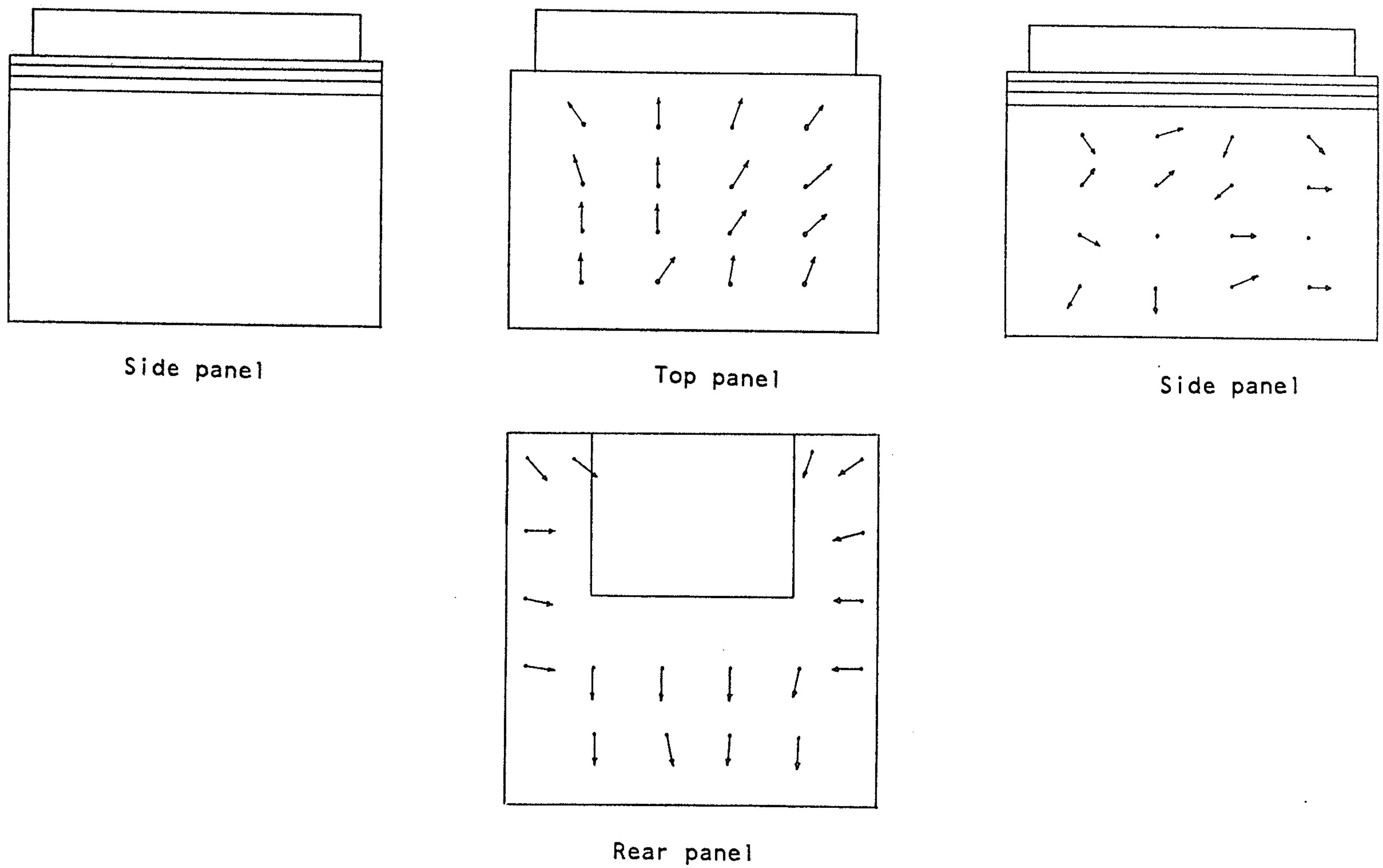

Figure 4.18 : One third octave band vibration intensity pattern on computer cabinet at 63 Hz. centre frequency with external excitation and no air flow.

of the cabinet which is known to be quite stiff. Some energy is transmitted from the hood to the top panel. Indeed, the flow pattern in Figure 4.18 suggests good structureborne vibration transmission from the rear to the top panel despite the intervening EMI seal. The structureborne path is presumably through the unisolated screws which attach the rear panel to the cabinet. Consequently greater consideration should be given here to better vibration isolation. Vibration energy is also transmitted to the computer's base through the lower half of the back panel. It seems that there is virtually no horizontal energy transmission from the area of the fan/hood to the rear panel. This might explain the "inflow" of energy from the side panels to the top half of the back panel. It would be prudent to stiffen the back to alleviate the "pivoting" action of the fan. It has been possible to identify this "pivoting" action with the aid of the flow pattern provided by the vibration intensity technique. Previous tests [55] relied solely on accelerations. Although high accelerations were observed at the centre of the rear panel, it was thought they were merely due to the rear panel's greater flexibility. The vibration intensity technique has shown a more detailed and detrimental consequence of this flexibility.

In summary, the vibration intensity pattern on the development computer in the 63 Hz. one-third octave band indicates a net flow of energy from the fan area to the top panel and also to the lower half of the rear panel. However, a small part of the structureborne energy flows to the side panels and re-enters the rear panel in its upper half. This intensity pattern is severely distorted by the flow of air through the computer's interior. Acceleration measurements on the computer cabinet have shown that the airflow induced vibration contributes significantly to the overall vibration levels in Figure 4.13 through 4.16. Thus, locations where the air stream impacts the panels of the cabinet act as vibration "sources". Consequently, the airflow within such machines must be examined carefully so that the airflow induced structureborne vibrations may be reduced.

Finally, vibration intensities were determined to identify the structureborne paths in the one-third octave band centered at 500 Hz. They are shown in Figure 4.19. At those locations were the internal PCB chassis is mounted directly to the external cabinet (locations 17,33,35,37,39 in Figure 4.11) the intensity pattern is distorted from its expected downward flow. This phenomenon occurs because internal computer components have structural resonances in the range 400 to 600 Hz. which, presumably, the air stream excites. This resonant energy is then transferred to the rest of the computer by the solid contacts. Consequently, locations where the internal PCB chassis is mounted on the cabinet essentially act as vibration "sources". This observation was corroborated by their acceleration levels which were up to 4 dB higher than elsewhere.

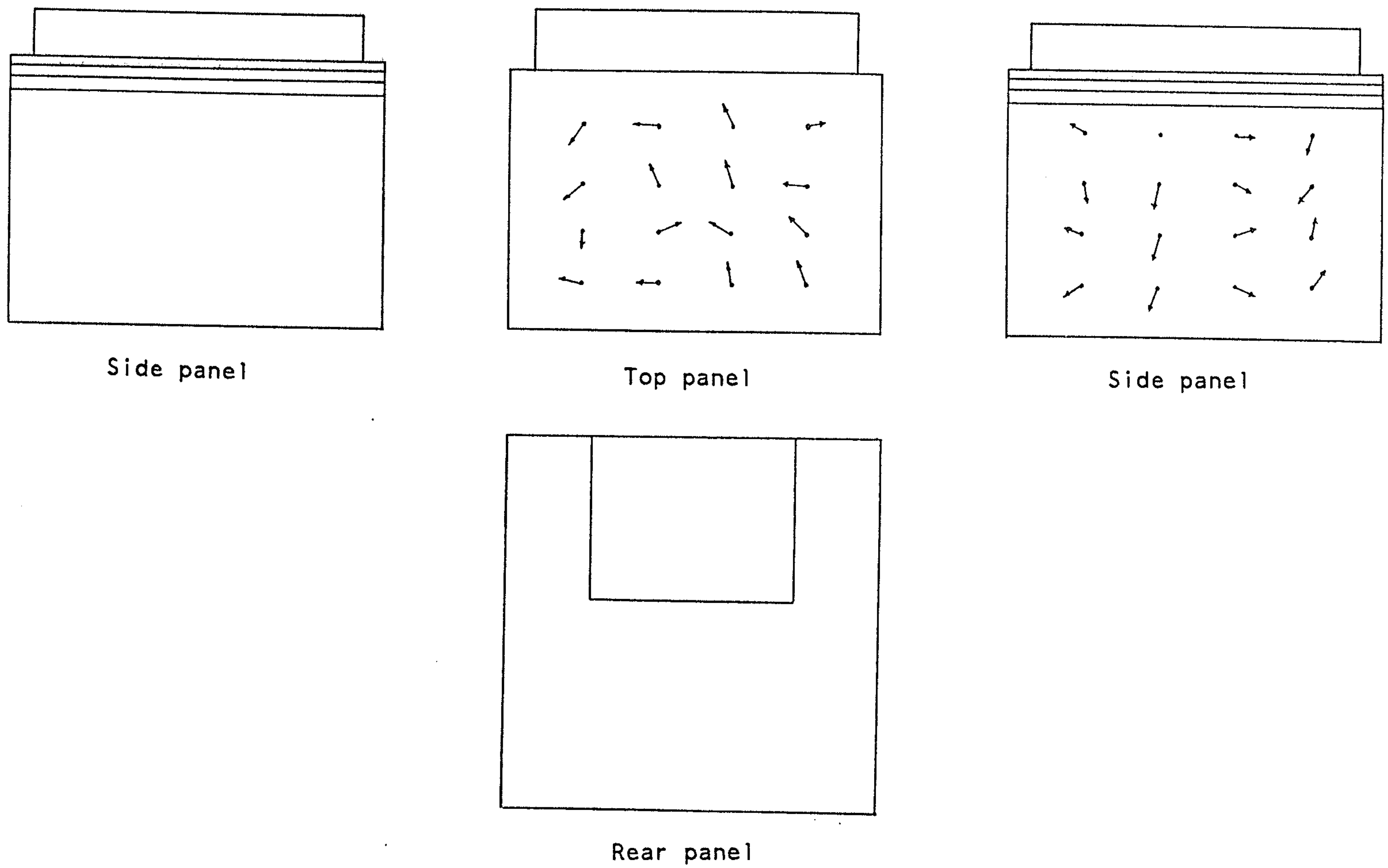

Figure 4.19 : One third octave band vibration intensity pattern on computer cabinet at 500 Hz. centre frequency with fan running.

4.3 CONCLUSIONS

Good correlation was established in Chapter III betwen the vibrating computer and the sound radiated in the octave bands centred from 500 to 2000 Hz. It was based primarily upon the assumption that the exterior panels could be idealised as a set of incoherent sound sources each moving fundamentally in a breathing mode. Furthermore, air flow noise was neglected. This last assumption was reasonable because the predominant source above about 200 Hz. was from structural resonances excited essentially by the mechanically mounted fan. Therefore, the correlation should not be surprising because similar agreement has been reported [40] for an engine with a comparable configuration involving one quite flexible (rear) panel. The rear panel has been shown to be the major cause of high structureborne vibration levels. The accompanying change in the computer's volume effectively generates much of the airborne sound too.

The vibration intensity technique has been shown to have good potential in solving vibration problems. Based upon the results of this study, the following recommendations may be made in order of priority. First, the air flow within the computer has to be modified to reduce both the airborne and structureborne noise. Second, the fan mounts need to be redesigned to give better isolation. Third, internal components and the PCB chassis should be isolated from the cabinet to reduce structureborne transmission caused by resonances of the internal components. Finally, the rear panel needs to be stiffened, particularly around the central portion to alleviate the pivoting action of the fan and hood assembly.

REFERENCES

1. S. Temkin 1981 Elements of Acoustics. John-Wiley and Sons.

2. D.A.Blaser, D.A.Feldmaier 1982 Engine noise - Kamal & Hickling. Plenum Press 247-278. Acoustic intensity measurement of noise emission from engines.

3. L.L.Beranek 1960 Noise Reduction. McGraw Hill.

4. M.J.Crocker 1982 Engine noise - Kamal & Hickling. Plenum Press. 279 - 311. Comparison between surface intensity, acoustic intensity and selective wrapping noise measurements on a diesel engine.

5. J.E.Cunningham 1982 NSERC brief #E 831072. Overview of the measurement of sound power over the last ten years.

6. T.Reinhart, M.J.Crocker 1980 Inter-noise, Florida U.S.A. 1129 - 1132. A comparison of noise source identification techniques on a diesel engine.

7. Bruel & Kjaer Application note # 1-0430062-2A

8. H.F.Olson 1932 U.S. Patent # 1892644. System responsive to the energy flow of sound waves.

9. C.W. Clapp, F.A. Firestone 1941 J.Acoust. Soc. Am. 13, 124-136. The Acoustic Wattmeter - an instrument for measuring sound energy flow.

10. R.W.B. Stephen 1966 Acoustic and Vibrational Physics, Edward Arnold Publishers Ltd.

11. L.L. Beranek 1949 Acoustic Measurements. John-Wiley and Sons.

12. S. Baker 1955 J.Acoust. Soc. Am. 27 #2, 269-273. An acoustic intensity meter.

13. G. Krishnappa 1981 J. Acoust. Soc. Am. 69 #1, 307-310. Cross spectral method of measuring acoustic intensity by correcting phase and gain mis-match errors by microphone calibration.

14. J.J. Kowalewski 1983 Canadian Acoustics 11, 25-36. Noise source identification - Acoustic intensity technique.

15. G. Pavic 1977 Journal of Sound and Vibration 51, 533-545. Measurement of sound intensity.

16. F.J. Fahy 1977 J. Acoust. Soc. Am. 62 #4, 1057-1059. Measurement of acoustic intensity using the cross spectral density of two microphone signals.

17. G. Rasmussen, M. Brock 1983 proc. 11 International Congress on Acoustics, Paris 6, 177-180. Transducers for intensity measurements.

18. J.K. Thompson, D.R. Tree 1981 Journal of Sound and Vibration 75 #2, 229 - 238. Finite difference approximation errors for acoustic intensity measurements.

19. P.M. Morse, K.V. Ingard 1968 Theoretical Acoustics McGraw-Hill, New York.

20. J.Y. Chung, J. Pope 1978 Inter-noise '78, San Francisco 893-899. Practical measurement of acoustic intensity - the two microphone cross spectral method.

21. J.Y. Chung 1977 J. Acoust. Soc. Am. 64, 1613-1616. Cross spectral method of measuring acoustic intensity without error caused by instrument phase mismatch.

22. D.A. Blaser, J.Y. Chung 1978 Inter-noise '78, San Francisco 901 - 908. A transfer function technique for determining the acoustic characteristics of duct systems with flow.

23. Bruel & Kjaer information booklet # 3-044-0029-2A.

24. Sperry Test procedure # PX-72000 -6862 Rev A.

25. Hewlett Packard model 3582A dual channel spectrum analyser user's manual.

26. N. Popplewell 1984. Lecture notes for Noise-Control University of Manitoba.

27. J.Y. Chung, D.A. Blaser 1981 SAE paper # 810396. Recent developments in the measurement of acoustic intensity using the cross spectral method.

28. R.J. Alfredson 1977 Noise-Control '77, Hampton Virginia 307-318. A new technique for noise source identification of a multi-cylinder automotive engine.

29. T.H. Hodgson 1977 J. Acoust. Soc. Am. 61 #2, 487-493. Investigation of the surface acoustical intensity method for determining the noise sound power of a large machine in-situ.

30. C.H. Hansen, D.A. Bies 1979 Journal of Sound and Vibration, 62 #1, 93-110. Near field determination of the complex radiation efficiency and acoustic intensity distribution for a resonantly vibrating surface.

31. O.K.O. Petterson 1979 Journal of Sound and Vibration 66 #4, 626-629. A procedure for determining the sound intensity distribution close to a vibrating surface.

32. G. Hubner 1973 J. Acoust. Soc. Am. 54 #4, 967-977. Analysis of errors in measuring machine noise under free field conditions.

33. B.G. van Zyl, F. Anderson 1975 J. Acoust. Soc. Am. 57 #3, 682-686. Evaluation of the intensity method of sound power determination.

34. G.C. Maling Jr., M.G. Clark 1983 inter-noise '83 111-114. Prediction of sound power level and sound pressure levels radiated by computer frames.

35. Bruel & Kjaer Application note # 1-0430023-1A.

36. Bruel & Kjaer Application note # Bo-00192-0430019-1A.

37. G. Porges 1977 Applied Acoustics. John Wiley and Sons, New York.

38. M.C. Junger, D. Feit 1972 Sound, Structures and their interaction MIT Press.

39. L.L. Beranek 1971 Noise and Vibration Control, McGraw Hill, New York.

40. N. Kojima, M. Fukuda 1983 11th. International Congress on Acoustics, Paris, 5, 259-262. Acoustic radiation from vibrating wall of engine.

41. N. Kojima et al. 1981 Bulletin of the JSME, 24 #3, 1233-1238. Estimation of noise emitted by the vibration of a plate.

42. D.L. Brown 1982 Sound and Vibration 1-6. Modal Analysis - Past, Present, Future.

43. C.J. Hemond Jr, 1983 Engineering Acoustics and noise control. Prentice-Hall.

44. T. ten Wolde 1978 Inter-noise '78 San Francisco 901-908. On the measurement of source strength of large industrual sources.

45. M.E. Wang, M.J. Crocker 1978 Inter-noise '78, San Francisco 375-382. Recent applications of coherence techniques for noise source identification.

46. A.F. Seybert 1980 Inter-noise '80, Florida 1067-1070. Source characterization using acoustic intensity measurements.

47. F. Laville et al 1980 Inter-noise '80. Florida 1083-1085. Sound power determination using intensity measurements under free field conditions.

48. S. Kumar, N.S. Srivastava 1975 J. Acoust. Soc. Am. 57 #4, 769 - 772. Investigation of noise due to structural vibrations using cross correlation technique.

49. G. Pavic 1976 Journal of Sound and Vibration 49 #2, 221 - 230. Measurement of structureborne wave intensity, part 1, formulation of the method.

50. G. Pavic 1976 PhD thesis, University of Southampton. Techniques for the determination of vibration transmission mechanisms in structures.

51. D. U. Noiseux 1970 J. Acoust. Soc. Am. 47 #1 238-247. Measurement of power flow in uniform beams and plates.

52. P. Rasmussen, G. Rasmussen 1983 proc. 11 International Congress on Acoustics, Paris, 6, 231-234. Intensity measurements in structures.

53. P. Rasmussen Bruel and Kjaer internal document, based on reference 52. Measurement of vibration intensity.

54. J.W. Verheij 1980 Journal of Sound and Vibration, 70 #1, 133-139. Cross spectral density methods for measuring structureborne power flow on beams and pipes.

55. A. Chawla, E. Semercigil and A. Fathi 1983. Structureborne tests on Sperry computers, Internal report, University of Manitoba.

56. T. Lahti 1983 proc. 11 International Congress on Acoustics, Paris, 5, 365-368. Two channel FFT analysis applied to transmission measurements.

57. S. Czarneki et al 1980 Inter-noise '80, Florida U.S.A. 1125 - 1128. Modal investigations on the identification of airborne and structureborne sounds.

58. M.J. Crocker et al 1980 Inter-noise '80. Florida 741-746. Measurement of transmission loss of panels by an acoustic intensity technique.

59. P. W. Keyte et al 1983 proceedings 11 International Congress on Acoustics, Paris, 5, 285-288. The measurement of sound transmission along bars and hydraulic pipes.

60. I. Yoshihiko. T. Shigeru 1978 Inter-noise '78 San Francisco 789 - 794. Structureborne noise transmission in steel structure like ship.

61. A.F. Seybert, D.F. Ross 1977 J. Acoust. Soc. Am. 61 #5. 1362-1370. Experimental determination of acoustic properties using a two microphone random excitation technique.

APPENDIX 1

According to ISO 3745 and ANSI. 31-1980, the sound power of a source is determined by surrounding it by a hypothetical hemisphere in the far field. The sound pressure level, L_p, is measured usually at twelve equally distributed locations on the hemisphere. Each location has the same elemental surface area of the hemisphere associated with it. The L_p are then averaged spatially to give $L_{\bar{p}}$. Then equation {A.1.1} is used to determine the sound power.

The sound power level of the source can be determined from the relationship [26],

$$L_W = L_{\bar{p}} + 10 \log_{10} \frac{S}{S_o} - 10 \log_{10} N + C \quad \text{dB re. } 10^{-12} W. \qquad \{A.1.1\}$$

where $L_{\bar{p}}$ is the average measured sound pressure level referenced to 20 μpa,

$S = 2\Pi r^2$ = surface area of hemisphere,

$S_o = 1m^2$

N = number of measuring locations

C = Correction term, in dB, for the influence of ambient pressure and temperature.

In order to determine $L_{\bar{p}}$, the sound pressure level of the source is determined at the 12 locations whose co-ordinates are listed in Table A.1.1.

Location Number	Axis X	Axis Y	Axis Z
1	0	5.58	2.16
2	3.48	3.48	3.48
3*	5.58	2.16	0
4	2.16	0	5.58
5*	5.58	-2.16	0
6	3.48	3.48	3.48
7	0	-5.58	2.16
8	-3.48	-3.48	3.48
9*	-5.58	-2.16	0
10	-2.16	0	5.58
11*	-5.58	2.16	0
12	-3.48	3.48	3.48

Table A.1.1 Cartesian Coordinates of Microphone Positions.

Note:

1. The above coordinates, expressed in feet, represent a set of twelve points uniformly distributed on the surface of a hemisphere with a radius of six feet, with the origin at the acoustic center of the source.

2. *Three decibels shall be subtracted from the sound pressure levels obtained at those points on the reflecting plane (Z=0).

APPENDIX 2

Measurement of sound power and error analysis:

Measurement of the sound power by using equation {A.1.1} is valid only if measurements are done in the free field. Due to the unavailability of an anechoic chamber, sound pressure measurements were carried out in a large room. The only large room available had hard plaster surfaces. Consequently, the standard ANS1 S1.31 - 1980 was replaced by the more appropriate ANSI S1.21-1976 to accommodate sound power measurements in a semi-reverberant field. To account for semi-reverberant conditions two new constants, Directivity factor, Q, and Room constant, R, are introduced. These constants account for the boundary materials etc., as shown by equation {A.2.1} [26].

$$L_W = L_{\bar{p}} - 10 \log_{10} \left(\frac{Q}{4\Pi r^2} + \frac{4}{R}\right) - 0.5 \quad \text{dB re } 10^{-12}\text{W.} \qquad \{A.2.1\}$$

Where L_W is the sound power level,

$L_{\bar{p}}$ is the average measured sound pressure level referenced to 20 μ Pa

r is the radius of the measurement control volume.

The sound pressure levels of the computer are shown in Table A.2.1.

Location Number	Co-ordinates (Ft) X	Y	Z	Sound pressure level in octave bands centred at (dB)* 500 Hz	1.000 Hz	2000 Hz
1	0.00	5.58	2.16	57.5	45.0	46.0
2	3.48	3.48	3.48	55.0	46.0	44.0
3	5.58	2.16	0.00	51.0	43.0	42.0
4	2.16	0.00	5.58	56.0	47.0	45.0
5	5.58	-2.16	0.00	52.5	41.0	39.0
6	3.48	3.48	3.48	56.0	46.0	44.0
7	0.00	-5.58	2.16	53.5	45.0	45.0
8	-3.48	-3.48	3.48	55.0	44.0	41.0
9	-5.58	-2.16	0.00	50.0	41.0	39.0
10	-2.16	0.00	5.58	56.0	45.0	45.0
11	-5.58	2.16	0.00	51.0	43.0	40.5
12	-3.48	3.48	3.48	56.0	47.0	45.0
			$L_{\bar{p}}$	54.4	44.5	42.9

*dB re 20 μPa

Table A.2.1: Sound pressure levels measured at 12 locations on the hypothetical hemisphere surrounding the computer.

For a sound source positioned close to a boundary, the Q-factor is approximately 2 according to reference [26].

Dimensions of the room are 27' x 18.5' x 12'.

Thus, floor area = 499.5 ft^2

ceiling area = 499.5 ft^2

wall area = 1092.0 ft^2

Σ area = 2092.0 ft^2

According to reference [26], $R \simeq \Sigma S\,\bar{\alpha}$ for small values of $\bar{\alpha}$. Values of $\bar{\alpha}$ have been obtained from reference [26] for various materials and the value of R is determined as shown in Table A.2.2.

Surface	$S\,\bar{\alpha}$ at octave band centre frequency (Hz.)		
	500	1000	2000
Wooden floor	499.5 x 0.03	499.5 x 0.03	499.5 x 0.03
Concrete Ceiling	499.5 x 0.01	499.5 x 0.02	499.5 x 0.02
Portable partitions	1092.0 x 0.20	1092.0 x 0.02	1092.0 x 0.15
$R \simeq \Sigma S\,\bar{\alpha}$	238.4	210.6	188.8

Table A.2.2: Determination of Room constant R.

Now, substituting for the variables in equation {A.2.1}, the measured sound powers in the 500, 1000 and 2000 Hz. octave bands are 70.6, 60.2 and 58.2 dB re 10^{-12}W, respectively.

Error Analysis:

The governing equation for the measurement of sound power level, L_w, is [26]

$$L_w = L_{\bar{p}} - 10 \log_{10} \left(\frac{Q}{4\pi r^2} + \frac{4}{R}\right) - 0.5 . \qquad \{A.2.2\}$$

Thus, the error e_{L_w} is

$$e_{L_w} = \left[\left(\frac{\partial L_w}{\partial L_p} e_{L_p}\right)^2 + \left(\frac{\partial L_w}{\partial Q} e_Q\right)^2 + \left(\frac{\partial L_w}{\partial R} e_R\right)^2 \right]^{1/2} \qquad \{A.2.3\}$$

or

$$e_{L_w} = \left[\left(e_{L_p}\right)^2 + \left(\frac{10 \log_{10} e}{\left(\frac{Q}{4\pi r^2} + \frac{4}{R}\right)} \frac{1}{4\pi r^2} \right)^2 + \right.$$

$$\left. \left(\frac{10 \log_{10} e}{\left(\frac{Q}{4 r^2} + \frac{-4}{R}\right)} \left(\frac{-4}{R^2}\right) \right)^2 \right]^{1/2} . \qquad \{A.2.4\}$$

$r = 6$ ft , $Q = 2$, $e = 2.718$

$R_{500} = 238.4\ ft^2$, $R_{1000} = 210.6\ ft^2$, $R_{2000} = 188.8\ ft^2$.

Variation in $L_p = \pm\ 0.5$ dB.

Thus percentage variation is $\frac{0.5}{54.4}$ %, $\frac{0.5}{44.5}$ %, $\frac{0.5}{42.9}$ % in $L_{\bar{p}}$.

Maximum error in Q is 12.5%, as Q-factors between 1.5 to 2.5 have been approximated as 2 [26]. The error in R will not significantly affect the final result so as a "worst case" estimate let that be 70% [26].

Corresponding errors e_{L_p}, e_Q, and e_R in L_p, Q and R have been tabulated in Table A.2.3 for quick reference.

Error	Octave band centre frequency (Hz) 500	1000	2000
e_{L_p}	0.9%	1.1%	1.1%
e_Q	12.5%	12.5%	12.5%
e_R	70 %	70 %	70%

Table A.2.3 : Errors in L_p, Q and R.

Substituting for e_{L_p} , e_Q and e_R in equation {A.2.4} for each of the 500, 1000 and 2000 Hz octave bands, the resulting errors are:

$$e_{500\ Hz} = \pm\ 5.8\% \text{ or } \pm\ 4.0\ dB$$

$$e_{1000\ Hz} = \pm\ 5.6\ \% \text{ or } \pm\ 3.4\ dB$$

$$e_{2000\ Hz} = \pm\ 5.6\% \text{ or } \pm\ 3.3\ dB.$$

There are two major sources of error using the acoustic intensity technique. They are due to:

a) the finite difference approximation for the pressure gradient of up to $\pm$ 1.5 dB and,

b) the averaging mode of the spectrum analyser of up to $\pm$ 1.0 dB.

The cumulative effect of these errors cannot be estimated directly so that an experimental technique was used. The ILG reference sound source was used to determine the error in the measured value of the acoustic intensity. For various measurements, the "worst case" error was approximately 1.8 dB in the 500, 1000 and 2000 Hz. octave bands. Thus the acoustic intensity measurement (and approximation) error has been estimated to be of the order of $\pm$ 1.8 dB.

APPENDIX 2A

Derivation of expression for the acoustic intensity of a source :

For a stationary ergodic signal, the acoustic intensity I can be expressed as,

$$I = E\{p\ u_r\} \ , \qquad \{A.2A.1\}$$

where E denotes the expected value of the pressure, p, and the particle speed, u_r . By expressing the pressure and speed in terms of complex numbers, equation {A.2A.1} may be re-expressed as,

$$I = \frac{1}{4} E\ \{(p + p^*)(u_r + u_r^*)\}, \qquad \{A.2A.2\}$$

where * denotes the complex conjugate. Equation {A.2A.2} may be re-arranged to yield,

$$I = \frac{1}{2} E\ \{Re(p\ .\ u_r) + Re(p\ .\ u_r^*)\}\ . \qquad \{A.2A.3\}$$

Equation {A.2A.3} may be modified by expressing the variables in terms of their Fourier components. Thus,

$$I = \frac{1}{2} E\ \{Re(F_p\ .\ F_{ur}) + Re(F_p\ .\ F_{ur}^*)\}\ . \qquad \{A.2A.4\}$$

Here F_p denotes the Fourier Transform of p .

As mentioned in equation {2.3}+, the particle speed, u_r, at some instant t may be represented as,

$$u_r = (1/\Delta r\rho) \int_0^t (p_2 - p_1)dt \quad , \qquad \{A.2A.5\}$$

+Numbers without a letter prefix indicate that the equation is in the main text.

For the particle speed, u_r , sensed midway between two pressure transducers, spaced Δr apart,

$$F_{ur} \cong i(F_{p2}-F_{p1})/\rho\Delta r\omega, \tag{A.2A.6}$$

where ρ is the density of air, and $i = (-1)^{1/2}$.

The Fourier Transform of the pressure midway between the transducers is,

$$F_p \cong \frac{1}{2}(F_{p1}+F_{p2}) . \tag{A.2A.7}$$

Substituting equation {A.2A.6} and {A.2A.7} into equation {A.2A.4} gives,

$$I = [E\{Re(F_{p1})\ Im(F_{p1}) - Re(F_{p2})\ Im(F_{p2})\}$$

$$+E\{Im(F_{p1} \cdot F_{p2}^{*})\}]/\rho\Delta r\omega . \tag{A.2A.8}$$

For stationary and ergodic signals with zero mean,

$$E\{Re(F_{p1}) \cdot Im(F_{p1})\} = 0, \tag{A.2A.9}$$

$$E[Re(F_{p2}) \cdot Im(F_{p1})] = 0. \tag{A.2A.10}$$

Consequently, the acoustic intensity spectrum is

$$I = E\{Im(F_{p1}\ F_{p2}^{*})\}/\rho\Delta r\omega, \tag{A.2A.11}$$

$$= Im(G_{12})/\rho\Delta r\omega . \tag{A.2A.12}$$

APPENDIX 3

In order to determine the predominant vibration mode of the computer's panels, two accelerometers were mounted on each panel to determine the magnitude of the transverse and axial accelerations. The resulting accelerations are listed in Table A.3.2 through A.3.5 for convenience. According to equation {3.3} and {3.4}

$$\Delta S_f = \frac{\pi}{f} \sqrt{\frac{D}{\rho_t h}} \quad \text{for} \quad f > \frac{\pi}{S} \sqrt{\frac{D}{\rho_t h}} \qquad \{A.3.1\}$$

where ΔS_f is the surface area of each "independent" vibrating surface and D is the stiffness of the plate. Now, the computer's box-like shell is assumed to be made wholly of aluminum. Consequently, the value of Young's modulus, E, is 70 GPa and the density, ρ_t, is 2870 kg/m^3. Furthermore, the panels of the box are considered homogeneous and uniform to simplify the analysis so that

$$D = \frac{Eh^3}{12(1-\nu^2)} = 246.09 \text{ Nm.}$$

The total surface area of the computer, S, is 0.82475m^2 so that for the centre frequency, f, of 500 Hz.

$$\frac{\pi}{S} \sqrt{\frac{D}{\rho_t h}} = 20.6\text{Hz.}$$

Now 500 Hz, 1000 Hz and 2000 Hz are all greater than 20.6 Hz. so that

$$\Delta S_{500} = 0.034\text{m}^2$$

$\Delta S_{1000} = 0.017m^2$

$\Delta_{2000} = 0.0085m^2$

and $n_{500} = \frac{S}{S_{f\ 500}} = \frac{0.8247}{.034} \cong$ 25 points

$n_{1000} = \frac{S}{\Delta S_{1000}} = \frac{0.8247}{0.017} \cong$ 50 points

$n_{2000} = \frac{S}{\Delta S_{2000}} = \frac{0.8247}{0.0085} \cong$ 100 points .

Next the square of the surface speed was measured at 25, 50 and 100 locations on the computer for the 500 Hz, 1000 Hz and 2000 Hz octave bands, respectively. Sixty-four averages were invariably used to improve the signal to noise ratio.

Thus

$$\underset{5000\text{ Hz}}{Ws} = \rho c S \frac{k^2 \Delta S_f}{(2\pi + k^2 \Delta S_f)} \sum_n < \dot{\xi}^2 > \quad . \qquad \{A.3.1\}$$

"Constants" ρ, c, S, k and ΔS_f are known so that the sound power level may be obtained next for

$\Delta S_f = 0.034m^2$, $k^2 = 83.39$, $S = 0.82475m^2$, $c = 343ms^{-1}$, $\rho = 1.16$ kg/m^3.

The octave band surface speeds are shown in Table A.3.1. The sum of the squared speeds in the octave band centered at 500 Hz, shown in Table A.3.1, is $196.4 \times 10^{-9} m^2/s^2$. Consequently, inserting appropriate values for the variables in equation {A.3.1} yields

$$\underset{500\text{ Hz}}{W_s} = \frac{1.16 \times 343 \times 0.82475 \times 83.89 \times .034 \times 1.964 \times 10^{-7}}{10^{-12} \quad \times \quad (2\pi + 83.89 \times 0.34)} \ .$$

$$= \quad 72.8 \text{ db re } 10^{-12} \text{ W.}$$

Location N	Velocity squared $<\dot{\xi}^2>$ in the 500 Hz. octave band (dB re $10^{-12} m^2/s^2$)
1	38.5
2	39.5
3	39.5
4	39.5
5	37.5
6	38.0
7	38.0
8	38.0
9	37.0
10	37.5
11	40.5
12	40.5
13	40.5
14	40.5
15	38.0
16	38.5
17	39.5
18	38.5
19	38.0
20	40.5
21	38.5
22	36.5
23	36.0
24	37.5
25	37.5

Table A.3.1. Octave band velocity squared values in the oactave band centred at 500 Hz.

One-third octave centre frequency (kHz)	Transverse acceleration dB re 1g	Axial acceleration dB re 1g
0.96	50.3	49.8
0.020	51.2	51.5
0.025	53.6	51.0
0.032	63.1	52.9
0.040	69.1	58.0
0.050	72.7	67.2
0.063	78.1	61.0
0.080	87.8	74.6
0.100	81.6	81.9
0.125	85.9	76.5
0.160	99.6	77.5
0.200	95.8	82.0
0.250	76.8	63.3
0.320	79.4	68.1
0.400	82.0	68.3
0.500	92.5	72.1
0.630	88.4	73.7
0.800	95.4	75.7
1.000	92.1	74.5
1.250	84.7	74.7
1.600	81.4	70.2
2.000	86.2	74.2
2.500	82.8	78.4
3.200	82.6	81.9
4.000	88.7	86.2

Table A.3.2: Relative transverse and axial acceleration levels on top panel of computer.

One-third octave centre frequency (kHz)	Transverse acceleration dB re 1g	Axial acceleration dB re 1g
0.016	61.4	59.3
0.020	60.4	58.1
0.025	59.9	57.6
0.032	59.0	60.0
0.040	60.5	66.8
0.050	59.3	65.5
0.063	69.2	62.7
0.080	73.3	72.3
0.100	70.8	79.8
0.125	69.3	74.6
0.160	73.8	72.4
0.200	75.7	78.0
0.250	72.3	62.7
0.320	74.4	70.7
0.400	77.4	68.2
0.500	85.4	72.1
0.630	81.2	73.9
0.800	88.1	75.2
1.000	78.5	66.8
1.250	83.2	71.9
1.600	77.4	71.3
2.000	80.7	73.7
2.500	79.2	78.3
3.200	82.8	79.9
4.000	87.3	86.8

Table A.3.3: Relative transverse and axial acceleration levels on left panel of computer.

One-third octave centre frequency (kHz)	Transverse acceleration dB re 1g	Axial acceleration dB re 1g
0.016	49.4	46.1
0.020	49.4	47.4
0.025	50.6	49.1
0.032	53.9	57.8
0.040	56.3	63.1
0.050	59.2	71.3
0.063	68.6	67.4
0.080	74.7	77.1
0.100	72.4	76.9
0.125	71.6	76.6
0.160	69.2	76.6
0.200	80.0	83.1
0.250	68.8	68.6
0.320	72.7	73.1
0.400	84.4	67.3
0.500	92.7	77.5
0.630	87.7	78.04
0.800	93.3	79.86
1.000	86.3	70.31
1.250	87.4	74.4
1.600	79.0	71.9
2.000	79.6	77.0
2.500	79.7	78.2
3.200	86.9	84.4
4.000	89.9	92.5

Table A.3.4: Relative transverse and axial acceleration levels on right panel of computer.

One-third octave centre frequency (kHz)	Transverse accelerat-ion dB re 1g	Axial accelerat-ion dB re 1g
0.016	53.3	48.1
0.020	59.7	49.8
0.025	66.8	53.6
0.032	72.7	60.2
0.040	78.7	68.6
0.050	86.7	70.8
0.063	96.0	75.4
0.080	106.8	88.8
0.100	97.8	85.7
0.125	99.4	78.6
0.160	96.5	78.5
0.200	100.7	84.9
0.250	87.3	66.8
0.320	85.9	73.7
0.400	85.6	70.1
0.500	85.5	72.5
0.630	77.5	74.8
0.800	79.1	76.7
1.000	82.8	75.1
1.250	80.6	76.1
1.600	72.9	75.2
2.000	75.3	75.9
2.500	77.1	77.3
3.200	84.0	82.9
4.000	89.6	91.4

Table A.3.5 Relative transverse and axial acceleration levels on rear panel of computer.

Error Analysis

Major errors are caused by the simplifications and assumptions associated with equation {3.3}. First, the computer is assumed to be in an infinite baffle; a condition that is obviously not satisfied in a semi-reverberant room. As in the acoustic intensity case the measured sound power levels would be higher due to the reflected waves from the room boundaries. Second, it is assumed that the sound sources are spaced uniformly throughout the computer; a condition that is evidently untrue as seen in Chapter II. In practice, more measurement points should be allocated to the regions with the greater radiation levels to prevent any bias in the measured sound power level. Third, the computer's exterior panels have been assumed to be homogeneous and free of local stiffeners and mass dampers. Once again, this assumption is not strictly valid due to the complexity of the computer's construction. On the computer, the external attachments occupy a significant proportion of the total surface area when compared to the area of the "homogeneous" panels. Consequently, this distorts the simple "pulsations" of the exterior panels. These errors can only be expressed qualitatively. The only error that can be quantified is that which occurs in the determination of the square of the surface velocity. This error has a magnitude of $\pm$ 1.0 dB when 64 averages are performed within the spectrum analyser. The following section determines the magnitude of the measurement error.

An error analysis, for the sound powers measured by using the surface velocity technique follows.

$$We = \sum_n \rho c S \frac{k^2 \Delta S_f}{2\pi + k^2 \Delta S_f} < \dot{\xi}^2 > \qquad \{A.3.2\}$$

and

$$\frac{\partial We}{\partial \dot{\xi}} = 2 \sum_n \rho c S \frac{k^2 \Delta S_f}{2\pi + k^2 \Delta S_f} < \dot{\xi} > \qquad \{A.3.3\}$$

$$e<\dot{\xi}> = \pm \; 12\% \text{ of } < \dot{\xi} > .$$

An estimate of the average surface velocity is, $< \dot{\xi} > = 2.75 \times 10^{-9} ms^{-1}$.

Thus,

$$e_{we} = 2 \times 1.14 \times 343 \times 0.826 \times \frac{2.85}{9.13} \times 0.12 \times (2.75 \times 10^{-9})^2$$

$$= 1.82 \times 10^{-16} W .$$

Now the sound power of the computer is of the order 1.9×10^{-5}W. This implies a negligible measurement error.

APPENDIX 4

Sample calculation of the power crossing sections AA' and BB' (Table 4.1) at 80 Hz.

The vertical components of the intensity vectors are marked in Figure A.4.1 for a spacing between measurement locations of 0.0889m. By using the sign convention of downward positive, the net intensity crossing section AA' is 86.4 dB whilst the net intensity crossing section BB' is 74.50 dB. Then the net power flow towards the sand pit across:

a) Section AA' is 10Log_{10}[Antilog 8.64 x .0889] = 75.90 db re 10^{-12}W; and across

b) Section BB' is 10Log_{10}[Antilog 7.45 x .0089] = 64.00 db re 10^{-12}W.

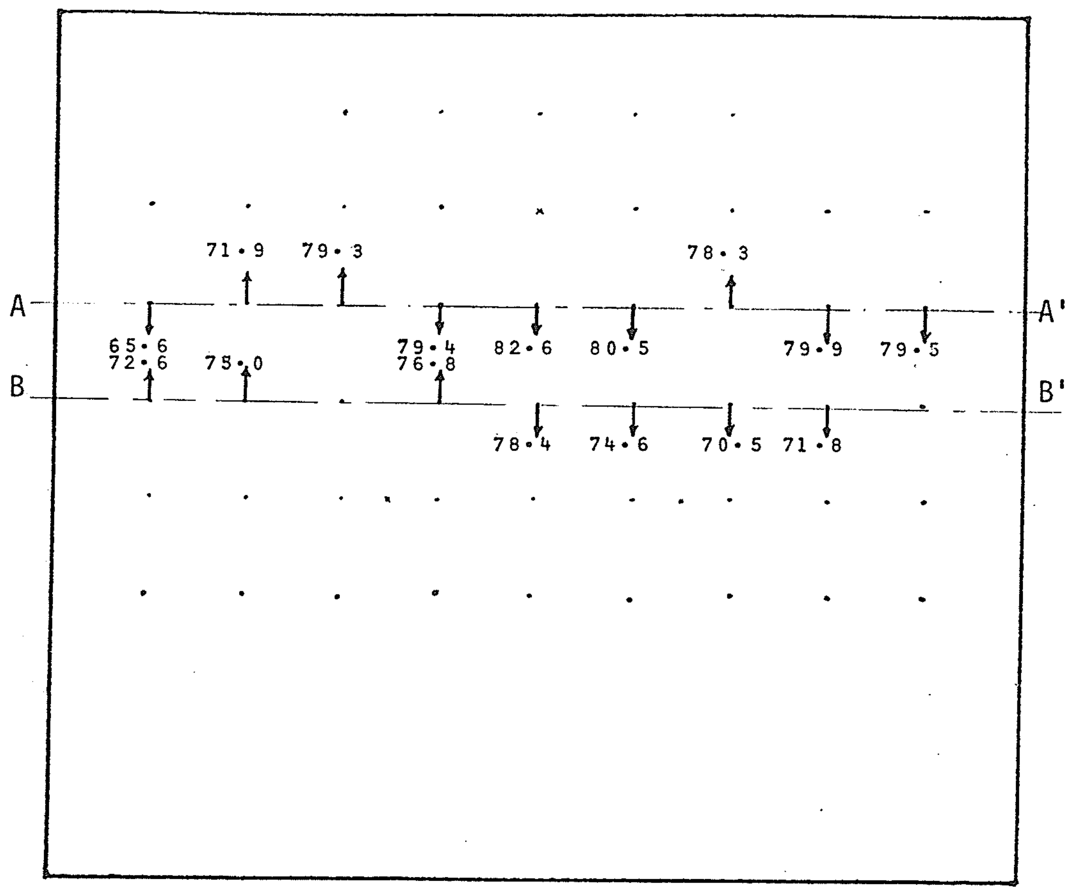

Figure A.4.1: Intensity levels crossing sections AA' and BB' (dB re 10^{-12} W/m)